Cape Peninsula University of Technology

A LAND-BASED HF TRANSMITTER FOR IONOSPHERIC PROPAGATION STUDIES USING SUPERDARN RADARS

by

LUSANDA LUNICA MDIBI

Student No. 216282799

Thesis submitted in fulfilment of the requirements for the degree Master of Engineering: Electrical Engineering in the Faculty of Engineering at the Cape Peninsula University of Technology

Supervisor: Prof Michael J. Kosch

Co-Supervisors: Prof Robert R. van Zyl

Mr Jonathan Ward

Bellville Campus

2019

DECLARATION

I, Lusanda Lunica Mdibi, declare that the contents of this dissertation/thesis represent my own unaided work, and that the dissertation/thesis has not previously been submitted for academic examination towards any qualification. Furthermore, it represents my own opinions and not necessarily those of the Cape Peninsula University of Technology.

Signed **Date**

ABSTRACT

The goal of this project is to design, build and characterize a low power High Frequency (HF) transmitter. The transmitter will be installed and operated in Antarctica to establish a beacon at the South Pole station to be received by the Super Dual Auroral Radar Network (SuperDARN) radar installed at SANAE IV. The transmitter is specified and designed to transmit at 12.57 MHz (continuous wave) from the South Pole. It must achieve a frequency drift of 41.8 mHz or better. The transmitter must operate normally under extremely low temperature conditions down to -40°C. The transmitted wave will be refracted by the ionosphere and received by the SuperDARN radar at SANAE IV. The ground distance between the HF transmitter and the radar is approximately 2000 km. The goal of the experiment is to form a bi-static radar configuration in order to study the ionosphere, especially travelling ionospheric disturbances (TIDs), which are signatures of atmospheric gravity waves (AGWs). A 25 dBm transmitter prototype was developed using a GPS disciplined oscillator in order to achieve the frequency stability required for this project. The HF transmitter proved to conform to the power and frequency stability requirements both during propagation tests conducted between Hermanus (34.4241° S, 19.2247° E) and Pretoria (34.0558° S, 18.4589° E) in South Africa, as well as when the device was exposed to temperatures that ranged from +40°C to -45°C. Although the antenna design was beyond the scope of this project, various determinations and considerations are presented in the link budget analysis, which have been confirmed during field tests. Therefore, certain recommendations on the antenna design are given. Propagation in Antarctica is expected to differ from the field tests conducted due to the differences in density and dynamics of the polar ionosphere, compared to the mid-latitude ionosphere.

ACKNOWLEDGEMENTS

I would like to take this opportunity to express my gratitude to the following:

- My ancestors, for watching over me throughout the journey of my studies and my life.
- My immediate family, for their support, love, encouragement and wisdom that I know I can always count on.
- The SANSA Space Science team, for their financial and moral support throughout the period of my studies for this degree.
- Prof. Michael J. Kosch, for his guidance, support and patience throughout the period of my studies for this degree.
- Prof. Robert R. van Zyl, for encouraging me and making it possible for me to be part of the F'SATI programme as well as his supervision and guidance.
- Jonathan Ward, for his assistance and engineering expertise that proved very useful during the execution and testing of the project.
- Juchelle Ontong, for going above and beyond for every student to ensure that we had all the assistance and resources we need to execute and complete research as well as comfort at SANSA.
- Dr. Phumzile Malindi, for always making time to assist whenever I needed it the most.
- Dr. Pierre Cilliers, for his contribution in the project and arranging with GEW technologies to assist with propagation tests.
- Hannes P. Coetzee, for taking time on his schedule and utilizing the equipment at his disposal to assist with propagation tests.
- Daniel van Niekerk, for assisting with the letter of recommendations when I applied for a bursary.
- My friends and classmates who contributed in any way towards the completion of my research.

Opinions expressed in this thesis and the conclusions arrived at are those of the author, and should not necessarily be attributed to the French South African Institute of Technology and to the South African National Space Agency.

DEDICATION

This study is whole heartedly dedicated to my beloved mother, whose strength, courage and effort made me the man that I have become.

TERMS AND CONCEPTS

AC	Alternating Current
AGW	Atmospheric Gravity Waves
BAS LPM	British Antarctic Survey Low Power Magnetometer
CW	Continuous Wave
DC	Direct Current
DEA	Department of Environmental affairs
DUT	Device under Test
GNSS	Global Navigation Satellite Systems
GPS	Global Positioning Satellites
GPSDO	GPS Disciplined Oscillator
HF	High Frequency
IC	Integrated Circuit
IEEE	Institute of Electrical and Electronics Engineers
ITU	International Telecommunications Union
LPDA	Log Periodic Dipole Antenna
LPF	Low Pass Filter
PIC	Peripheral Interface Controller
Radar	Radio Detection and Ranging
RF	Radio Frequency
SANAE	South African National Antarctic Expedition
SANSA	South African National Space Agency
SuperDARN	Super Dual Auroral Radar Network
TID	Travelling Ionospheric Disturbances

1 Table of Contents

LIST OF FIGURES

CHAPTER 1 INTRODUCTION

1.1. INTRODUCTION

A global network of scientific HF radars, known as the Super Dual Auroral Radar Network (SuperDARN), measures the velocity of the plasma at ionospheric altitudes (200 – 300 km) over a large region of the northern and southern hemispheres. The network is currently operated by 11 countries and is made up of 34 radars. SuperDARN measures the drifting plasma at ionospheric altitudes in the polar regions of the Earth for scientific purposes (Shepherd, 2017). The HF radars give several advantages over polar orbiting satellites (which can also be used for similar studies), such as the cost of operation, maintenance and construction. They also allow continuous monitoring of these regions.

Travelling ionospheric disturbances (TIDs) are a result or ionospheric manifestation of atmospheric gravity waves (AGW). TIDs of different scales are primary factors that determine ionospheric dynamics (Podlesnyi, 2014). These disturbances are important because of the change of direction they have been observed to cause to signals travelling through the ionosphere. They are consequently detrimental to the accuracy of high frequency (HF) geolocation systems because they cause refraction of the radio signals (Mitchell et al., 2017). SuperDARN radars have been successfully used to study TIDs in high latitudes for a while now (Ogawa et al., 2009).

SuperDARN radars operate on the principle of coherent backscatter in order to measure the motion of the magnetic field-aligned ionospheric irregularities that exist in the F-layer of the ionosphere at a height of approximately 125km. This is best achieved with radars that operate at HF (3-30 MHz) compared to VHF and UHF radars (Chisham et al., 2008). The SuperDARN is monostatic because they do not receive each other's signals even though one can access data of multiple radars. A bi-static radar configuration may be used as a method of ionospheric sounding that can increase the ability to study the dynamics of ionospheric irregularities (Berngardt et al., 2015).

1.2. RESEARCH PROBLEM

Spacecraft have been used for space weather research purposes since the early 1960's when the Canadian satellite, Alouette 1, was launched to study the ionosphere. The evolution of satellite technology has since provided more ionospheric data about low- and mid-latitude locations. There is no doubt that data from satellites are useful, but these satellites orbit Earth, which makes them incapable of monitoring the polar zones continuously to provide real time data.

Space weather impacts many technological systems, and can lead to serious disruptions, such as (Lanzerotti, 2013):

- power grid outages;
- disruption to Global Navigation Satellite Systems (GNSS), for example the Global Positioning System (GPS);
- high frequency (HF) radio communications outages;
- satellite damage; and
- increased radiation threat at high altitude.

These are graphically presented in Figure 1.

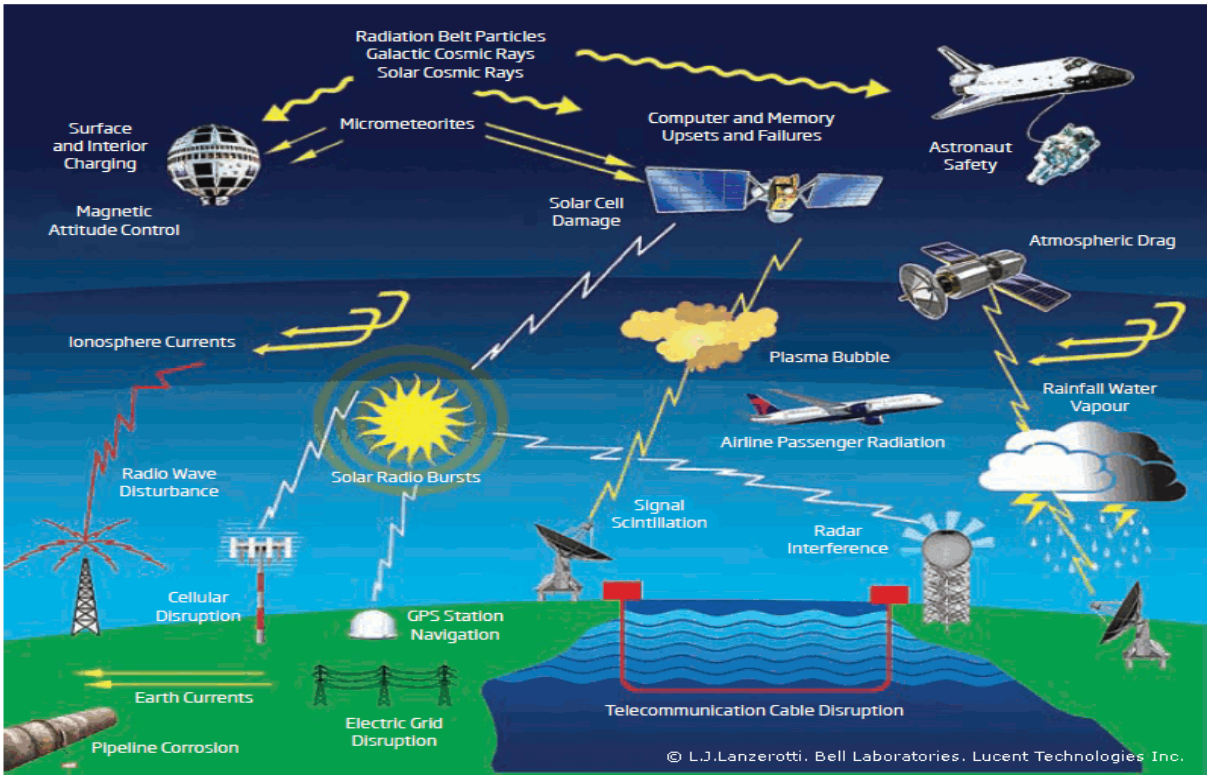

Figure 1: Solar radiation / space weather effects on technological systems

The high latitude ionosphere is less predictable compared to the mid- and low-latitude ionosphere. The geometry of the magnetic field lines, which are almost vertical, exposes the ionosphere to influencing forces and activities, such as space weather storms. This makes it susceptible to AGWs/TIDs that may travel as far as mid-latitudes. Studying these gravity waves is a challenge that the SuperDARN radars are trying to address, but limitations like power and distance coverage are to be expected when only the backscatter portion of the SuperDARN signal is observed.

1.3. RESEARCH BACKGROUND

In order to understand the polar ionosphere to a point where models can predict it accurately, it is necessary to measure, monitor and document the results continuously. SuperDARN radars partially address this issue, but backscatter, which the radars rely on, is a small portion

of all the energy radiated by the radar. This means most of the wave energy that may be useful, continues to travel outward and is wasted.

High-latitude locations, such as Antarctica, are difficult to access. This makes research in these areas extremely difficult and expensive to plan and execute. Equipment and electronic devices are difficult to operate in these areas because of the considerably low temperatures as low as -40°C. Although advances in technology have made it easier to access several platforms to share research data, Antarctica still presents a challenge of accessibility to researchers. Due to the above reasons, there is very limited data available about the ionosphere and its dynamics in this region.

The primary objective of SuperDARN is to provide direct, continuous, global-scale observations of high-latitude ionospheric convection. SuperDARN radars are sensitive to scatter from decameter-scale irregularities in the ionospheric plasma density. These irregularities tend to be aligned along the magnetic field direction and present an appreciable cross-section for backscattering only when the HF ray is within a few degrees off perpendicular to the magnetic field (Baker et al., 2008).

Unlike polar orbiting satellites, which only pass over a specific area a few times per day, HF radars permit continuous monitoring of these regions. Ground-based systems are also much cheaper to build, operate and maintain than spacecraft. The SuperDARN network is still expanding, with new radars joining the network almost yearly.

South Africa takes part in the SuperDARN network through the South African National Space Agency (SANSA), which uses and operates the SANAE IV SuperDARN radar in Antarctica.

It is proposed that it may be possible to do propagation studies using the radar and a fixed frequency, ground-based HF transmitter beacon. This beacon will be placed somewhere between the South African base (SANAE IV) and the South Pole, possibly even at the South Pole Station itself. This will allow continuous measurements of the ionosphere between the radar and the beacon. This also means that the radar will not only rely on backscatter to study the ionosphere. Forward propagation means that more power is directed towards the receiver or radar.

1.4. OBJECTIVES OF THE RESEARCH

- This project requires the HF transmitter to be designed, built and then tested under the conditions expected in Antarctica using an environmental chamber.
- The design must be verified through relevant simulations and/or field tests.

1.5. RESEARCH QUESTIONS

- Can a low cost HF beacon that meets the project requirements be designed to operate in Antarctic conditions?
- How does a bi-static radar configuration improve ionospheric studies?

- How is the ionosphere in high latitudes different from the mid-latitude and low-latitude ionosphere?

1.6. HF TRANSMITTER DESIGN SPECIFICATIONS

The environment in which the device is to be installed is known to be covered in ice all year round. The device must,therefore, meet the following specifications:

- The device should be powered by a 12V DC supply.
- The output power of the device should be 100 mW at a maximum of 10 W input power.
- The device must operate over a range of 8 – 20 MHz with a nominal frequency of 12.57 MHz because the SuperDARN radar operates at this specific frequency.
- The device must operate in temperatures that range from -40 °C to 0 °C.
- The frequency of the device must be stable enough to achieve a Doppler shift observation better than 1 m/s for TID studies.
- The device must be able to transmit CW and Morse code signals.

1.7. BACKGROUND OF IONOSPHERIC WAVE PROPAGATION

1.7.1. Ionosphere

The ionosphere refers to the upper regions of the atmosphere. This region is weakly ionised, that is, it has a significant density of free electrons (negative charges) and positively charged ions. It has practical importance because, among other functions, it enables HF radio propagation to distant places on Earth (Khoder, 2014). Waves that can be refracted by the ionosphere are referred to as sky waves (see Figure 2).

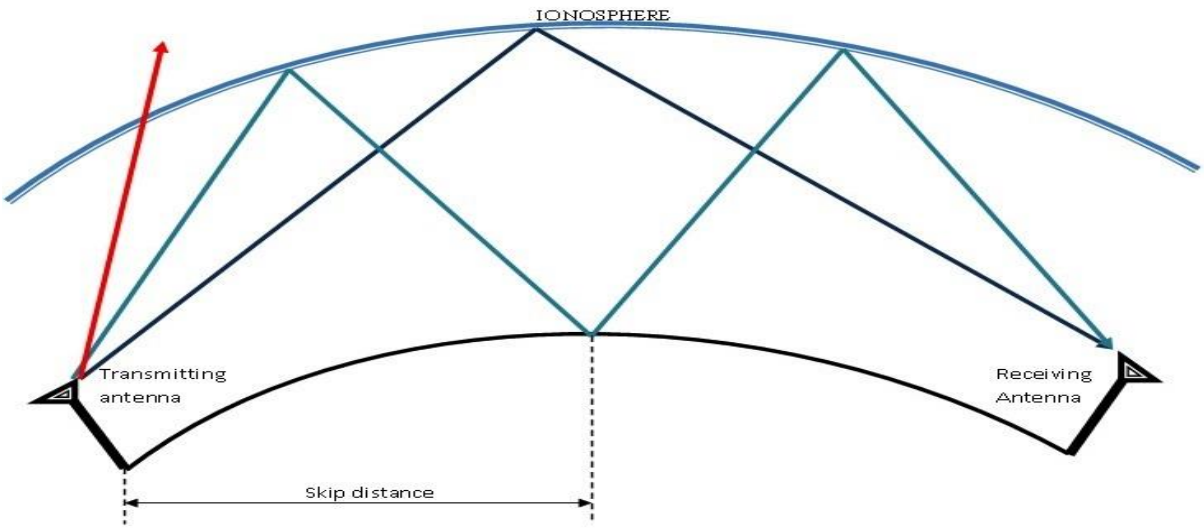

Figure 2: Sky wave propagation

The ionosphere is divided into the following layers:

- D layer, which is at the bottom (from 60 - 90 km) and can refract VLF and LF waves, but higher frequency signals pass through;
- E layer, which is the middle layer (from 90 – 125 km) and is capable of refracting signals of up to 20 MHz; and the
- F layer, which is the highest layer of the ionosphere (above 125 km) and refracts signals of up to approximately 30 MHz.

Each layer causes some attenuation of signals passing through to the next layer. The distance between the transmitter station and the point where the refracted waves return to the ground is called the skip distance (Malindi, 2013).

Refraction and reflection of sky waves depend on three factors:

- *Density of the ionosphere*. This depends on the solar radiation and particle precipitation causing ionisation at high latitudes. At night, the D layer disappears and the E layer becomes thinner and that increases the skip distance.
- *Frequency of operation*. Frequencies above 30 MHz cannot be refracted back to Earth; they are therefore unsuitable for sky wave transmission as they will be lost into space.
- *Angle of radiation.* Each frequency has a maximum angle at which it can be radiated and refracted back by the ionosphere. This angle is called the critical angle of that frequency (Malindi, 2013).

1.7.2. Atmospheric Gravity waves

Atmospheric gravity waves (also known as atmospheric internal waves) occur when a layer of air of determined velocity encounters a large obstacle like a mountain or island and then changes direction and travels upwards. Each layer of the atmosphere has a uniform temperature and pressure density that only changes with height. When the air collides with the obstacle, the horizontal ribbons of uniform air are disturbed, which forms a wave pattern. These waves are formed because there are forces that try to restore the hydrostatic equilibrium of the atmosphere. The gravitational force drags the air parcel towards the Earth and the buoyancy raises the air parcel due to density differences of the stratified atmosphere. The differences in density are primarily caused by temperature differences between the parcel and the surrounding air (Wirth & Hofer, 2017). AGWs are also caused in the F-layer of the atmosphere because of the heating due to space weather storms. It is these AGWs and their associated TIDs that the SuperDARN radars observe. The vertical movement is observed through its associated Doppler shift.

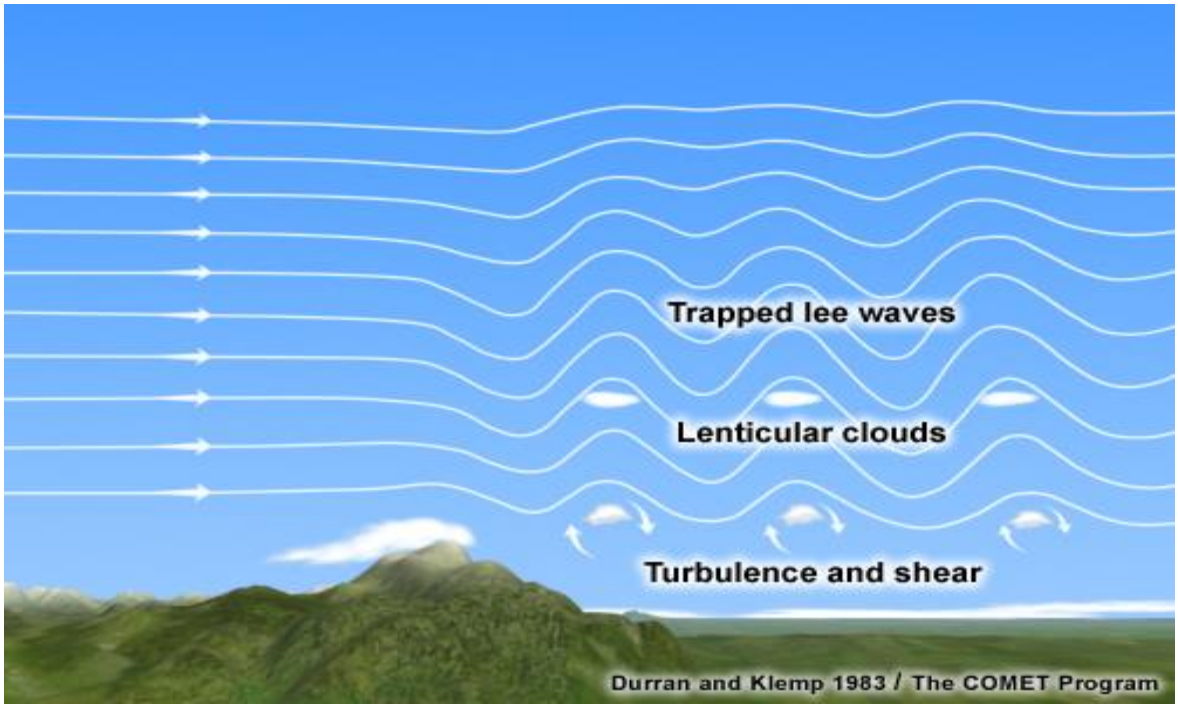

Figure 3: Ground waves caused by mountains (adapted from Wirth & Hofer, 2017)

Figure 3 shows trapped atmospheric waves that occur when wind speeds above the mountain increase sharply with height and stability decreases in the layer above the mountain top.

1.8. HYPOTHESIS

A high frequency signal that is bounced from the ionosphere and returned to ground may be used to characterize the ionosphere that reflected or refracted it. As the wave propagates between the transmitter and the receiver, it is subjected to attenuation and frequency drift that may be used to identify some characteristics of traveling ionospheric disturbances, such as their speed, height and wavelength. It is hypothesized that placing a transmitter at a distance from the receiver will provide results (in terms of the power and frequency drift of the signal) similar to the backscatter of the Doppler radars when observing TIDs.

1.9. PROPOSED SOLUTION

A low power, continuous wave (CW) transmitter is designed to be utilised in a bi-static radar configuration. Its signal will be received by the SuperDARN radar at SANAE IV. SANAE IV is the South African base that is operated by the Department of Environmental Affairs (DEA). A CW transmitter is less complex, easier to operate, and at a lower cost compared to pulse radars that may require the transmitter and receiver to be synchronized. It is technically suitable for the task of measuring the change in velocity of a moving target, i.e. the vertical motion of the ionosphere due to TID.

1.10. RESEARCH DESIGN AND METHODOLOGY

The following approach is followed to ensure that the research is carried out effectively and the expected results are achieved:

- **Literature survey:** A thorough survey of literature pertaining to HF transmitter design is conducted. These sources include books, reliable internet sites, journals and consulting people with expertise in the field relating to the study undertaken.
- **Simulations and analyses:** This research is design- and construction-based. Circuit simulations are important prior to construction. There is a variety of software packages that can be used. Simulations are also necessary because the device is not deployed in the Antarctic to obtain real field results. It can only be simulated to obtain the expected performance.
- **Construction and testing:** The final and most crucial part of this project is the construction and testing. The designed prototype has to be tested under conditions that emulate the weather conditions of Antarctica. An environmental chamber is used for this purpose. Field tests are conducted in Hermanus.

In future, the beacon will be placed at the South pole with its antenna radiating towards SANAE IV, as presented in Appendix B.

1.11. DELINEATION OF THE RESEARCH

The focus of this project is the design and implementation of, specifically, an HF transmitter that can operate efficiently under the harsh weather conditions of Antarctica. The literature survey will include a suitable antenna design for the project but the design and construction of the antenna is not part of this project. The HF beacon is not deployed in Antarctica at this point in time due to the logistical challenges in deploying the transmitter there, but the design has been validated through experimental results.

1.12. SIGNIFICANCE OF THE RESEARCH

This project is of great significance to:

- SANSA Space Science – Space weather, including forecasting atmospheric gravity waves and determining the expected electron density profile mid-way of the skip distance, is of great science interest to this organization. The data received from the HF beacon will be used to study and characterize the ionosphere of the region between the South pole and SANAE IV. Parameters of the ionosphere, such as electron density, geomagnetic storm effects, ionospheric motions and sky wave propagation paths will be better understood from analysing the signal received from this transmitter after it has been refracted by the ionosphere.
- HF radar operators – These researchers can make use of this design to accomplish ionosphere path profile studies and verification of results that may be achieved by software simulations. The ability to change the operational frequency without

changing any circuit components will make this project flexible enough to be used by HF radar operators that might not be operating in the frequency range specific to this project.

1.13. SYNOPSIS OF THE CHAPTERS

Chapter 1 gives an introduction and background to this project, space weather and its effects. It also highlights the research methodology, the significance of the research, and sets forth the specifications and delineation of this project.

Chapter 2 discusses the structure of the ionosphere and how it affects HF radio wave propagation and relates to atmospheric gravity waves that are the result of the disturbed ionosphere. A background on radar techniques is introduced in this chapter as well as some HF antenna designs.

Chapter 3 focuses on the parameters that make up an HF radio link and how each parameter affects the power in the link. A link budget specific to this project is also carried out in this chapter.

Chapter 4 presents the design of each of the stages of the HF beacon.

Chapter 5 discusses the test setup, procedures and results obtained during the tests.

Chapter 6 presents the conclusion of the project and recommendations for future work.

2.1. INTRODUCTION

Radar systems play a major part in space communications and space weather. SANSA Space Science is responsible for monitoring these weather conditions as a national organization representing South Africa and being part of the SuperDARN international network. SANSA Space Science is the entity or organization that is responsible for research, infrastructure and data for monitoring the near-Earth space environment in South Africa. SANSA leads the South African space programme and is part of the South African National Antarctic Programme (SANAP) with several ongoing space science and space weather related projects in Antarctica and surrounding islands. The South African National Antarctic Expedition (SANAE) IV base is operated by the Department of Environmental Affairs (DEA) in Antarctica. It was built between 1993 and 1997, and is considered to be one of the continent's most modern stations. The location of the base is considered special because of the fact that magnetic field lines reach down to the ground in the polar regions. The map of the existing SuperDARN network in the Southern and Northern hemispheres is as shown in Appendix C.

2.2. IONOSPHERE

The ionosphere is the ionised component of the atmosphere that is made up of free electrons and positive ions. They exist in a medium that is electrically neutral. Charged particles have a rather large influence on the electrical properties of a medium even though they are not the dominant particles; in fact they are a minority amongst the neutral particles. These charged particles make it possible to create and design radio communications over a long distance by reflecting or refracting radio waves in the ionosphere. Gradients in refractive index or plasma density allow signals in the High Frequency (HF) band (3-30 MHz) to be bent gradually towards the horizon as the refractive index of the ionospheric medium decreases with height (Hunsucker & Hargreaves, 2003).

2.2.1. Ionospheric layers

Molecules are in a combined state and remain electrically neutral in most parts of the atmosphere. When gas molecules are hit by the intense solar ultraviolet (UV) radiation from the sun, the molecules split, ionise and electrons escape, creating positive ions and free electrons. Although the ionosphere is named after ions, free electrons are the actual concern when it comes to radio waves. The number of electrons starts to increase at an altitude of about 30 km, but the electrons are not dense enough to affect radio waves until about 60 km. The ionosphere is generally thought of as having a number of distinct layers. This makes it easier to explain the structure of the ionosphere, but it is not entirely accurate as the entire ionosphere contains ionised atoms, molecules and free electrons. Instead, the layers are best thought of as peaks in ionisation levels. The so-called layers are commonly identified by letters D, E and F. Different literature sources have presented different opinions on the height and thickness of each layer (Poole, 1999).

2.2.1.1. D layer

The lowest layer of the ionosphere is called the D layer and is found at an altitude of approximately 60 km to 90 km above the surface of the Earth. Lyman series alpha hydrogen radiation that has a wavelength of 121.5 nanometer (nm) is the main cause of ionisation in this layer. A high number of active sunspots enhance hard X-ray ionisation in the air during the day, while a residual amount of ionisation is due to cosmic rays at night. The recombination rate is high in this layer, which means the total ionisation effect is very low and as a result the HF radio waves are not reflected by the D layer. The frequency of collision between electrons and other particles in this region is rather high; it can reach millions of collisions per second. The lower range of HF waves, i.e. 10 MHz and lower, are subjected to higher levels of attenuation in this layer; an increase in frequency reduces the effect of D layer absorption. It is then reasonable that absorption at night is much lower than during the day since the layer is considerably reduced after sunset, mainly due to recombination. The little of it that remains is due to re-ionising galactic cosmic rays. The effect of the D layer increasing and reducing may be recognised by the disappearance of distant AM broadcast band stations in the daytime, or rather, the reception distance gets closer to the broadcaster or transmitter (Oshiorenoya, 2004).

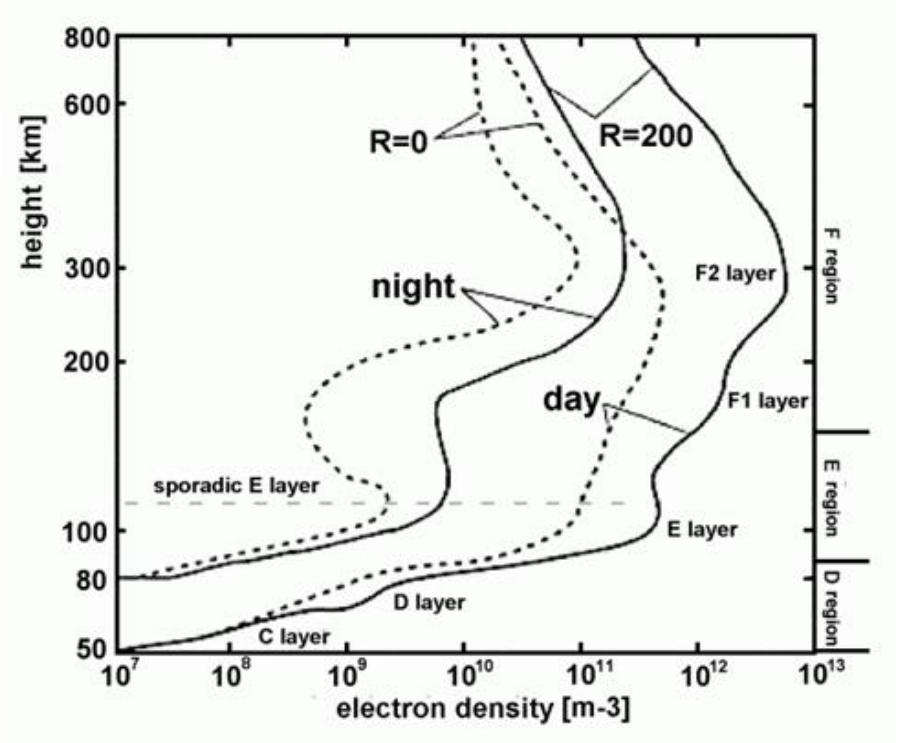

Figure 4: A typical electron density profile for various times and seasons

2.2.1.2. D layer absorption

The D region is responsible for most of the absorption encountered by HF signals that make use of the skywave mode. The D layer acts as an attenuator mostly at low frequencies. In

fact, the attenuation varies as the inverse square of the frequency, i.e. doubling the operating frequency reduces the level of attenuation by a factor of four. This is why low frequency signals are inhibited from reaching the higher layers, except at night when the D layer disappears. Free electrons in the D layer vibrate as electromagnetic signals traveling in this layer collide with the neutrals, which results in attenuation of the signal itself. A minute amount of energy is consumed and a small amount of the signal of the radio signal is dissipated as vibrating electrons collide with other molecules. The number of collisions that occur determines the level of attenuation. The number of collisions is dependent on several factors, such as electron temperature, and number of neutral gas molecules present in the layer, i.e. a higher number of gas molecules results in higher attenuation levels. One of the primary factors that determine the attenuation experienced by the signal is the frequency of the signal itself. Signals with shorter wavelengths do not cause as many collisions between free electrons and neutral particles, resulting in less absorption compared to longer wavelength signals (Poole, 1999). In most cases, the absorption in the D region is a principal factor when determining the lowest usable frequency (LUF) in order to achieve successful communication over a fixed skywave path (Goodman, 2006). The lowest usable frequency is defined as the minimum frequency in the HF band that is capable of providing sufficient reception for a given distance and transmission power. There are several other mechanisms that affect the LUF, making it difficult to evaluate the expected performance of the radio link, such as (Maslin, 2003):

- the characteristics of the ionosphere between the transmitter and receiver;
- scattering of radio waves;
- the signal-to-noise ratio at the receiver; and
- polarisation changes that are caused by the magnetic field of the Earth.

Abnormally high levels of absorption in the D region sometimes cause blackouts in high frequency sky wave propagation during the day. The blackouts are referred to as shortwave fadeouts (SWFs). Absorption in the D layer is given by:

$$A = 4.5\text{x}10^{-5} \cdot \int \frac{N_e V_{en}}{(\omega \pm \omega_e)^2 + V_{en}^2} dh \qquad (1)$$

$$\omega = 2\pi f$$

where:

A – Absorption in dB

N_e – Electron density in m^{-3}

V_{en} – Electron-neutral collision frequency in Hz

ω_e – Electron gyro frequency in rad/sec

f – Operational frequency in Hz

The electron gyro frequency is usually about 10 times smaller than the operational frequency and can be neglected for this calculation. Absorption is therefore approximated by:

$$A = 4.5\text{x}10^{-5} \cdot \int \frac{N_e V_{en}}{\omega^2 + V_{en}^2}\, dh \;\; (dB) \qquad (2)$$

The relationship between the shortwave fadeouts (SWFs) and solar flares was discovered several decades ago by Dellinger (1937). The condition of high absorption can last from a few minutes to a few hours. Sudden Ionospheric Disturbances (SIDs) are so named because the start of this absorption is usually very sudden, although not always, and is followed by a relatively slow recovery. SWFs are occasionally followed by brief variations in the magnetic field of the Earth, which indicate the presence of electric currents in the D region. The National Bureau of Standards describes the SWFs as sudden, slow, or gradual, depending on the time variation of the recorded signal, i.e. not all shortwave fadeouts are sudden (Davies, 1965).

2.2.1.3. D layer collision frequency

The amount of energy that is lost, depends on the number of collisions that take place, which in turn is also dependent upon a number of other factors. The first is the number of neutrals, electrons and ions that are present. In the D layer the density of the air is relatively high, so there are a large number of neutrals around and the number of collisions is high. The second factor is the frequency of the signal. As the frequency is decreased, so the displacement of the vibrations increases and consequently the number of collisions (Poole, 2016). The atmosphere of the Earth is made up of about 78% nitrogen, 21% oxygen and 1% argon. The formula to determine the collision frequency is given below.

$$\begin{aligned} V_{e,n} = {} & 2.33\text{x}10^{-11}[N_2](1 - 1.21\text{x}10^{-4}T_e)T_e \\ & + 1.82\text{x}10^{-10}[O_2]\ \left(1 + 3.6\text{x}10^{-4}\sqrt{T_e}\right)\sqrt{T_e} \\ & + 8.9\text{x}10^{-11}[O](1 + 5.7\text{x}10^{-4}T_e)\sqrt{T_e} \end{aligned} \qquad (3)$$

where:

$V_{e,n}$ – Electron-neutral collision frequency in Hz
T_e – Electron temperature in K
$[N_2]$ – Nitrogen density in the D layer in m^{-3}
$[O_2]$ – Oxygen density in the D layer in m^{-3}
$[O]$ – Atomic oxygen density in the D layer in m^{-3}

2.2.1.4. E layer

The E layer is a unique layer above the D layer even though their boundaries blend together, and is also known as the Kennelly-Heaviside layer. The amount of ionisation of the E layer is

greater than that of the D layer and normally follows the position of the sun in the sky closely. This layer begins at 90 km and stretches up to 125 km above the surface of the Earth.

The E layer is a stable layer but its maximum ionisation is most substantial at midday. It exists in every season of the year but its height may differ depending on the position of the Sun in the sky and it disappears at night. It provides absorption as well as reflection of low frequency radio waves (Lee, 1991). This layer is also capable of refracting HF signals of up to 20 MHz in some regions (Bertrand, 2002).

"Sporadic E" refers to the mostly unpredictable formation of regions of very high electron density in the E region. Sporadic E regions may form at any time during the day or night, occurring at any altitudes of the E region. Areas of coverage vary greatly from a few kilometers to hundreds of kilometers and it can occur for minutes to several hours. They have practical importance because they are often dense enough to affect radio propagation quite seriously. There are about a dozen types of these sporadic E regions, but there are three main physical types (Rishbeth, 1989):

- Mid-latitude sporadic E layers are usually much denser than the normal E layer or even the F2 layer, and are thought to be produced by wind shears. The wind shears interact with the geomagnetic field in such a way to compress the long-lived metal ions into thin layers, typically a kilometer thick but several hundreds of kilometers in extent.
- In the electrojet that flows by day along the magnetic dip equator, the fast electron drift generates plasma instabilities that cause equatorial sporadic E regions.
- In the auroral oval at high latitudes, sporadic E is produced by the precipitation of energetic electrons, which causes ionisation through collisions, particularly during auroral sub-storms.

2.2.1.5. F layer

The F layer is a major part of the terrestrial ionosphere and the most important from the point of view of radio communications and navigation systems. It exists at altitudes between 140 km and 600 km, and occasionally at altitudes extending to the upper limits of the ionosphere (Cander & Zolesi, 2013). During the day, the F region is separated into two different layers, named F1 and F2. The ionisation levels in these layers can be high and fluctuate considerably depending on the intensity of the ultraviolet radiation from the Sun, which also depends on the time of the day or the position of the Sun. The F1 layer will have decayed by midnight. Due to the F layer's ability to refract signals of up to 30 MHz and long skip distances provided by refraction from such high elevation, it supports long distance communication (Bertrand, 2002).

2.2.1.6. Spread F

Spread F happens when the F layer becomes diffuse because of irregularities that cause radio waves to scatter. The signal that is then received is the composition of several waves that are

reflected from different altitudes and positions in the ionosphere at slightly different times. Spread F usually happens at night and at low latitudes, while this phenomenon is less probable at mid-latitudes compared to low and high latitudes. When it does occur at mid-latitude it is more likely to occur in winter and at night, unlike at the magnetic poles where spread F is observed during both the day and night. Spread F is frequently associated with ionospheric storms and happens at all latitudes (Zolesi & Cander, 2014). Spread F reflects HF radiation at different heights within the F layer, causing the received HF signals to be scattered in time and space. This in turn makes accurate frequency determination and identification difficult. It is regarded to be due to large "bubbles" in the ionosphere and is usually associated with ionospheric storms that lower the Maximum Usable Frequency of the F layer.

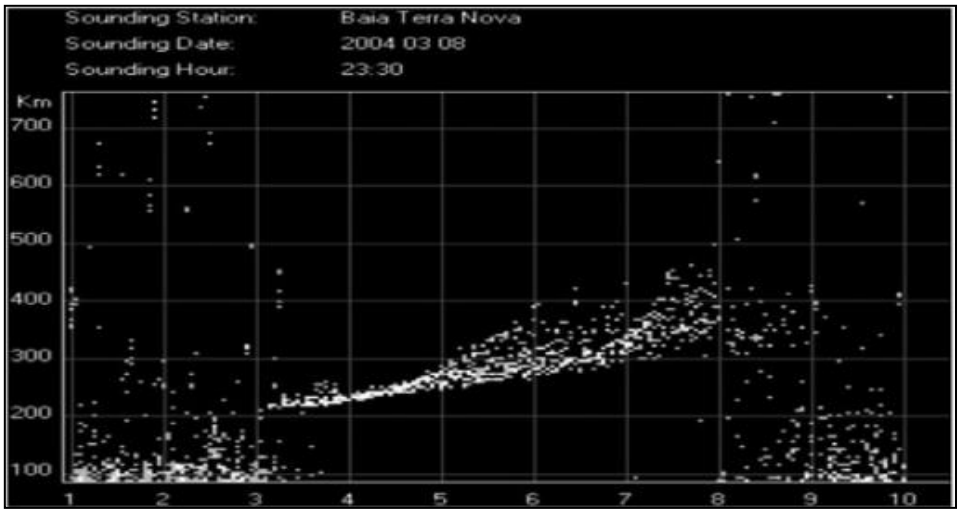

Figure 5: A spread F ionogram obtained from an ionosonde station (Baia Terra Nova) in Antarctica (Zolesi & Cander, 2014)

2.2.2. High latitude ionosphere

The Earth-bound ionosphere can be categorised into three regions that have different properties that depend on their geomagnetic latitudes. The three regions are:

- The mid-latitude region, which is well-studied and explored. Ultra-violet and X-ray emissions from the Sun are mostly responsible for the ionisation in this region. The ionisation is then removed by a chemical recombination process that involves neutral atmosphere as well as ionised species.
- The low-latitude region, which exists and extends up to 30° of both sides of the magnetic equator and is heavily influenced by electromagnetic forces that are caused by the geomagnetic field that flows horizontally over the equator. This results in a very large measure of electrical conductivity in this region.
- The high-latitude region is rather more complicated compared to the mid- and low-latitude regions due to the geomagnetic field direction that is almost vertical in this region, as well as ionising particle precipitation from space.

High-latitude challenges

The complexity of this region is caused by magnetic field lines that connect high latitudes to the outer part of the magnetosphere that is driven by solar wind. The ionosphere at mid-latitudes is connected to the inner magnetosphere that essentially rotates with the Earth and is, therefore, less susceptible to external influences. There are usual or common repercussions of operating at high latitudes, which are (Hunsucker & Hargreaves, 2003):

- The ionosphere in this area is dynamic due to the variation of solar wind, which controls the circulation pattern of the high latitude ionosphere.
- This area is a victim of sporadic events due to the fact that this region is more accessible to energetic particle emission of the Sun that may cause more ionisation. This might negatively affect polar radio propagation. During the day, the ionosphere is directly accessible to material from the solar wind over a limited range of latitudes.
- The auroral zones occur within the high-latitude region and they are not at all favourable for radio propagation due to the fact that they increase the amount of D-layer absorption due to ionising particle precipitation from space.

2.2.3. Atmosphere refraction and reflection

2.2.3.1. Total internal reflection

The magnetic field of the Earth causes the ionosphere to have a non-uniform refractive index. This causes the radio wave to split when it reaches the ionosphere (Terman, 1943) as presented in Figure 6.

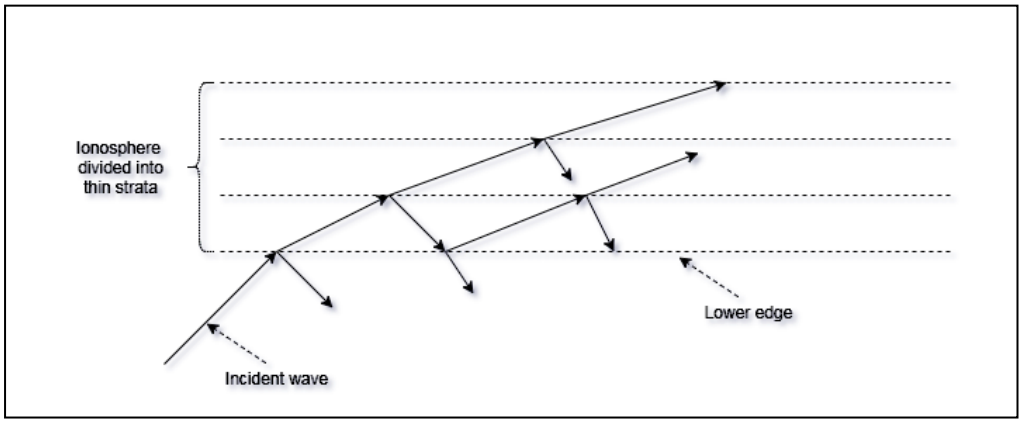

Figure 6: Waves split as they travel in different densities of the ionosphere

A refractive index is basically expressed and defined as the ratio of the velocities of an electromagnetic wave as it travels through different media relative to a vacuum; in this case the ionosphere and free space, respectively (Wilson & Ford, 2009). The most general form of a refractive index is a complex function. The real term of the complex function is known as the phase refractive index and is given by:

$$n = \frac{c}{v} \tag{4}$$

where:

c - Speed of light in a vacuum (3x10^8 m/s)

v - Speed of wave propagating in a certain medium in m/s

The Appleton-Hartree equation is the formula that defines the refractive index of an ionized medium in a magnetic field. The complex refractive index n that is appropriate for the E and F layers is given by:

$$n^2 = 1 - \frac{X}{1 - iZ - \frac{\frac{1}{2}Y^2\sin^2\theta}{1 - X - iZ} \pm \frac{1}{1 - X - iZ}\left(\frac{1}{4}Y^4\sin^4\theta + Y^2\cos^2\theta(1 - X - iZ)^2\right)^{1/2}} \tag{5}$$

where:

n - Complex refractive index

v - Electron collision frequency

$\omega = 2\pi f$ - Frequency

f - Wave frequency in Hz

$\omega_0 = 2\pi f_p$ - Electron plasma frequency

$\omega_H = \sqrt{\frac{n_e q^2}{m\,\varepsilon_0}}$ - Electron gyro frequency

B_0 - Ambient magnetic field strength

e - Electron charge

m - Electron mass

θ - Angle between the ambient magnetic field vector and the wave vector identified as $\boldsymbol{k}$

$i = \sqrt{-1}$

$X = \frac{\omega_p^2}{\omega^2}$

$Y = \frac{\omega_H}{\omega}$

$Z = \frac{v}{\omega}$

The Appleton-Hartree equation produces two separate solutions for the refractive index because of the $\pm$ sign in the equation. For $\theta = 90°$, i.e. the wave vector of the propagation plane is perpendicular to the magnetic field ($k \perp B_0$), the mode of propagation represented by the '+' sign is known as the ordinary mode, and the mode of propagation represented by the '-' sign is known as the extraordinary mode. For $\theta = 0°$, i.e. the wave vector of the propagation plane is parallel to the magnetic field ($k \parallel B_0$), the mode of propagation represented by the '+' sign is known as the left-hand circularly polarized mode, and the mode of propagation represented by the '-' sign is known as the right-hand circularly polarized mode. Wave polarization is further discussed later in this chapter (see Section 2.6.1).

To consider the propagation of a wave within a particular medium utilising a ray theory model, it is necessary to take account of the refractive index of the dielectric medium. A wave travels slower in a denser medium than in a less dense medium and the refractive index gives a measure of this effect. Refraction is known to occur when a ray is incident on the interface between two dielectrics that have different refractive indices, as illustrated in Figure 6 and Figure 7. The incidence angle θ_0 and the refraction angle θ_1 are related to each other and to the refractive indices of their dielectrics. This relationship is defined by Snell's law of refraction, which states that (Senior J. M., 2009):

$$n_0 \sin\theta_0 = n_1 \sin\theta_1 \qquad (6)$$

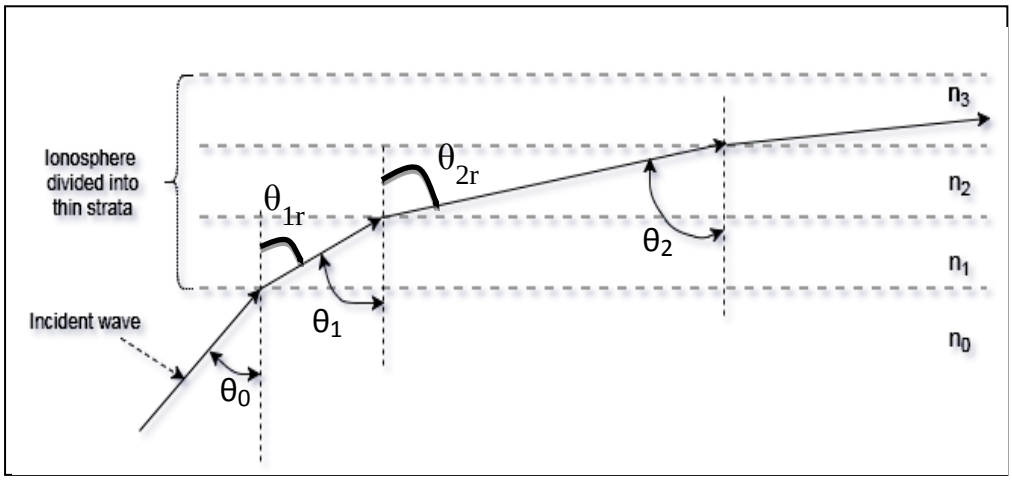

Figure 7: An illustration of a wave being refracted as it travels through layers of different refractive indices

It is important to note that $\theta_{1r} = \theta_1$ and $\theta_{2r} = \theta_2$.

If the ionosphere is subdivided into many thin layers, each with a different electron density, Snell's law of refraction may be applied as follows:

$$n_0 \sin\theta_0 = n_1 \sin\theta_1 = n_2 \sin\theta_2 = \cdots = n_k \sin\theta_k \qquad (7)$$

As seen in Figure 7, the refractive index decreases as the electron density rises with each layer and every layer introduces some measure of refraction to the wave. One of the conditions for a wave to return to earth is to have total internal reflection and that begins to happen when the refracted angle $\theta_r = 90°$ (Hum, 2007) at the k^{th} layer and may be expressed as:

$$n_0 \sin\theta_0 = n_k \sin 90° \quad (8)$$

n_0 is the refractive index of air, which is approximated to $n_0 = 1$. This equation can be further written as:

$$\sin^2\theta_i = n_k^2 = \varepsilon_{r,k} \quad (9)$$

where:

$\varepsilon_{r,k}$ – Dielectric of the *k*th layer and it is given by (Hum, 2007):

$$\varepsilon_{r,k} = \sin^2\theta_i = 1 - \frac{81\,N_{min}}{f_{ob}^2} \quad (10)$$

where:

N_{min} - Minimum electron density required to achieve total internal reflection
f_{ob} - Oblique incidence frequency
θ_i - Angle of incidence in the i^{th} layer

When the maximum electron density is present in the ionosphere, the only possible way for the radio wave to be totally internally reflected is if the dielectric of the k^{th} layer is zero ($\varepsilon_{r,k} = 0$). This necessitates the operational frequency to be less than the critical frequency. The critical frequency is the minimum frequency that will not be reflected back when transmitted vertically. It is given by (Hum, 2007):

$$\frac{81\,N_{max}}{f_c^2} = 1 \Rightarrow f_c = 9\sqrt{N_{max}} \quad (11)$$

The value of f_{ob} is called the maximum usable frequency (MUF) and is defined by the Secant Law. It is expressed as:

$$f_{ob} = f_c \sec\theta_i \quad (12)$$

2.2.3.2. Virtual height and actual height

The virtual reflection height (denoted by *h*' in Figure 8) is the height that the electromagnetic wave would reach if it travelled in a straight line through the ionosphere at the speed of light,

and instead of being gradually refracted back, it is reflected by a flat mirror-like surface. The incident angle and the reception angle are the basis on which the virtual height is estimated or calculated. It is also the measured distance from the returning high frequency pulses when pulse radar is in use (Terman, 1943). The actual reflection height (denoted by h_1 in Figure 8) is the height where the wave is actually returned from and is usually less than the virtual height because the refractive index of the ionosphere is greater than 1. Even though these heights are different, the time delay experienced by the wave is said to be the same if the wave travelled the virtual height rather than the actual height, because the actual wave velocity is less than the speed of light.

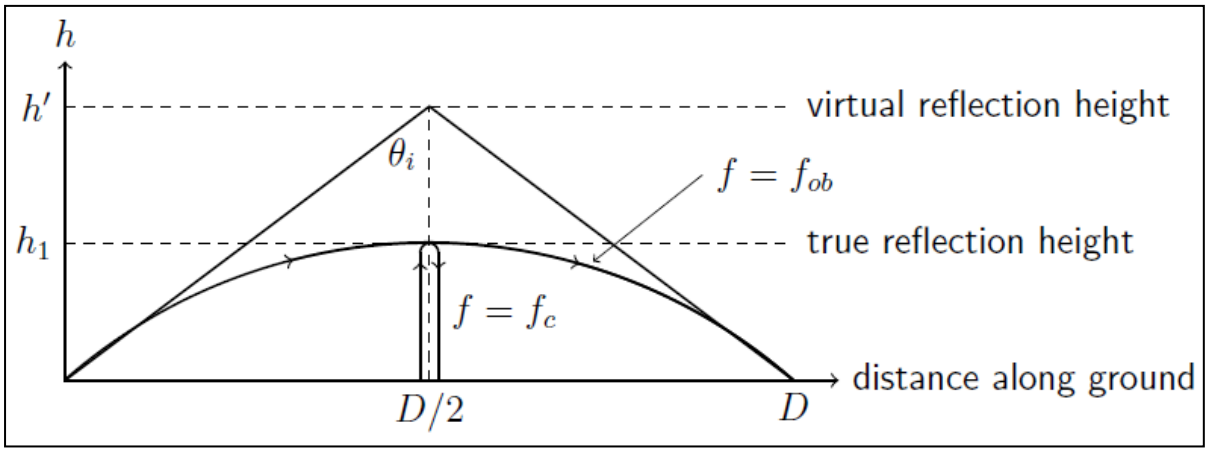

Figure 8: Virtual reflection height vs. true or actual reflection height of a radio wave

An ionosonde is used to determine the virtual height of the ionosphere. Table 1 below shows typical virtual heights of different layers of the ionosphere at different times of the day.

Table 1: Virtual heights of various regions of the ionosphere

Layer	Day-time virtual height	Night-time virtual height
F2	250 – 400 km	----
F1	200 – 250 km	----
F	----	300 km
E	110 km	110 km

2.2.4. Atmospheric Gravity Waves

Fluctuations of the neutral atmosphere, which are usually considered to be triggered by events that cause upward movements of the atmosphere in localized regions, are known as atmospheric gravity waves (AGWs) or auroras at high latitudes. These waves may be caused by severe weather systems and winds over mountains (Hickey, 2011). AGWs occur when the

boundary between any stable layer of different densities is disturbed. As the gravity and buoyancy forces attempt to restore equilibrium, there is an overshoot between the layers that results in oscillations that propagate as waves (Hocking, 2001). Most of these waves at high latitudes are caused by auroral heating sources. They propagate horizontally over long distances, influencing the ionosphere; thus, producing travelling ionospheric disturbances (TIDs) (Bristow & Greenwald, 1997). The terms *atmospheric gravity waves* and *travelling ionospheric disturbances* are sometimes used interchangeably in the literature. Some TIDs are said to originate at conjugate magnetic latitudes in the polar zones and travel meridionally towards the equatorial latitudes (Balthazor & Moffett, 1997).

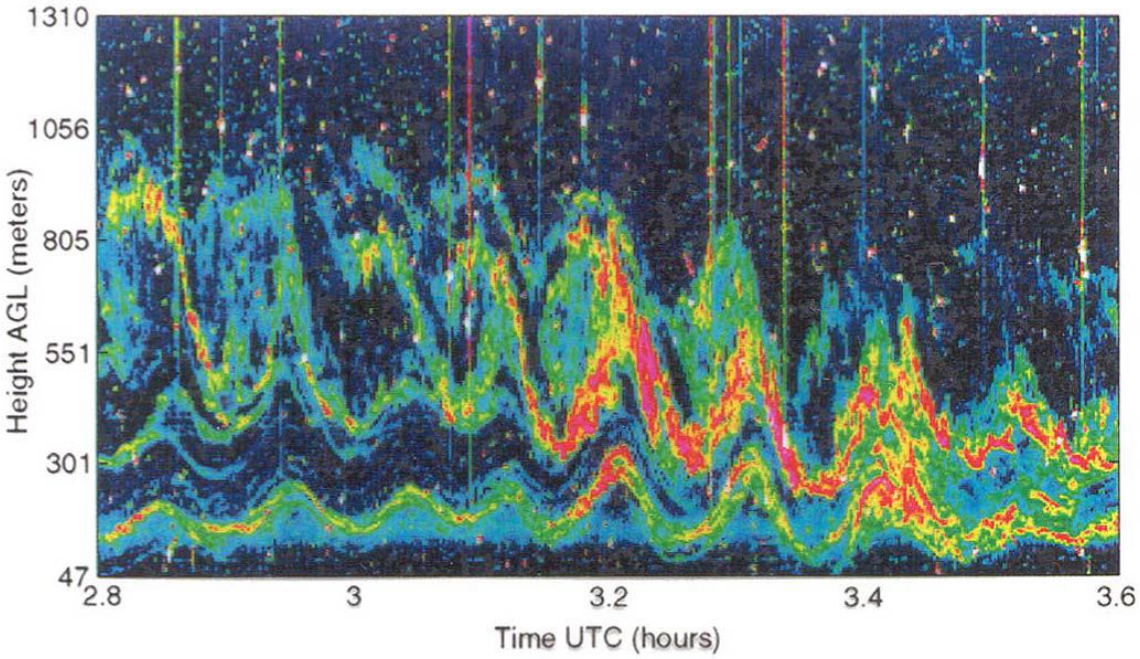

Figure 9: Travelling ionospheric disturbances as observed by a radar (adapted from Alpers & Huang, 2011)

TIDs have been mostly assigned to two categories according to their periods or wavelengths. The two categories of TIDs are described below:

- Large-scale traveling ionospheric disturbances (LSTIDs) are due to gravity waves produced in the auroral or sub-auroral regions when a geomagnetic storm or auroral sub-storm occurs. Such storms are caused by the intense precipitation of charged particles and/or the enhancement of the auroral electrojet. When these waves interact with the ionosphere, they cause LSTIDs that propagate towards the equator. As these LSTIDs propagate through the mid-latitudes, they experience changes in period, velocity, amplitude as well as energy dissipation, which are due to ionic drag, thermal conductivity and molecular viscosity (Ding et al., 2008). LSTIDs are said to travel horizontally at speeds of 400 m/s to 1000 m/s with wavelengths of more than 1000 km and have periods that range between 30 minutes to several hours (Senior, Kosch, Yeoman, Rietveld & McCrea, 2006).

- Medium-scale traveling ionospheric disturbances (MSTIDs) travel a little slower than LSTIDs, with speeds ranging from 50 m/s to 300 m/s. Their wavelengths have been recorded to reach up to 300 km and their periods are shorter with values of between 10 minutes and 60 minutes (Zolesi & Cander, 2014).

According to Harris et al. (2012), smaller and shorter scale disturbances that are temporal also exist in the ionosphere. These small-scale disturbances are said to have wavelengths shorter than 300 km and periods of less than 30 minutes.

2.3. THE HF TRANSMITTER

The function of a radio transmitter in a communication system is to modulate the audio-frequency signal to the required part of the frequency spectrum and to amplify the signal to the required transmitted power level (Green, 1978). Basic communication transmitters include continuous wave (CW), amplitude modulated (AM), frequency modulated (FM), and single sideband (SSB) types. As shown in Figure 10, a typical CW transmitter consists of an RF oscillator, buffer, Morse code controller (or another type of signal modulator) and a power amplifier.

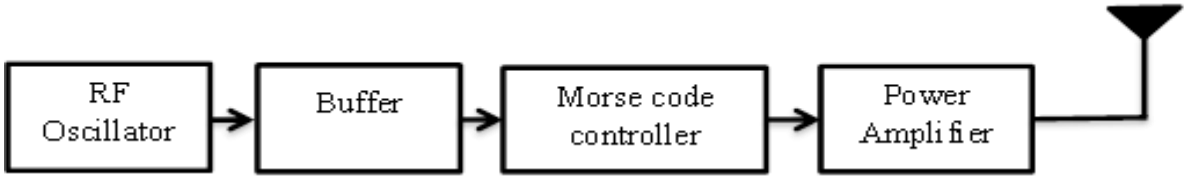

Figure 10: CW transmitter block diagram

2.3.1. RF oscillator

Every RF transmitter makes use of an oscillator (Patrick & Fardo, 2008). An oscillator converts electrical energy from direct current (DC) to alternating current (AC). In an RF transmitter, the carrier oscillator generates the RF carrier signal. The basic concept of an oscillator is illustrated in Figure 11. The shape of the output signal is dependent on the type of oscillator; it can either be sinusoidal or non-sinusoidal.

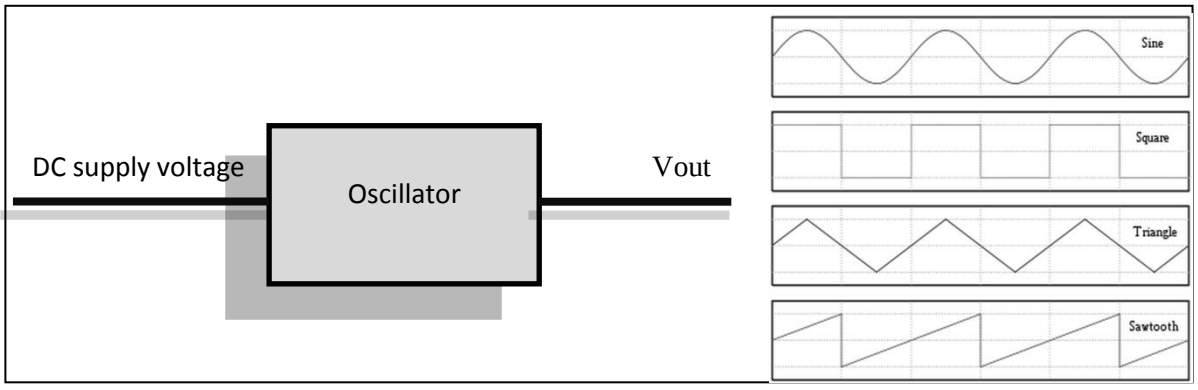

Figure 11: Basic operational diagram of an oscillator

2.3.2. Modulated Transmitters

In a telecommunication link, an electromagnetic signal that has a steady base frequency is generated at the transmitting side of the link. A carrier is a radio frequency signal and carries no information on its own and is given by:

$$v_c = V_c \sin \omega_c t \tag{13}$$

where:

V_c - Voltage amplitude of the signal

ω_c - Angular frequency of the signal

t - time interval

Modulation is a process of incorporating a useful information signal in the carrier signal so as to be transmitted. There are several types of modulation. The three most common types of modulation are (Freeman, 1999):

- Amplitude Modulation (AM) – The carrier amplitude varies in accordance with the amplitude of the baseband or information signal. The information signal is also called a modulating signal.
- Frequency Modulation (FM) - The carrier frequency varies in accordance with the amplitude of the baseband signal.
- Phase Modulation (PM) - The carrier phase varies in accordance with the amplitude of the baseband information signal.

Figure 12 illustrates these 3 common modulation schemes.

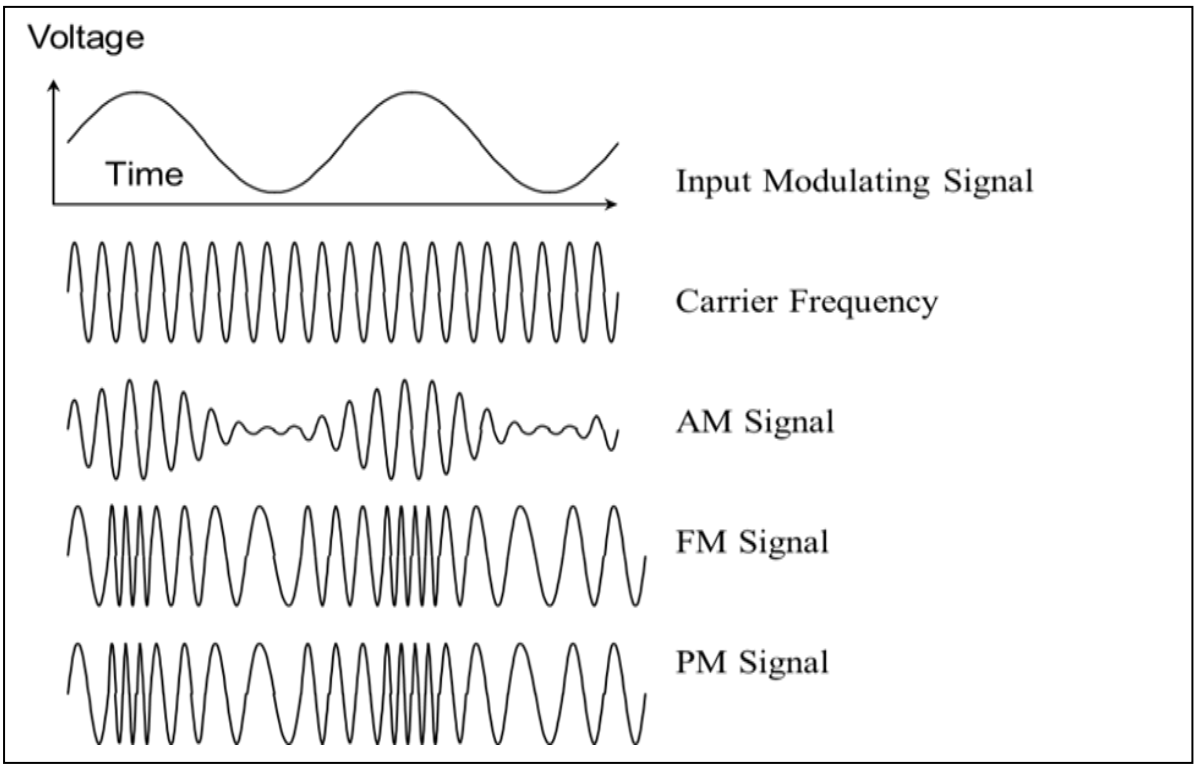

Figure 12: Illustration of the three most common modulation techniques (adapted from Faruque, 2017)

2.3.3. Buffer amplifier

The purpose of the buffer amplifier is to isolate the carrier oscillator and pre-amplify the signal. This stage is necessary to avoid the power amplifier drawing too much current from the oscillator, which will cause frequency instability; it also amplifies the oscillator signal to a suitable level to drive a power amplifier (Grebennikov, 2007).

2.3.4. Morse code controller

This section is responsible for encoding the messages that are transmitted. It may be as simple as a switch that is manually operated by a human or it could be an electronic device that is programmed to execute Morse code encoded information. Further information about the Morse code is discussed in Section 4.2.2.1.

2.3.5. Power amplifier

The power of the carrier signal is amplified in the power amplifier stage. RF power amplifiers must be able to meet broad and sometimes conflicting sets of requirements, which include but are not limited to linearity, power, reliability, gain, efficiency, thermal management, bandwidth and cost effectiveness (Walker, 2011), Cripps (2006). Amplifiers form the starting point for many electronic systems in a very wide range of applications. An output may vary from values in the range of milliwatts to kilowatts depending on the design and application the device is intended for. Efficiency is one of the most crucial parameters of RF power amplifiers. This is especially important in equipment and devices that are powered by a limited supply power. Efficiency is usually defined as a ratio of output power over input

power; however, this is an ambiguous definition as the term “input power” can have more than one meaning as it may or may not include the DC power. Efficiency can be defined according to the active device used. Collector efficiency is most appropriate when referring to bipolar junction transistor (BJTs) amplifiers; drain efficiency may be used when referring to MOSFET amplifiers. Figure 13 shows a typical configuration of a BJT based power amplifier.

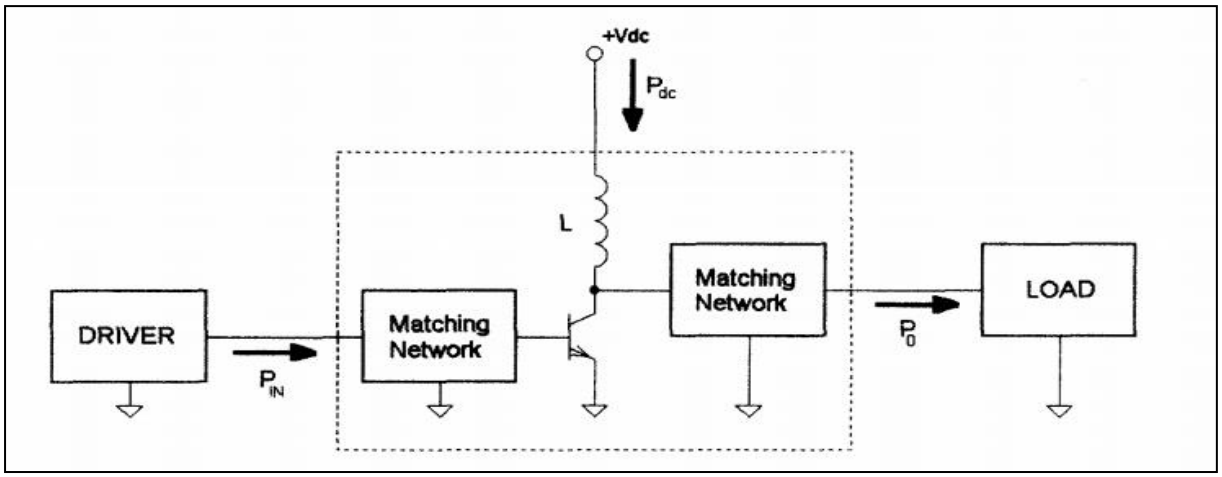

Figure 13: Basic configuration of a PA that uses a BJT (adapted from Floyd, 2000)

Collector efficiency of the above circuit is given by:

$$\eta = \frac{P_O}{P_{dc}} \tag{14}$$

where:

P_O – RF output power of the fundamental signal, sometimes including harmonics [W]

P_{dc} – Input dc supply power applied to the collector [W]

The input DC supply power is given by:

$$P_{dc} = V_{dc} I_{dc} \tag{15}$$

Power Added Efficiency (PAE) is a more accurate measure as it accounts for all powers and is specific. It is defined as the efficiency of the network in converting the input DC power into output RF power when the contribution of the RF input component is removed (Albulet, 1962). PAE is given by:

$$PAE = \frac{P_O - P_i}{P_{dc}} \tag{16}$$

There are several classes of power amplifiers. Only a few will be covered in this document. Power amplifiers mostly use transistors as the main amplifying device. These devices require a steady voltage or current to operate optimally. Biasing is the process of ensuring that the amplifier operates at the optimal DC operating point for the specific application. This point is known as the quiescent point (Q-point), or a bias point.

Class A amplifier

Power amplifiers are classified according to the conduction angle that is observed in the output signal with reference to the input signal. The conduction angle measures the segment of the input cycle that the output of the power amplifier reproduces. A Class A power amplifier has a transistor that is biased in a manner that allows operation in the linear region for the entire 360° of the input cycle. Class A amplifiers do not go into saturation, which means that the shape of the output signal is the same as the shape of the input. This class of amplifiers can be inverting or non-inverting amplifiers (Floyd, 2000).

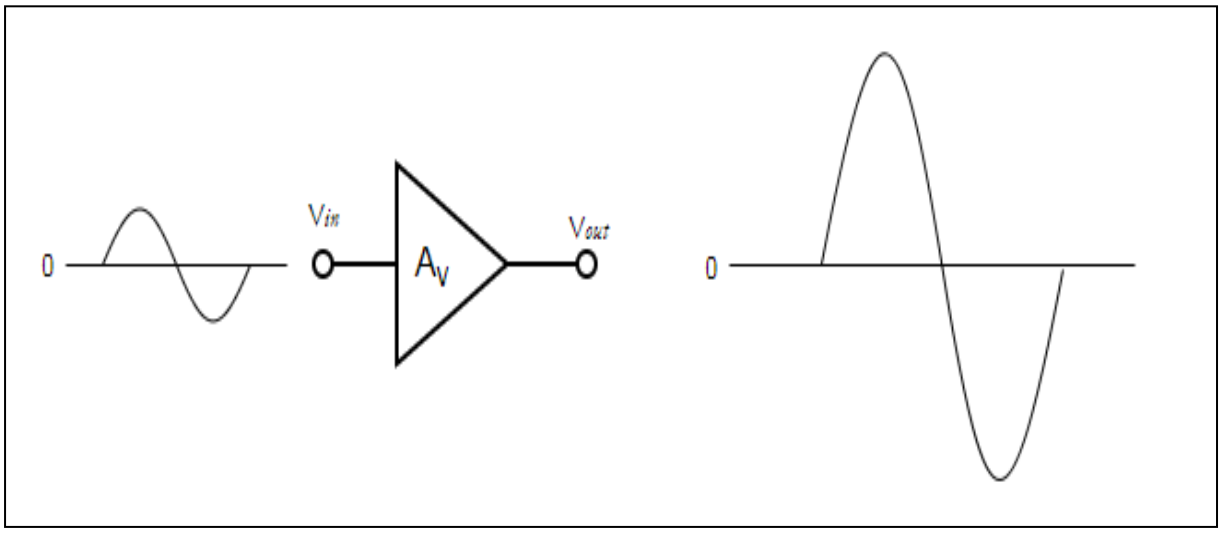

Figure 14: Class A output from a non-inverting amplifier is shown to be in phase with the input (Floyd, 2000)

The maximum possible efficiency a Class A amplifier can achieve is 25% and that is only achieved when a Q-point is well chosen. Class A applications are limited by the efficiency of the amplifier but its linearity gives it an advantage when it comes to audio applications where signal distortion cannot be tolerated.

Class B amplifier

A Class B amplifier is biased in the cut-off region of the active device in a manner that allows it to operate linearly in only half the cycle (180°) of the input signal and switches off during the other half. This operation is illustrated in Figure 14. Class B amplifiers can achieve an ideal efficiency of around 80%, although practically they only achieve about 50% efficiency (Floyd, 2000).

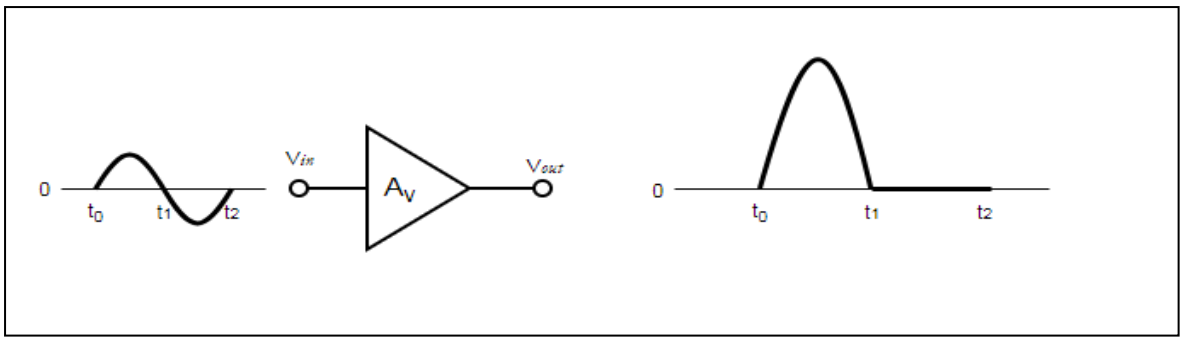

Figure 15: Class B amplifier output waveform relative to the input (Floyd, 2000)

Class C amplifier

Class C amplifiers are biased in a way that its conduction angle is less than 180°. A Class C amplifier produces an output that is considerably distorted. This makes Class C amplifiers unsuitable for audio applications; they are preferred for RF applications over Class A or B amplifiers. Theoretically, a Class C amplifier can achieve 100% efficiency but in reality it achieves approximately 70% efficiency (Floyd, 2000).

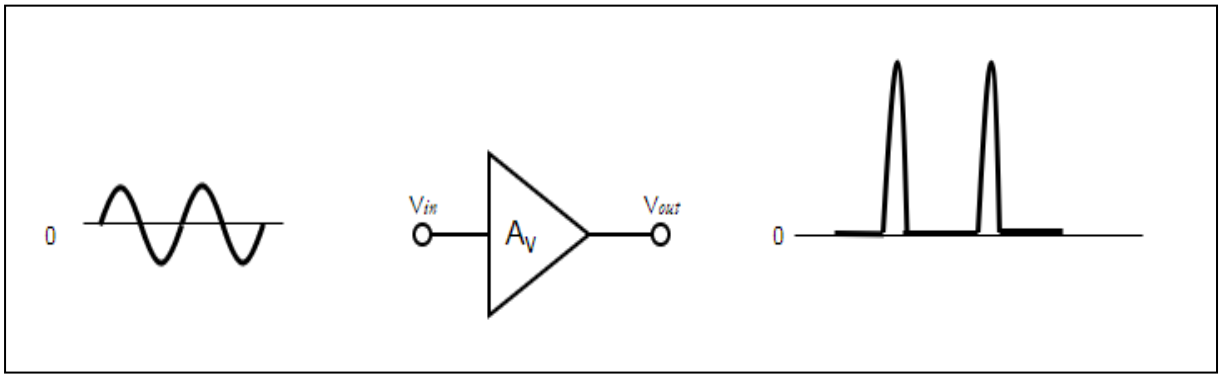

Figure 16: Non-inverting Class C amplifier output (adapted from Floyd, 2000)

2.4. RADARS

The term *radar* is an abbreviation for *Radio Detection and Ranging,* which is an electromagnetic system or device that is designed for detecting as well as locating objects. Radar transmits an RF pulse or an RF continuous wave, and sometimes a combination of the two, in order to detect the target parameters, such as velocity and distance of the target, by analysing the reflected signals from the object. Properties, such as conductivity, permittivity or permeability of the object are useful in object identification. HF radar has gained advantage over other types of radar due to the ability to also detect beyond the local horizon because of refraction.

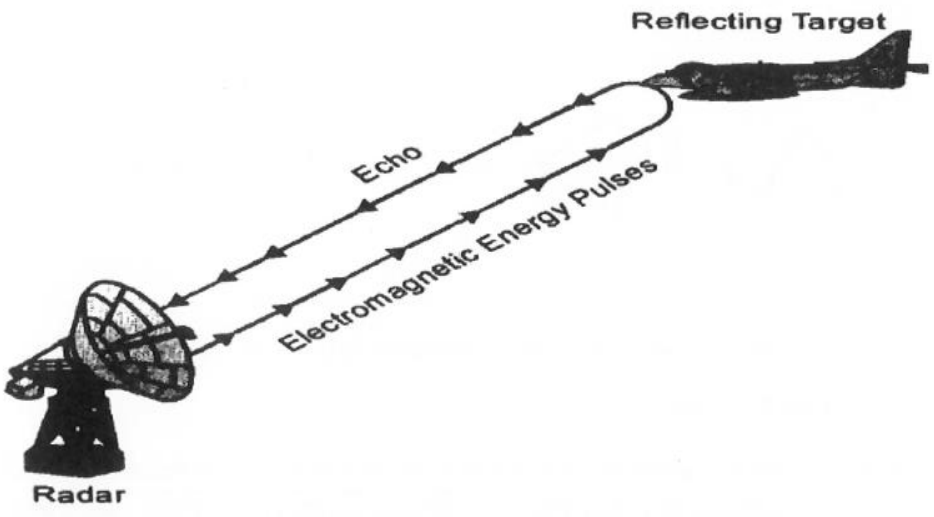

Figure 17: Pulse Radar detection and location (adapted from MMUST, 1999)

There are two types of radars that are commonly used:

- A pulse radar, which transmits a number of consecutive short RF energy pulses at predefined time intervals. The time delay of the echoes of the pulses that are scattered back to the radar by the target provides a measurement of the distance to the target.
- Continuous wave (CW) radar, which as the name says, continuously transmits an electromagnetic wave. CW radars are not ideal for range measurements as it lacks the obvious basis of time reference. CW radars are, therefore, useful for measurements of instantaneous rate-of-change in the range of the target. This is done by measuring the change in frequency of the returned electromagnetic wave that is caused by the motion of the target. This change of frequency due to motion is called the Doppler shift (Sisodia et al., 2011).

Pulse Doppler radar and moving target indication (MTI) radar are pulse radars that make use of Doppler shift for detecting moving targets (Singh et al., 2013).

2.4.1. Monostatic and bi-static radar

Monostatic radar is a radar that has its transmitter in the same physical location as its receiver. This type of radar makes it easy to use one local clock source for both the receiver and transmitter, which simplifies synchronization of the device as well as making the radar fully coherent (Kulpa, 2005). Monostatic radars furthermore generally make use of one antenna for both radiation and reception. This kind of radar configuration requires the use of a circulator or transmit/receive (T/R) switch or even a hybrid ring coupler to separate the transmitted and received signals (Issakov, 2010). This is not a compulsory feature as some

monostatic radar installations still use two different antennas; one to transmit and one to receive. Figure 18 illustrates the operation of a monostatic radar.

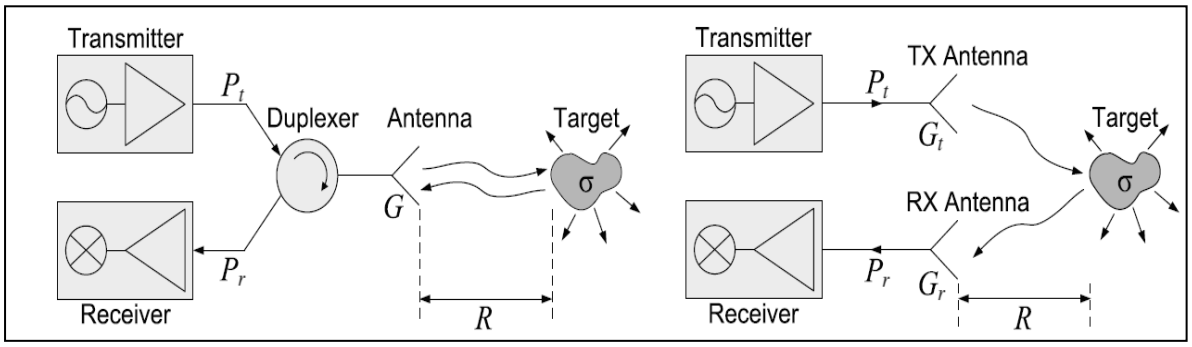

Figure 18: Operation of a monostatic radar

A bi-static radar is a radar that has the transmitter and receiver separated by a considerable distance. By this definition, it is apparent that a bi-static radar must utilise separate antennas, i.e. one to transmit and another one to receive. It is worth mentioning that there is a variation of a bi-static radar, called a multi-static radar, which makes use of multiple receivers and one transmitter in many separate locations. Bi-static radars have been to known to operate with dedicated transmitters that are designed specifically for bi-static operation. Such transmitters are named *transmitters of opportunity*. A bi-static radar is then called a hitchhiker when it utilises a transmitter of opportunity from a monostatic radar. It is called a passive radar, passive coherent radar, parasitic radar, or piggyback radar when the source of the signal is not even a radar signal (Willis & Griffiths, 2007). Figure 19 below shows the basic operation of a bi-static radar.

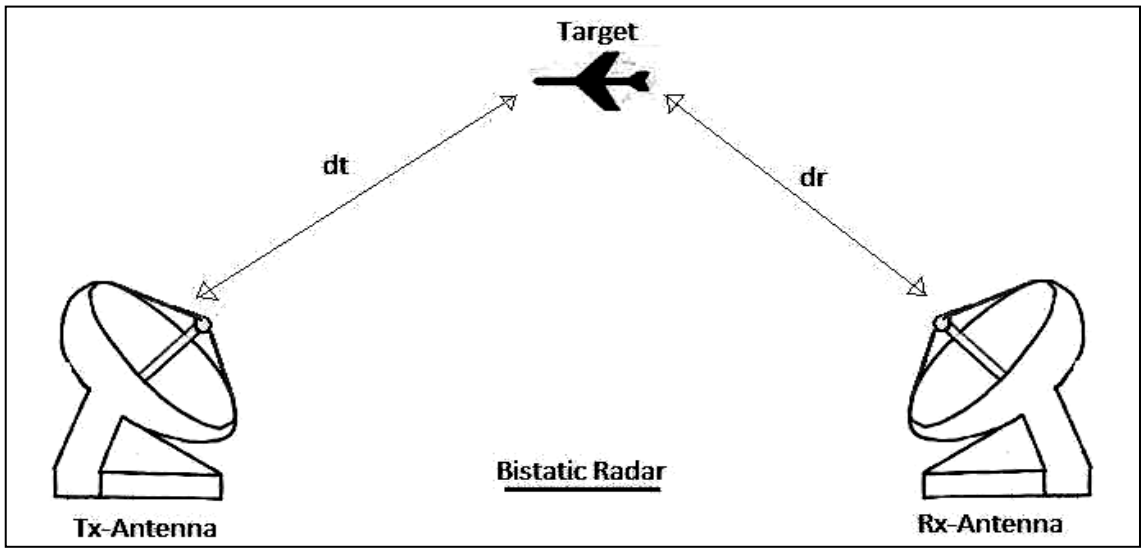

Figure 19: Operation of a bi-static radar

2.4.2. Monostatic radar Doppler effect

When there is relative motion between the source of the signal or transmitter and the observer of the signal or receiver along a line joining the two, there will be an apparent shift

in frequency experienced by the observer or receiver even though the signal emitted by the source is of constant frequency. This frequency shift is the basis of CW radars and it is known as the Doppler shift. If a monostatic radar transmits a signal at frequency f_0 and the target is moving towards the radar at the speed v_r, the returned signal will have a frequency $f_0 + f_d$, where f_d is the Doppler frequency shift that is expressed by:

$$f_d = \frac{2.v_r}{c}.f_0 \tag{17}$$

where:

f_d – Doppler frequency shift in Hz
f_0 – Operational frequency of the radar in Hz
v_r – Relative velocity of the target in m/s
c – Speed of light ($3x10^8$ m/s)

The target's relative velocity is a geometric term that is also expressed by:

$$v_r = v_a \cos\theta \tag{18}$$

where:

v_a – Actual velocity of the object
θ – Angle between the target trajectory and the line- of-sight (Figure 20)

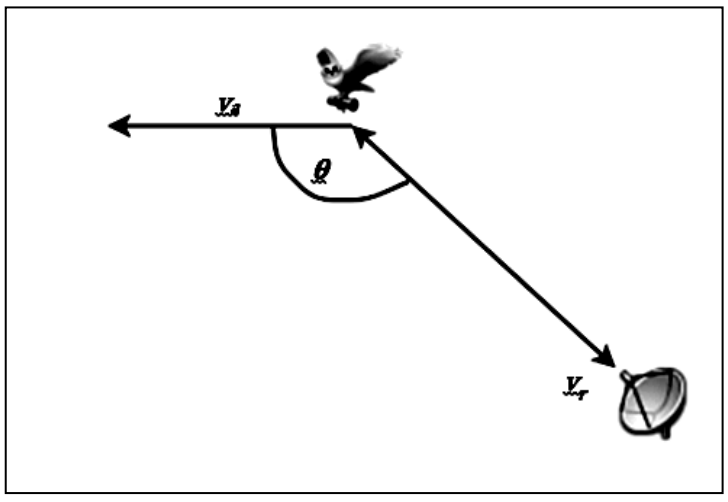

Figure 20: Velocity of a target moving at an angle that is not perpendicular to the radar wave

2.4.3. Bi-static radar Doppler effect

In bi-static radar operation, the positions of the transmitter (Tx), the receiver (Rx) and the target define a plane, called a bi-static plane, which changes with every position of the target as illustrated in Figure 21. The bi-static angle β is the angle that exists between vectors from the target towards the transmitter and receiver.

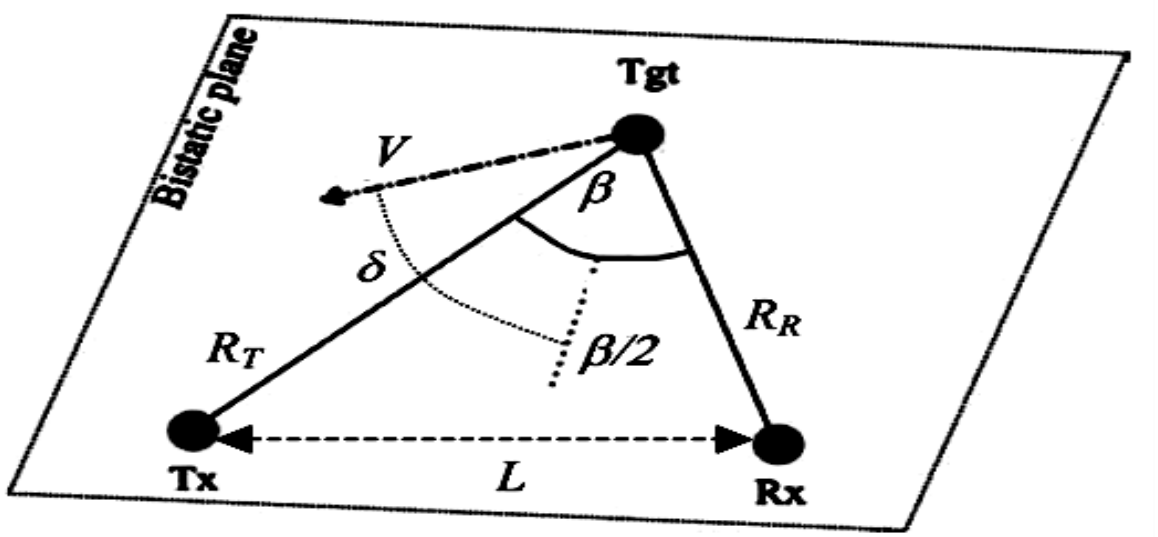

Figure 21: Bi-static geometry quantities in the bi-static plane (adapted from Johnsen and Olsen, 2006)

The bi-static Doppler shift $f_{d,b}$ is described by the contribution of range rates of both the distance vector from the transmitter to the target R_T and the distance vector from the target to the receiver R_R and is expressed as:

$$f_{d,b} = \frac{1}{\lambda}\left(\frac{dR_T}{dt} + \frac{dR_R}{dt}\right) \tag{19}$$

The range rates can be expressed in terms of the target velocity V and the above expression can be rewritten as:

$$f_{d,b} = 2\frac{V}{\lambda}\cos(\delta)\cos(\beta/2) \tag{20}$$

where:

λ – Operational wavelength in m

V – Target velocity in m/s

$(\beta/2)$ – Half of the bi-static angle, named the bi-static vector

δ – Angle between the bi-static vector and the vector resulting from the direction of the target

In the rare event that the target is at equidistance from both the transmitter and receiver (i.e. $R_M = R_T = R_R$), the bi-static Doppler shift is the same as the monostatic Doppler shift, which is given by:

$$f_{d,b} = f_{d,m} = 2\frac{v_m}{\lambda} = 2\frac{(dR_M/dt)}{\lambda} \tag{21}$$

The above discussed radar equations are applicable to radars whose transmitters and receivers are stationary (Johnsen & Olsen, 2006).

2.4.4. SuperDARN

These HF radars observe the backscatter that arises from plasma irregularities in the F layers of the ionosphere. The backscatter is then analysed to study the behaviour of the plasma in the auroral oval and the polar cap (Jenkins et al., 1998). Standard SuperDARN radars compute the autocorrelation function to estimate the backscatter power, Doppler velocity and the spectral width of the echoes.

Figure 22 below illustrates the operation of a typical HF SuperDARN radar.

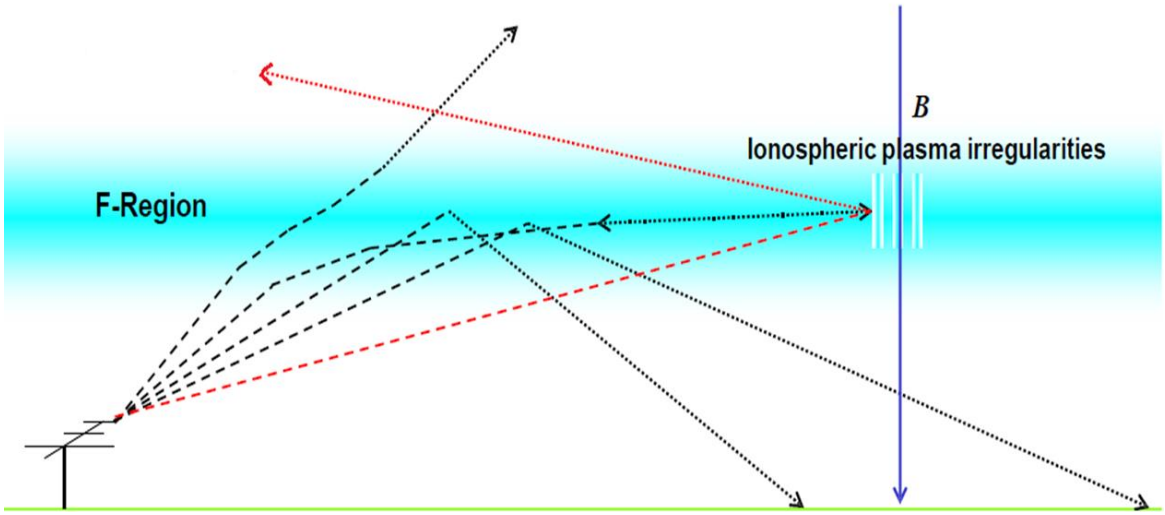

Figure 22: Operation of a SuperDARN radar (adapted from Baker, 2011)

The electromagnetic waves transmitted by the radar at an oblique angle are reflected by periodic structures that exist in the ionosphere. Only the backscatter wave is returned to the radar. Bragg scattering is the primary mechanism responsible for such reflections. Bragg diffraction takes place when an electromagnetic wave with a wavelength equivalent to double the spacings of the atomic structures is scattered and experiences constructive interference. This can be observed in Figure 23. When the spacing between structures is given by d, the distance travelled by the lower beam is $2\mathrm{d}\sin\theta$. The condition of θ that describes the strongest constructive interference is called Bragg's Law and is given by:

$$n\lambda = 2\mathrm{d}\sin\theta \qquad (22)$$

where:

n - Positive integer

d - Distance between ionospheric structures in m

θ - Scattering angle

λ - Wavelength of the incident wave in m

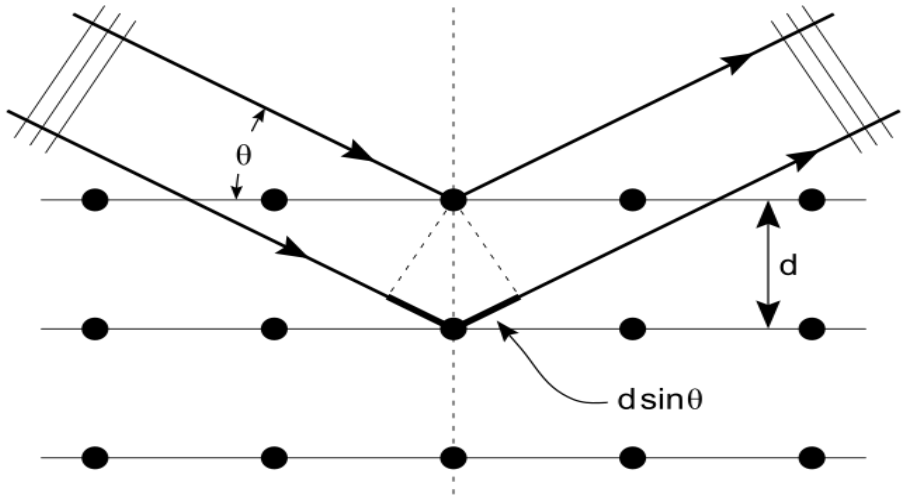

Figure 23: Bragg diffraction. Two beams with identical wavelengths and phases are scattered by periodic structures

For EM waves to transverse on the same path from the radar and back, its propagation path must be perpendicular to the plasma irregularities of the ionosphere, i.e. $\theta = 90°$. This results in the Bragg scatter condition being expressed as:

$$n\lambda = 2\mathrm{d} \tag{23}$$

When the radar is tuned to transmit and receive only one frequency, i.e. $n = 1$, the distance between the plasma structures is given by

$$\mathrm{d} = \frac{\lambda}{2} \tag{24}$$

Figure 24 below shows the determination of line-of-sight velocity. A signal is transmitted by the radar from the ground, and refracted back down by the F layer of the ionosphere. As it interacts with the ionosphere, it is scattered and the focus is on the portion of it that is returned to the radar along the same path. The velocity of the returning wave is considered to correspond to twice the component along the radar beam of the rate of change of the reflection height (Bristow & Greenwald, 1997).

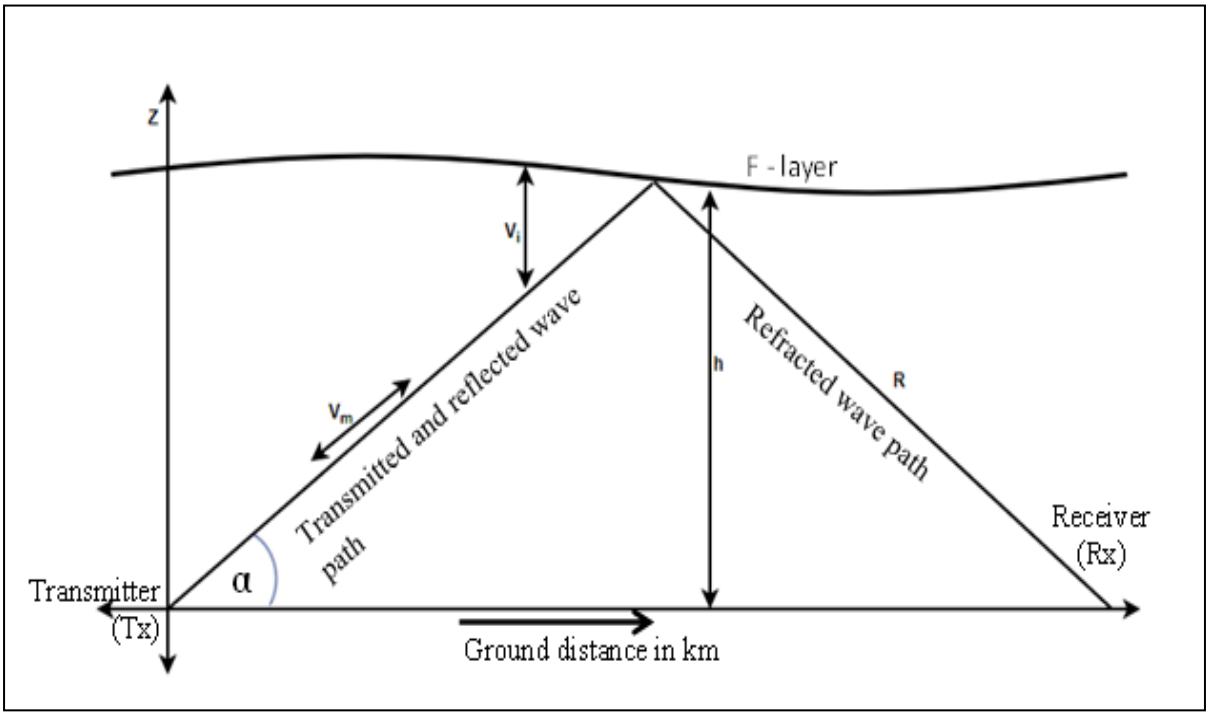

Figure 24: Parameters involved in determining the speed of the wave

The velocity of the AGW/TID is given by:

$$v_m = 2v_i \sin(\alpha) \tag{25}$$

with

$$v_i = \frac{\partial h}{\partial t} \tag{26}$$

where:

v_m – Measured line-of-sight velocity in m/s

h – Height of reflection in km

α – Take-off angle of the radar signal

SuperDARN radars make use of the Bragg-scatter power that is reflected from magnetic field aligned irregularities (FAI's) in the ionosphere across a vast field of view. Magnetic field lines in the high latitude regions of the Earth extend into the magnetosphere and that is where interaction with the solar wind takes place. The mobility of the plasma that is parallel to the magnetic field lines results in field lines being equipotential. SuperDARN radars observe the plasma motions in the outer magnetosphere as they are communicated along the field lines into the ionosphere.

2.4.5. An ionosonde

The ionospheric sounding system, or ionosonde, is an HF radar system probing the ionosphere in real-time. The primary purpose of the ionosonde is ionospheric research and HF channel management. An ionosonde uses basic radar techniques to detect the electron density of the ionospheric plasma as a function of height (Owens, 2004). The operation of a vertical ionosonde operation is shown in Figure 25.

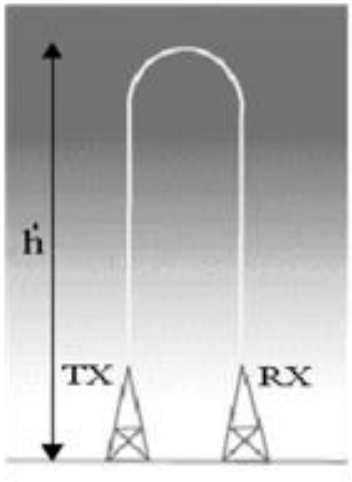

Figure 25: Vertical ionospheric sounder operation

The ionosonde investigates the ionosphere by transmitting short pulses of radio energy into the ionosphere at different frequencies. If the wave is reflected back, the receiver records the time it took for the signal to travel from the transmitter and back down to the receiver.

An ionogram, such as shown in Figure 26, is a record of all the information processed by the receiver. An ionogram is a basic data product of an ionospheric sounder. It is a two-dimensional image representing the power reflected from the ionosphere as a function of frequency and height. The ionogram can be useful to deduce many parameters of the ionosphere, such as critical frequency and the height of the F layer peak, which are considered to be the most important parameters. Ionogram reduction is the process of translating an ionogram to specific parameters, which is mostly done by computers.

It may be observed from Figure 26 that frequencies below the critical frequency are reflected back to ground by the ionosphere, while frequencies above the critical frequency pass through the ionosphere.

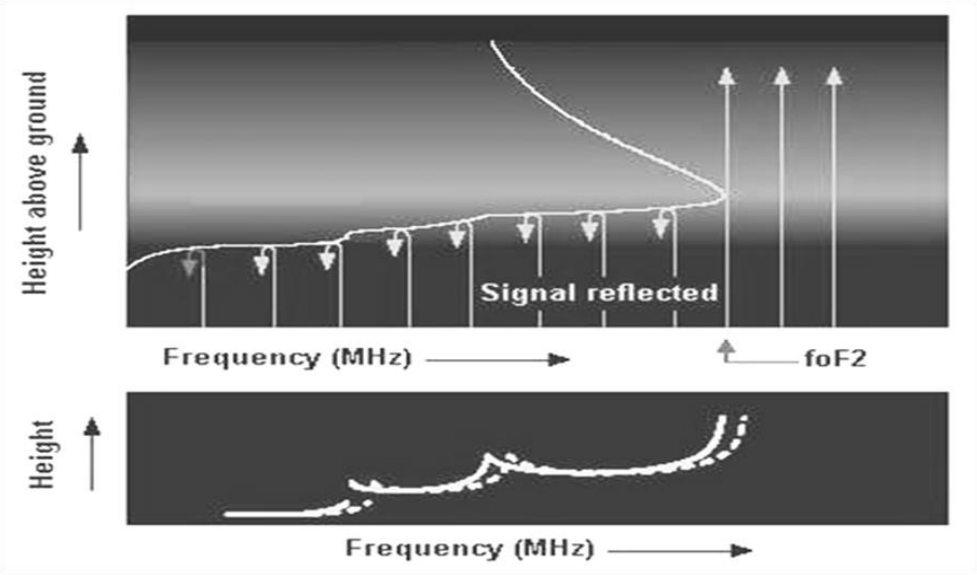

Figure 26: Ionosphere probing with an ionosonde

2.5. LINK BUDGET

A link budget is the process of accounting for all the various gains and losses between a transmitter and receiver to ensure a successful communication link under operable conditions (Graham, 2011). There are several ways to perform a link budget because of various applications, but there are common practices, such as including factors like fade margin, to accommodate for various equipment thresholds and miscellaneous losses. One of the most common of these additions is fade margin (Ellingson, 2016).

2.5.1. Link equation

A successful end-to-end transmission requires consideration of all the power, gain and loss mechanisms between the transmitter and receiver. Figure 27 presents these terms of the link equation.

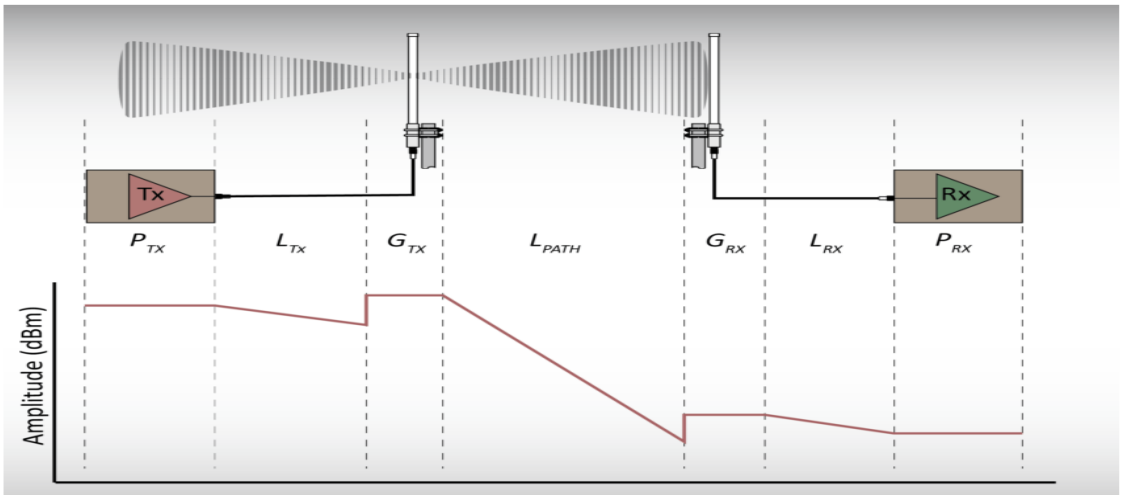

Figure 27: Radio link illustration (Scientific, 2016)

For a line-of-sight radio link or sky wave radio link, the link budget is given by the following formula:

$$P_{RX} = P_{TX} + G_{TX} - L_{TX} - L_{PATH} - L_M + G_{RX} - L_{RX} \quad (27)$$

where:

P_{RX} – Received power in dBm

P_{TX} – Transmitter output power in dBm

G_{TX} – Transmitter antenna gain in dBi

L_{TX} – Transmitter cable and connector losses in dB

L_{PATH} – Path loss or free space propagation loss in dB

L_M – Miscellaneous losses, including fade margin, polarisation and pointing losses in dB

G_{RX} – Receiver antenna gain in dBi

L_{RX} – Receiver cable and connector losses in dB

2.5.2. Losses

As the signal is radiated into free space between the radio transmitter and a radio receiver, it fades. Below is a list of the most significant losses suffered by an HF signal or a sky wave:

- Free Space Propagation Loss (FSPL)
- D region/layer absorption
- Miscellaneous losses (cable losses, antenna polarization losses, etc.)

2.5.2.1. Cable losses

The most used RF cable type in radio communication is the coaxial cable. This type of cable consists of a center metallic conductor that is surrounded by an insulating material, which is further surrounded by a tube-like metallic conductor. It is called coaxial because of the fact that both the wire in the center and the tube surrounding it share the same center axis. There are several coaxial cable names and standards, such as the RG-standard and the more recent LMR standard (Jackman, Swartz, Burton, & Head, 2011).

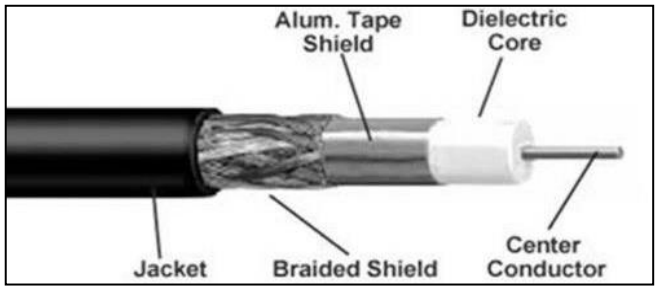

Figure 28: A typical structure of a coaxial cable

Cable loss is a function of frequency and length and is provided in the cable specifications by the vendor. Generally, cable losses increase as the frequency of operation increases, as shown in Figure 29.

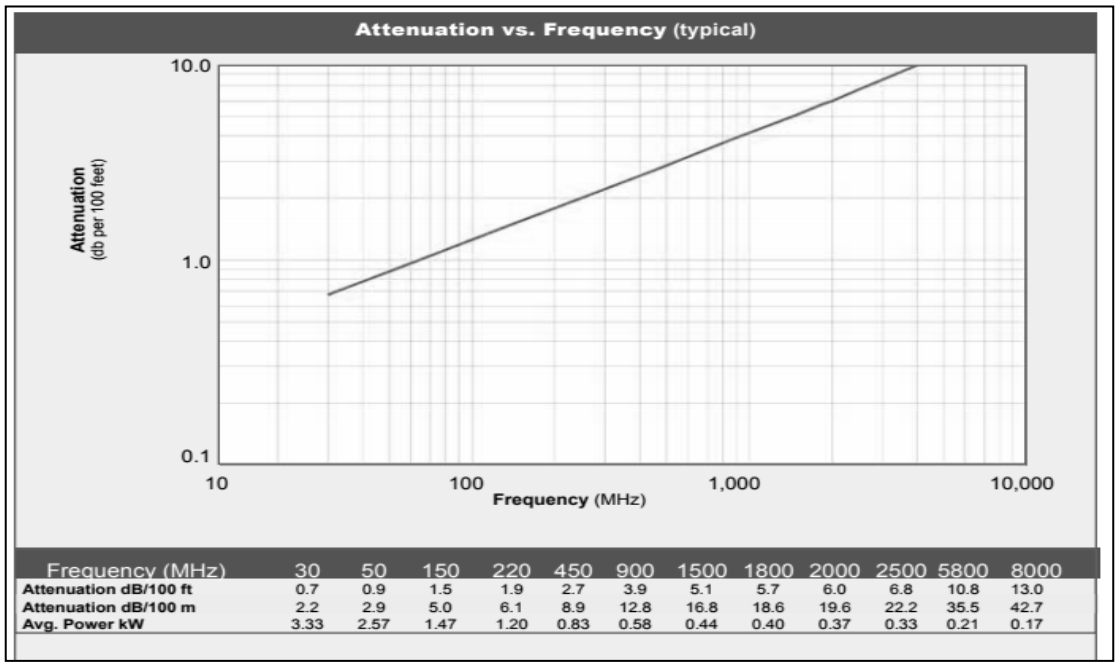

Frequency (MHz)	30	50	150	220	450	900	1500	1800	2000	2500	5800	8000
Attenuation dB/100 ft	0.7	0.9	1.5	1.9	2.7	3.9	5.1	5.7	6.0	6.8	10.8	13.0
Attenuation dB/100 m	2.2	2.9	5.0	6.1	8.9	12.8	16.8	18.6	19.6	22.2	35.5	42.7
Avg. Power kW	3.33	2.57	1.47	1.20	0.83	0.58	0.44	0.40	0.37	0.33	0.21	0.17

Figure 29: Attenuation as a function of frequency for an LMR-400 coaxial cable

2.5.2.2. Free space losses

The loss or gain characteristics of the equipment and antennas can be obtained from the manufacturer's data sheets, but the effective loss that exists in the space between the two antennas needs to be formulated in a manner that allows characterisation of the transmission path. The ratio between the power that is radiated by the transmitting antenna and the power measured at the receiving end is called *path loss* and is normally expressed in dB. Free space path loss is the minimum loss that occurs along any given path that exists between two isotropic antennas when there are no reflections, ground losses or any obstruction intervening. Free space loss is expressed by the Friis equation (Whitaker, 1996).

Figure 30: Transmit and receive antennas separated by distance *D*

To understand the Friis formula, an isotropic antenna that transmits power P_T is assumed as the transmitting antenna. The power density p that should be measured at a distance D is given by:

$$p = \frac{P_T}{4\pi D^2} \ (W/m^2) \tag{28}$$

If the antenna is considered to be a directional antenna, which means it has a gain G_T in the direction of the receiving antenna, the power density formula is now given by:

$$p = \frac{P_T . G_T}{4\pi D^2} \ (W/m^2) \tag{29}$$

When the antenna on the receiving end is considered, one of the most important parameters to consider is the effective aperture, which is defined as a measure of the antenna's effectiveness at receiving the power of radio waves. If the receiving antenna has an effective aperture A_{eff}, P_R is the power received by the antenna and is given by:

$$P_R = \frac{P_T . G_T . A_{eff}}{4\pi D^2} \ (W) \tag{30}$$

The effective aperture of a receiving antenna is given by:

$$A_{eff} = \frac{\lambda^2}{4\pi} G_r (m^2) \tag{31}$$

where G_r is the gain of the receiving antenna.

The received power may now be expressed as:

$$P_R = \frac{P_T . G_T . G_R . \lambda^2}{(4\pi D)^2} \quad (32)$$

The above equation is known as the Friis Transmission Formula (Bevelacqua, 2015). As per the explanation of the free space propagation loss, the ratio between the transmitted and received power from directional antennas is:

$$\frac{P_T}{P_R} = G_T . G_R . \left(\frac{4\pi D}{\lambda}\right)^2 \quad (33)$$

Since omnidirectional antennas have no gain, the above formula can be rewritten for omnidirectional or isotropic antennas to specifically express free space propagation loss ($FSPL$), and is given by:

$$FSPL = 10 \log \left(\frac{4\pi D}{\lambda}\right)^2 (dB) \quad (34)$$

$$FSPL = 20 \log \left(\frac{4\pi D f}{v}\right) (dB) \quad (35)$$

$$FSPL = 20 \log \left(\frac{4\pi}{v}\right) + 20 \log f + 20 \log D \ (dB) \quad (36)$$

where:

v – Speed of light (3×10^8 m.s^{-1})

f – Operating frequency in Hz

D – Distance from transmitter to receiver in m

For frequencies in MHz and distance in km the above formula can be rewritten as:

$$FSPL = 20 \log \left(\frac{4\pi . 10^6 . 10^3}{3 . 10^8}\right) + 20 \log f_{MHz} + 20 \log D_{km} \ (dB) \quad (37)$$

$$FSPL = 32.44 + 20 \log f_{MHz} + 20 \log D_{km} \ (dB) \quad (38)$$

2.5.2.3. D layer absorption

Table 2 tabulates the simulated absorption experienced by HF wave propagating through the D layer. These values are calculated for the propagation path between SANAE, which is located approximately at 72°S 3°W, and the South Pole on 21 December 2016 at 12:00 UT. This period is in the middle of summer in Antarctica and is also the period where propagation should be more successful than during equinox and winter. Since the wave travels at a slant angle, the wave encounters the D layer twice in two different geographical areas of the ionosphere. For the simulations reported in Table 2, the

following models were used: Virtual Ionosphere, Thermosphere, Mesosphere Observatory (VITMO), Mass-Spectrometer-Incoherent-Scatter (MSIS), and the International Reference Ionosphere (IRI).

Table 2: Simulated absorption for HF propagation through the D layer (extract)

Height(km)	*Ven (Hz)*	*Absorption (dB)*	*Ven (Hz)*	*Absorption (dB)*
65	2.71E+07	0.0226016	2.56E+07	0.0233538
66	2.37E+07	0.0250702	2.23E+07	0.0258914
67	2.07E+07	0.0271169	1.94E+07	0.0279555
68	1.80E+07	0.0286265	1.68E+07	0.0294805
69	1.56E+07	0.0295721	1.46E+07	0.0304092
70	1.35E+07	0.0299289	1.26E+07	0.0307222
71	1.17E+07	0.0297377	1.08E+07	0.0304459
72	1.00E+07	0.0290225	9.31E+06	0.0296607
73	8.61E+06	0.0278825	7.97E+06	0.028438
74	7.37E+06	0.0263957	6.82E+06	0.0268905
75	6.28E+06	0.0246185	5.81E+06	0.0250743
76	5.33E+06	0.0226355	4.92E+06	0.0230235
77	4.49E+06	0.0205045	4.15E+06	0.0208554
78	3.75E+06	0.0183148	3.47E+06	0.0186335
79	3.11E+06	0.016134	2.89E+06	0.0164185
80	2.56E+06	0.0140317	2.38E+06	0.01429
81	2.09E+06	0.0120605	1.95E+06	0.0122977
82	1.69E+06	0.0103419	1.58E+06	0.010551
83	1.36E+06	0.00921375	1.27E+06	0.00942157
84	1.09E+06	0.00897553	1.02E+06	0.00919811
85	860950	0.01004	808407	0.0103262
86	679368	0.01327	639716	0.0136998
87	533751	0.0174329	503679	0.0180181
88	418248	0.0217957	396227	0.0225442
89	327589	0.0260521	311274	0.0268956
90	256741	0.0298768	244539	0.0307194
91	201639	0.0329998	192790	0.0338041
92	159170	0.0352952	152673	0.0359636
93	126442	0.0366836	121567	0.0371277
94	101209	0.0371841	97615.8	0.0373989
95	81744.1	0.036897	79060.9	0.0368564
96	66689.6	0.0359568	64658.5	0.035663
97	54950.6	0.0344877	53385.4	0.0339589
98	45764.6	0.0326532	44585.4	0.031958
99	38524.6	0.0305846	37599.9	0.0297403
100	32769.5	0.0283924	32045	0.0274532
Total loss		0.89238718		0.90513868

2.5.3. Link budget calculated values

All receivers have a minimum acceptable average signal power that must be received in order to ensure proper demodulation and decoding of the transmitted signal for an acceptable level of performance. This threshold power is known as the receiver sensitivity. The SuperDARN radar at SANAE has a 50 $\boldsymbol{\Omega}$ system impedance and a threshold voltage of 100nV, or -127 dBm.

2.5.3.1. Link margin

The link margin, also referred to as fade margin, is an expression of how much margin in dB there is between the received signal strength level and the receiver sensitivity of the radio. It is a design allowance that provides for sufficient system gain or sensitivity to accommodate expected fading for the purpose of ensuring that the required quality of service is maintained. The recommended value in HF communications is any value between 20 and 40 dB (Malindi, 2013). The minimum received power is then expressed as:

$$\begin{aligned} P_r &= Rx\ senstivity + Fade\ Margin \\ &= -127dBm + 40dB \\ &= -87dBm \end{aligned} \tag{39}$$

2.5.3.2. Free space losses

The free space propagation loss is used to predict the strength of a RF signal at a particular distance. This is a theoretical value, as in the real world there are many obstacles, reflections and losses that need to be accounted for when estimating the signal strength at a location. However, the FSPL is a good approximation for estimating the loss is signal strength when propagating through free space. It is given by:

$$FSPL = 32.45 + 20\ \log d_{km} + 20\ \log f_{MHz} \tag{40}$$

The FSPL for a 12.57 MHz signal over a distance of approximately 2000 km between the South Pole and SANAE IV is calculated as:

$$\begin{aligned} &= 32.45 + 20\log 2000 + 20\log 12.57 \\ &= 32.45 + 66.3\ + 22 \\ &= 120.75dB \end{aligned}$$

2.5.3.3. Miscellaneous losses

These are losses, such as cable losses, connector losses, etc. The recommended value for these losses is L_M = 7.3 dB.

The total loss of the link is therefore given by:

$$L_{TL} = FSPL + L_D + L_M \tag{41}$$
$$= 120.75dB + 2dB + 7.3dB$$
$$= 130.05\ dB$$

At this point it is essential to determine the minimum power required from the transmitter to ensure communication between the transmitter and the receiver.

At SANAE IV an antennae array with the following specifications is installed:

- Frequency: 8 MHz – 20 MHz (12.57 MHz nominal)
- Antenna Gain: approximately 20 dB (frequency dependant)
- Horizontal beam width: 4°
- Vertical beam width: 52°

At the South Pole, it is proposed to make use of a Yagi antenna that operates at 12.5 MHz and has a gain of 10 dB.

The required transmitted power is, therefore, given by:

$$P_r = P_t + G_t + G_r - L_{TL} \tag{42}$$
$$P_t = P_r - G_t - G_r + L_{TL}$$
$$= -87dBm - 20dB - 10dB + 130dB$$
$$= 13dBm$$
$$= 20mW$$

2.6. ANTENNA DESIGNS

An antenna is any conductive device that is used for radiation or reception of radio waves. It is regarded as a means to transition between free space and the device or system used for radiating or receiving electromagnetic waves (Bakshi et al., 2008). Antennas are reciprocal and can be used for both transmitting and receiving (Malindi, 2013).

Depending on the application, several parameters of an antenna are relevant:

- polarization;
- antenna types and radiation pattern;
- directivity; and
- power gain.

2.6.1. Polarization

A radio wave, also known as an electromagnetic wave, consists of an electric field and a magnetic field; they are at 90° to each other as well as 90° to the direction of propagation in the case of transverse electromagnetic (TEM) waves. The magnetic field is referred to as the H-field, while the electric field is referred to as the E-field. The E-field is used as the reference vector to determine the polarisation of an electromagnetic wave. Polarisation of the wave can be vertical, horizontal, an intermediate angle or circular (left hand or right hand circular) (Silver, 2008). Figure 31 illustrates a TEM wave and its properties.

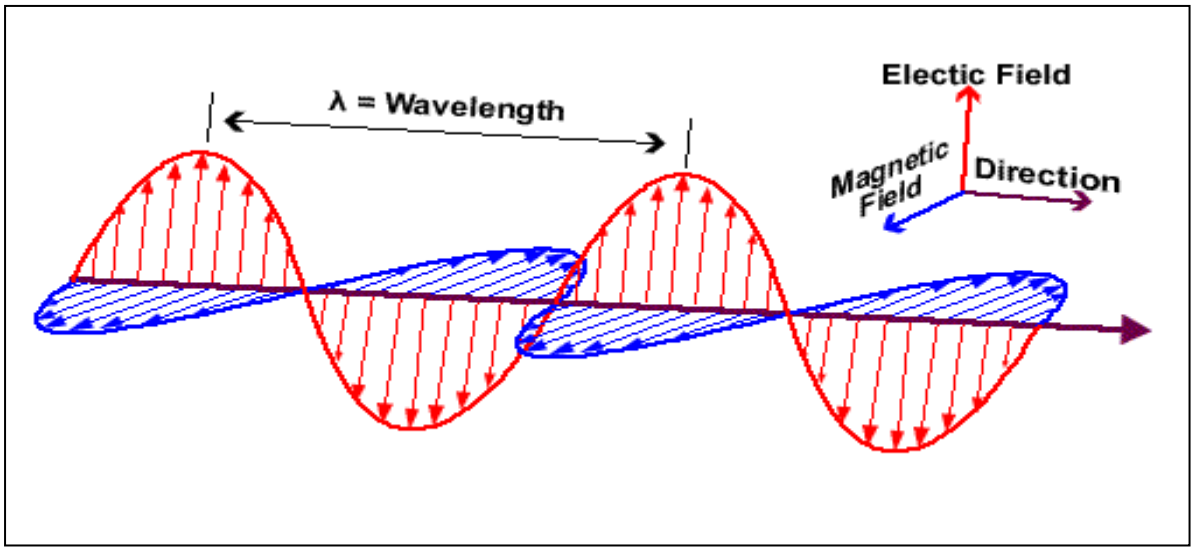

Figure 31: TEM wave and its properties (adapted from Tang, 2015)

Polarization of an antenna is defined by the polarization of the electromagnetic wave being radiated by the antenna. For maximum reception, both the transmitting antenna and the receiving antenna should have the same polarization. Polarization mismatch loss is given by:

$$L_{mismatch} = 20\log(\cos\varphi)\, dB \qquad (43)$$

where φ is the misalignment angle between the two antennas.

2.6.2. Antenna types and radiation pattern

The radiation from the antenna in any direction is measured in terms of field strength at a certain spatial point at a particular distance from the antenna. This is an important characteristic of an antenna because it indicates the distribution of energy radiated by an antenna.

A radiation pattern is a 3-dimensional representation of the variation of actual field strength of the electromagnetic field at every point that is equidistant from the antenna. There are two basic types of radiation patterns; the field strength pattern, which is expressed in terms of field strength E, and the power pattern or power radiation pattern, which is expressed in terms of power per unit solid angle (Bakshi et al., 2008).

A 3-dimensional pattern to represent all radiation angles θ, which represents all the angles in the x-z plane as illustrated in Figure 32 (a), and ϕ, which represents all the angles in the x-y plane as illustrated in Figure 32(b), cannot be presented in a plane. Polar plots of the relative magnitude of the field in any desired plane are plotted instead. The polar plots are plotted in two planes, named principle planes, and the resulting plots or patterns are called principle plane patterns. The E-plane pattern or vertical pattern contains the antenna and is obtained by plotting the magnitude of the normalised field strength against θ with constant ϕ. The H-plane pattern, or horizontal pattern, is normal to the antenna and is obtained by plotting the normalized field strength against ϕ for $\theta = \frac{\pi}{2}$.

The principle plane patterns of a dipole antenna are illustrated in Figure 32.

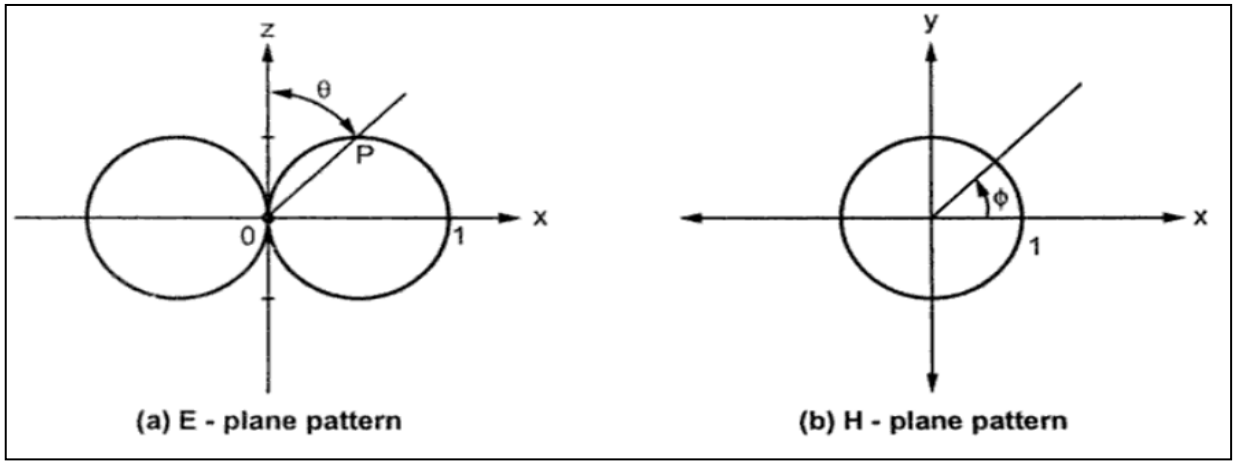

Figure 32: (a) Vertical radiation pattern and (b) horizontal radiation pattern for a hertzian dipole (adapted from Bakshi et al., 2008)

2.6.2.1. Isotropic antenna

An isotropic antenna is a lossless, ideal antenna that radiates uniformly in all directions in 3-dimensional space. In practice, an isotropic antenna does not exist. It is an antenna that is used as a reference antenna.

Figure 33 illustrates the radiation pattern of an isotropic radiator.

If the antenna radiates the power P_{rad} equally in all directions of the sphere with surface area given by:

$$Surface\ Area = 4\pi r^2 \tag{44}$$

where *r* is the radius of the sphere, the average power density on the spherical surface is given by:

$$P_{avg} = \frac{P_{rad}}{4\pi r^2}\ \ (W) \tag{45}$$

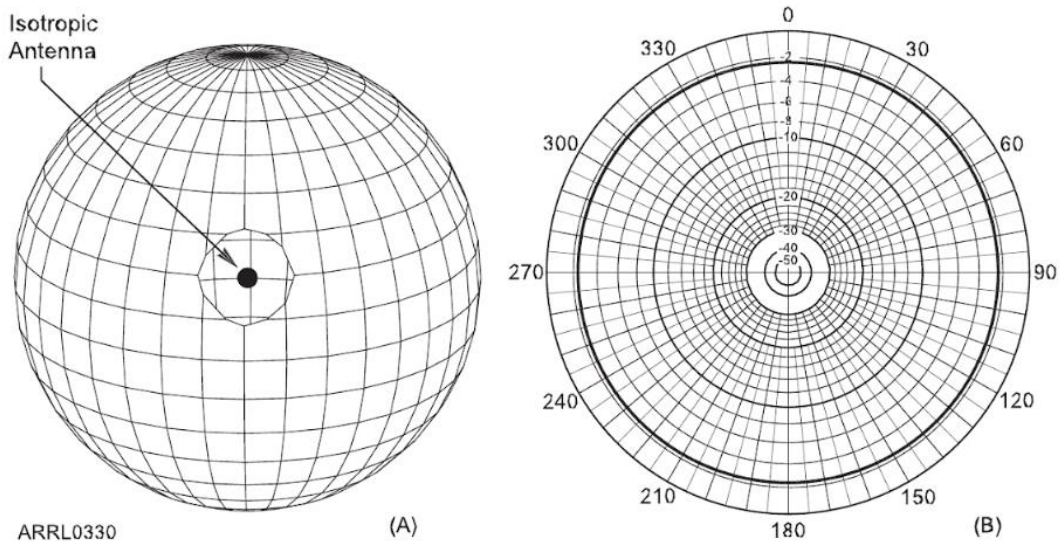

Figure 33: (A) 3-dimensional radiation pattern of an isotropic antenna, (B) radiation pattern of an isotropic antenna in any plane (adapted from Silver, 2008)

2.6.2.2. Dipole antenna

The electrical size of an antenna is given in terms of the wavelength at which it operates. A typical dipole antenna is 0.5λ long and its feed-point is usually at the center. Different lengths of the antenna will produce different radiation patterns; an increase in the length of the antenna will increase the number of lobes (Malindi, 2013). This is illustrated in Figure 34.

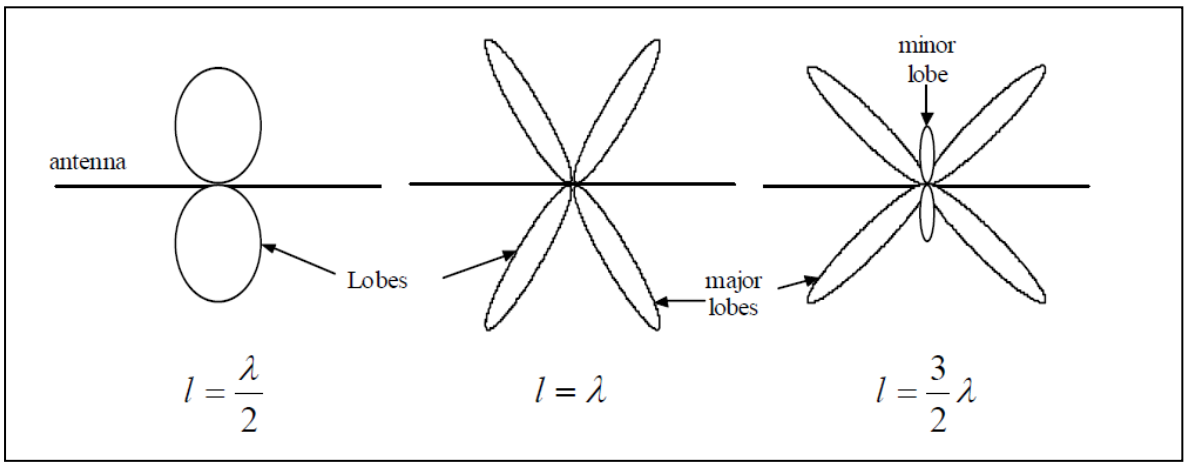

Figure 34: Radiation pattern for dipole antennas of different lengths

2.6.2.3. Directionality

Practically, no antenna can distribute energy with the same strength in every direction. A directional antenna is an antenna that radiates a large amount of power in one direction and a minimum amount in other directions (Bakshi et al., 2008). Directive gain is the ratio of the

power density that is radiated by a specific antenna in a particular direction and the power density that is radiated by an isotropic antenna with both power densities measured at the same distance from the antennas while both antennas are radiating the same power.

Directional transmitting antennas minimise radiation in other directions by concentrating their radiation; thus, minimising interfering with stations in other directions. The radiation patterns of various antennas are shown in Figure 35 and Figure 36.

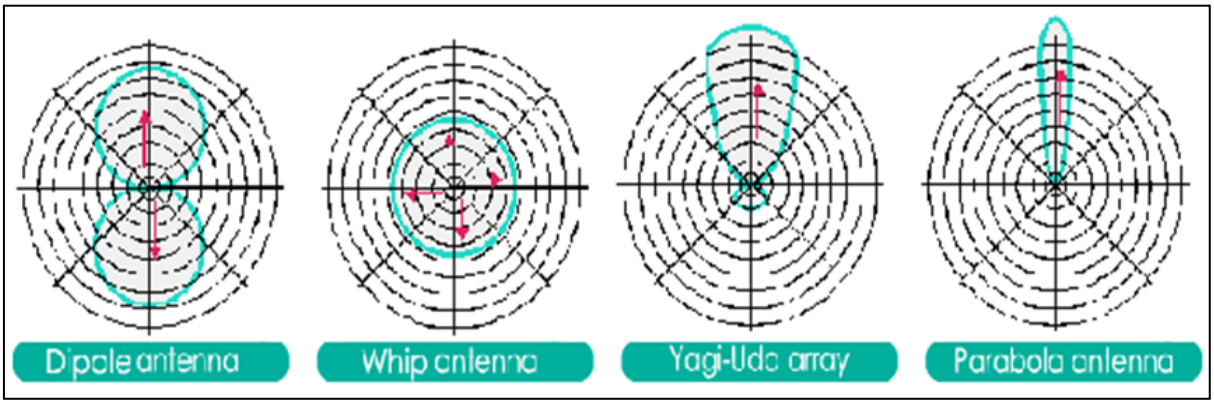

Figure 35: Directivity of typical antennas

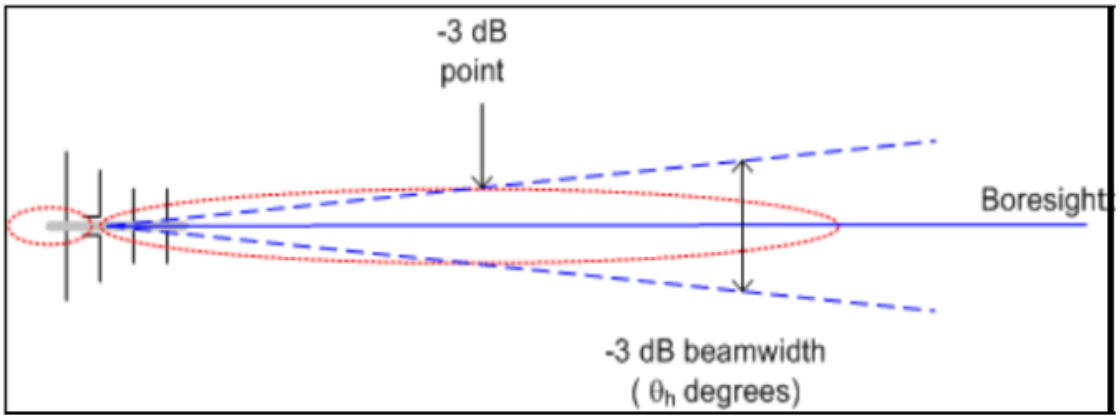

Figure 36: Radiation pattern of a directional antenna

It can be observed from Figure 36 that the gain of a directional antenna decreases at directions off boresight. Higher gain is achieved by reducing the width of the main lobe of the radiation pattern of an antenna. The -3 dB beamwidth is defined as being the angle between the directions in which the radiated power has reduced to half the value at boresight.

Directivity may be defined with the concept of radiated power per steradian as:

$$D = \frac{4\pi}{\Omega} \qquad (46)$$

The steradian is the unit of a solid angle; the solid angle Ω of a cone is the surface it defines on a concentric sphere of a unit radius as seen in Figure 37 (b). The solid angle is then expressed in S_r.

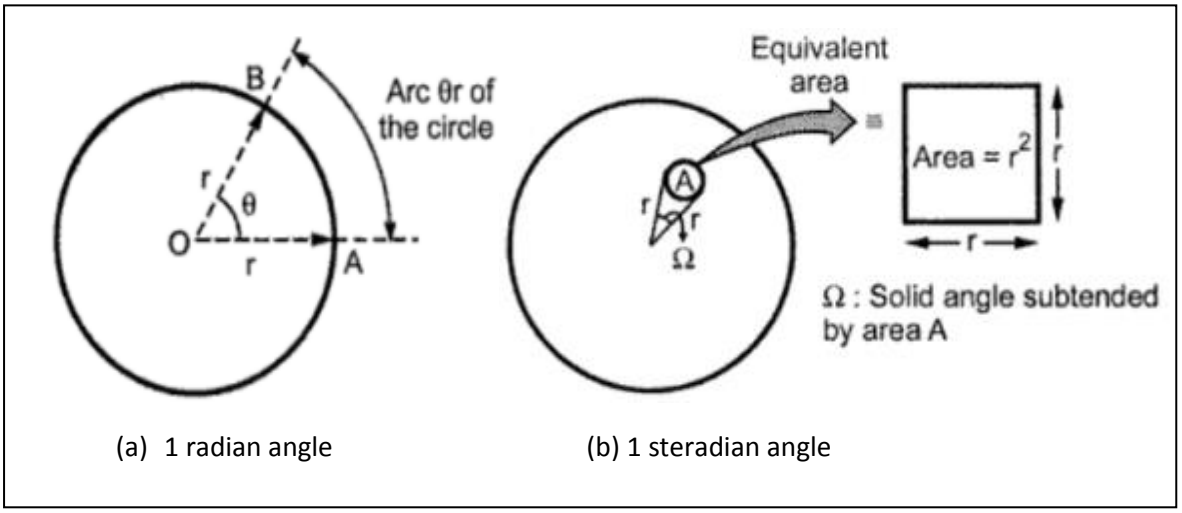

(a) 1 radian angle (b) 1 steradian angle

Figure 37: An illustration of a radian angle and a steradian angle

2.6.2.4. HF antennas

Different HF antennas exist with different operating merits.

Long wire antennas are some of the most popular antennas in this range of frequencies. The term "long wire" antenna means long wires can be combined to make antennas of different shapes that will increase gain as well as directivity over a single wire. Long wire is therefore a configuration rather than just a straight wire antenna. There are several configurations that are used, such as a V-configuration, inverted V-configuration, rhombic, etc. Long wire antenna systems generally operate over a frequency range that includes several amateur bands. The electrical characteristics of long wire antennas change slowly with length. This means that the need to establish resonance at a particular frequency for optimum antenna operation is eliminated as length is not a critical parameter for these antennas.

Figure 38 shows the gain of a long wire antenna as a function of its electrical length. It is also observed that for longer antennas, the lobes narrow and directivity increases.

Figure 39 shows (A) a typical radiation pattern for a terminated long wire antenna that has a length of two wavelengths and (B) a typical radiation pattern for a terminated long wire antenna that has a length of four wavelengths. These patterns are idealised cases where there is no current decrease experienced along the wire. A practical radiation pattern would be somewhat distorted due to attenuation introduced by the wire.

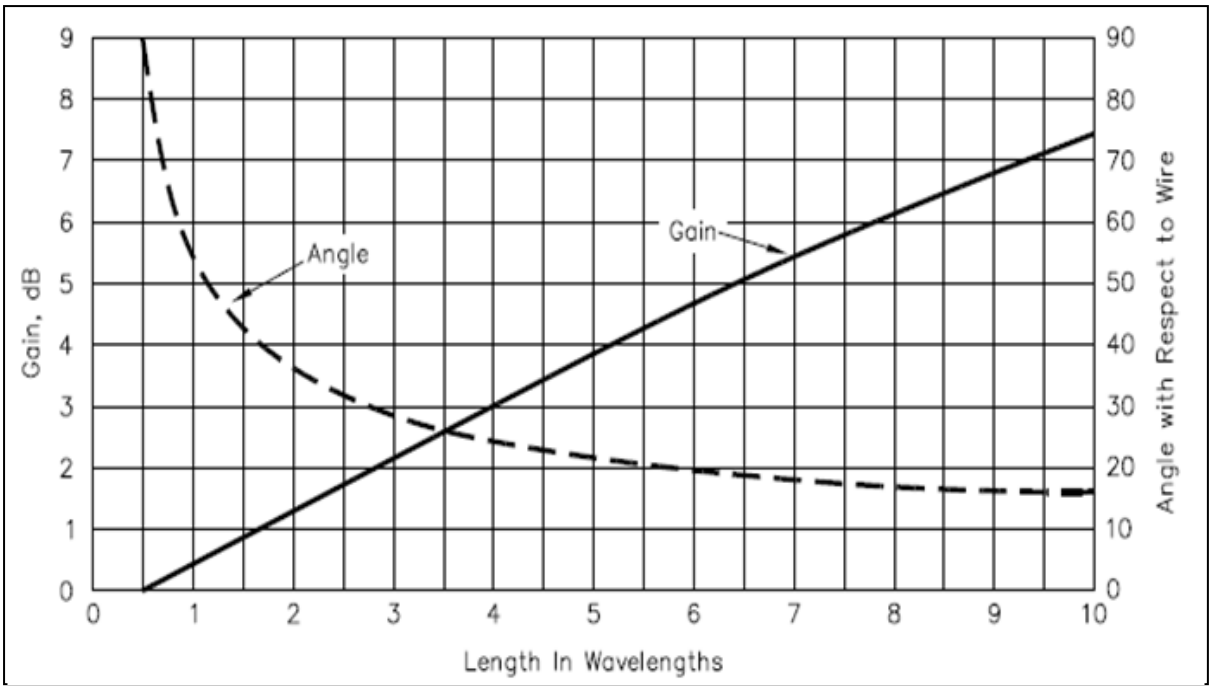

Figure 38: Theoretical gain of a long-wire antenna (adapted Straw, 1997)

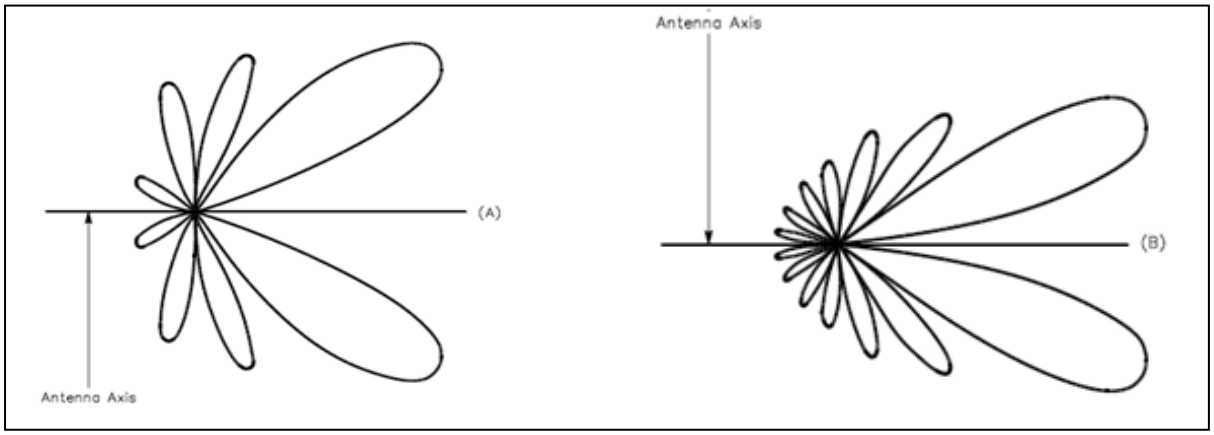

Figure 39: Typical radiation patterns of long wire antenna (adapted from Straw, 1997)

If a scenario of two directive antennas having the same theoretical gain is considered, such as a long wire antenna and a single multi-element array, amateur radio operators have observed that the long wire antenna is more effective during reception, which can be explained by the radiation pattern of the long wire antenna that tends to be horizontally spread out as shown in Figure 40. Figure 40 is an illustration of the radiation pattern produced by a rhombic (wire) antenna with a 9 dBi gain.

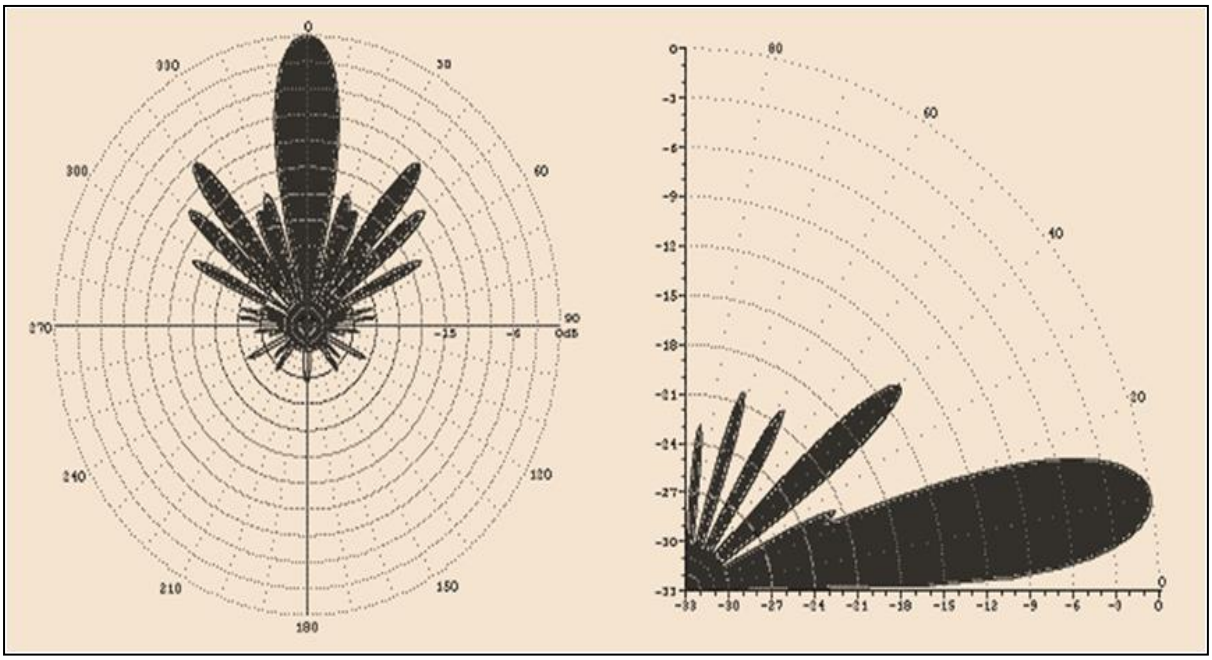

Figure 40: H-plane (left) and E-plane (right) of the long wire antenna radiation pattern (adapted from Straw, 1997)

A log-periodic antenna is an antenna system that is made up of driven elements that are designed to be operated over a wide range of frequencies. There are many varieties of log periodic antenna systems. Some of the popular systems are zig-zag, planar, trapezoidal, slot, dipole, etc. Amateur operators have been known to prefer the log-periodic dipole antenna (LPDA). This type of antenna is shown in Figure 41.

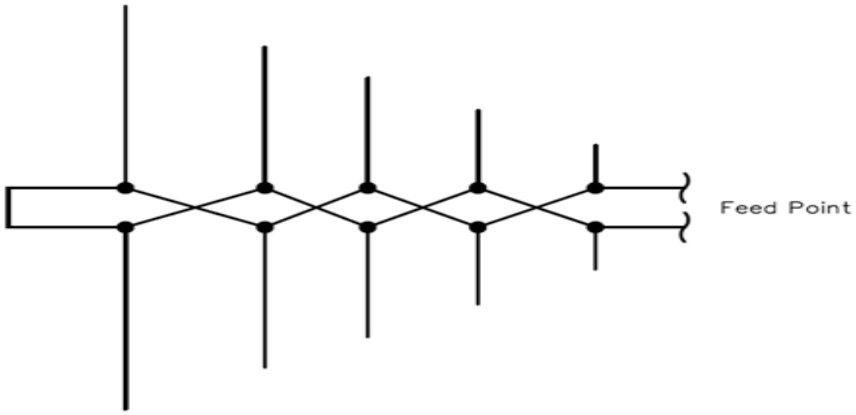

Figure 41: A log periodic dipole array (adapted from Straw, 1997)

The forward direction of the array as shown above is to the right. Sometimes the elements of the antenna are sloped forward and at times parasitic elements are utilised to enhance operational parameters of the antenna, such as the gain and front-to-back ratio. Depending

on the design parameters of the antenna, the LPDA can operate over a range of frequencies with its electrical parameters (gain, feed-point impedance, front-to-back ratio, etc.) remaining relatively constant. This is one advantage of the log periodic antenna over other antennas. As seen in Figure 41, the LPDA is made up of several dipole elements that are each of different lengths and with different relative spacings. The individual elements are excited by a distributive type of feeder system. Beginning from the feed point for the array, the element lengths and relative spacings are seen to increase smoothly in dimension. It is this feature upon which the design of the LPDA is based, and which permits changes in frequency to be made without greatly affecting the electrical operation.

The Yagi-Uda antenna, also referred to as a Yagi, is one of the most successful RF antenna designs for directive antenna applications. This antenna is used in a wide variety of applications where an RF antenna design with gain and directivity is required. A Yagi is a type of end-fire multi-element array. At the minimum, it consists of a single driven element and a single parasitic element. The driven element is the element of the Yagi antenna to which power is applied. It is normally a half-wave dipole or often a folded dipole. When the parasitic element is placed behind the driven element, it is named a reflector. The Yagi antenna will generally only have one reflector. More reflectors behind the first one add little to the performance; however, many designs use reflectors consisting of a reflecting plate, or a series of parallel rods simulating a reflecting plate. This gives a slight improvement in performance, reducing the level of radiation or pick-up from behind the antenna. Normally, a reflector will add around 4 or 5 dB of gain in the forward direction. When the parasitic element is placed in front of the driven element, it is named a director. The purpose of the director elements is to focus and direct the radiated power. Each director is expected to add about 1 dB in the forward direction, but this level reduces as the number of directive elements increases.

Figure 42 shows a typical construction of a Yagi antenna. It may be observed that directors are of equal length while the driven element is slightly longer. This difference in length is 5% longer than the reflector(s). The reflector is also 5% longer than the driven element.

Below are some of the advantages that Yagi antennas offer:

- A Yagi-Uda is a high gain antenna, i.e. more power to reach further distances.
- A Yagi-Uda is a directional antenna, which minimizes interference in other directions.
- The antenna can be made up of inexpensive material; its construction is simple and easy to mount on poles and other standard mechanical fixings.

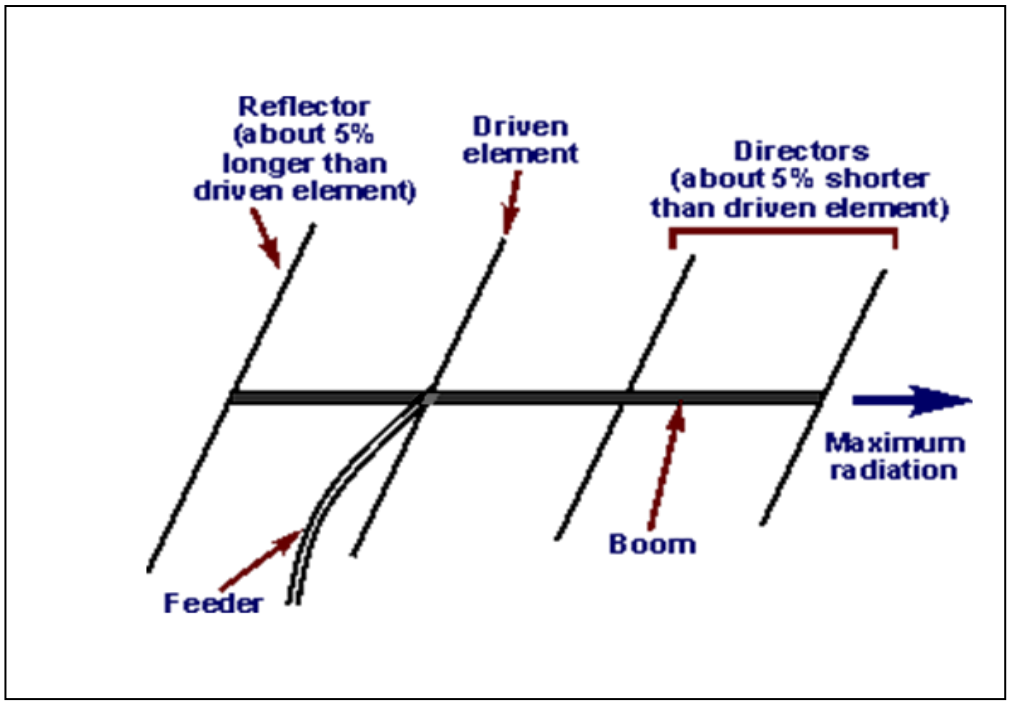

Figure 42: A typical Yagi-Uda antenna configuration

Figure 43 illustrates a typical radiation pattern of a 14.174 MHz Yagi antenna that is made up of 6 elements and is 20 meters long. The antenna is mounted approximately 21 m above ground. The Yagi antenna pattern is compared to that of a dipole antenna at the same frequency and same height above ground.

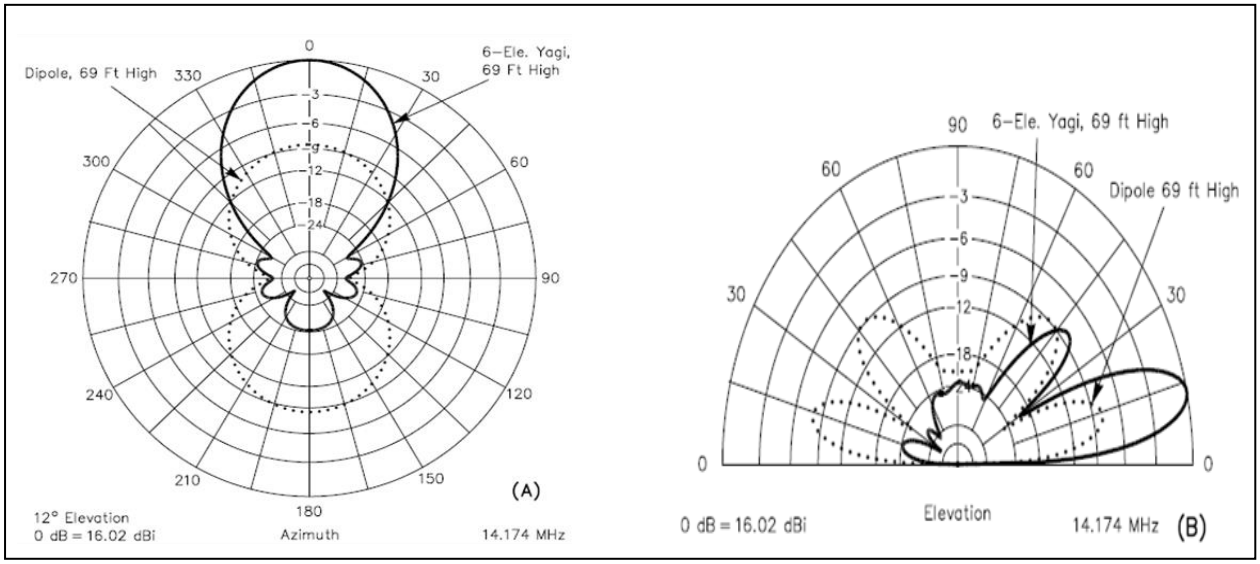

Figure 43: Radiation pattern of a Yagi-Uda antenna (bold line) against a radiation pattern of a dipole antenna (dotted line) (adapted Straw, 1997)

There are no simple formulas for designing Yagi-Uda antennas due to the non-linear relationships between physical parameters, such as element length, diameter and position, and electrical characteristics, such as input impedance and gain. Consequently, designs are found experimentally either through direct measurement or computer simulation, or by modifying existing designs.

2.6.2.5. Impedance matching of antennas

An antenna is presented as the load impedance to the system that is connected to its driving terminal. The impedance of the driving point of the system is ideally equal to the radiation resistance of the antenna. This will hardly be the case in practical systems as the driving point impedance includes some resistive losses that exist within the antenna. Other contributing complex impedance factors will be connectors and cabling between the driving device and the antenna. For maximum power transfer, it is a requirement that the antenna impedance and the impedance of the driving point be matched. Maximum power transfer is just as important for both the transmitting and receiving antenna. When there is a mismatch between the antenna and the driving point, a standing wave with a voltage standing wave ratio (VSWR) is created on the cable. Power loss is the result of the VSWR on the cable (Seybold, 2005).

3.1. INTRODUCTION

This chapter covers the design of each of the sub-circuits that make up the HF transmitter. Certain performance criteria have to be considered in the design and selection of components for the HF beacon circuit.

The operating temperature range is one of the most important factors when selecting components. Failure or malfunction of components due to very low temperatures could prove fatal to the entire project.

It is also important to note the noise that may be introduced by the circuit components to the signal. Susceptibility of components to noise may also cause issues to the frequency stability of the device.

Availability of components may prove to be challenging because of the operational frequency of the project. HF components have become scarce. The options for carrier generation that may be used for this project are mostly limited by the fact that the device must have the ability to be programmed to a different frequency within the SuperDARN operating frequency range, i.e. between 8 MHz and 20 MHz. This presents a challenge because most oscillators operate at only one frequency and, therefore, will require extra circuitry to implement the function of varying the frequency.

The Texas Instrument RI-R6C-001A transceiver IC is utilised in this project as the primary transmitter. This S6700 multi-protocol IC belongs to a family of HF reader systems that operate at 13.56 MHz. The RI-R6C-001A transceiver is primarily designed to be used in wireless identification applications. The chip was selected for its ability to operate in the HF range, wide operating temperature and small size. Using a compact transmitter built into a chip will also makes the circuit less susceptible to noise. The temperature of this transceiver remains stable over a wide range of temperatures. The chip is specified to provide a maximum RF output power of 200 mW (i.e. 23 dBm) when supplied with a 5V DC power supply and under 50Ω matched load conditions.

Figure 44 shows a simplified block diagram of the transceiver IC. The blocks within the green dotted line are utilised for reception and will not be used in this project because the purpose of the project is simply to transmit. The blocks within the solid line are used in this project as they are the transmitter blocks of the IC. The chip operates according to a “reader talks first” principle. In this case, the reader is the microcontroller chip. This means that the transponder will be quiet until the microcontroller sends a request to the transceiver. The pin-out layout is presented in Appendix E.

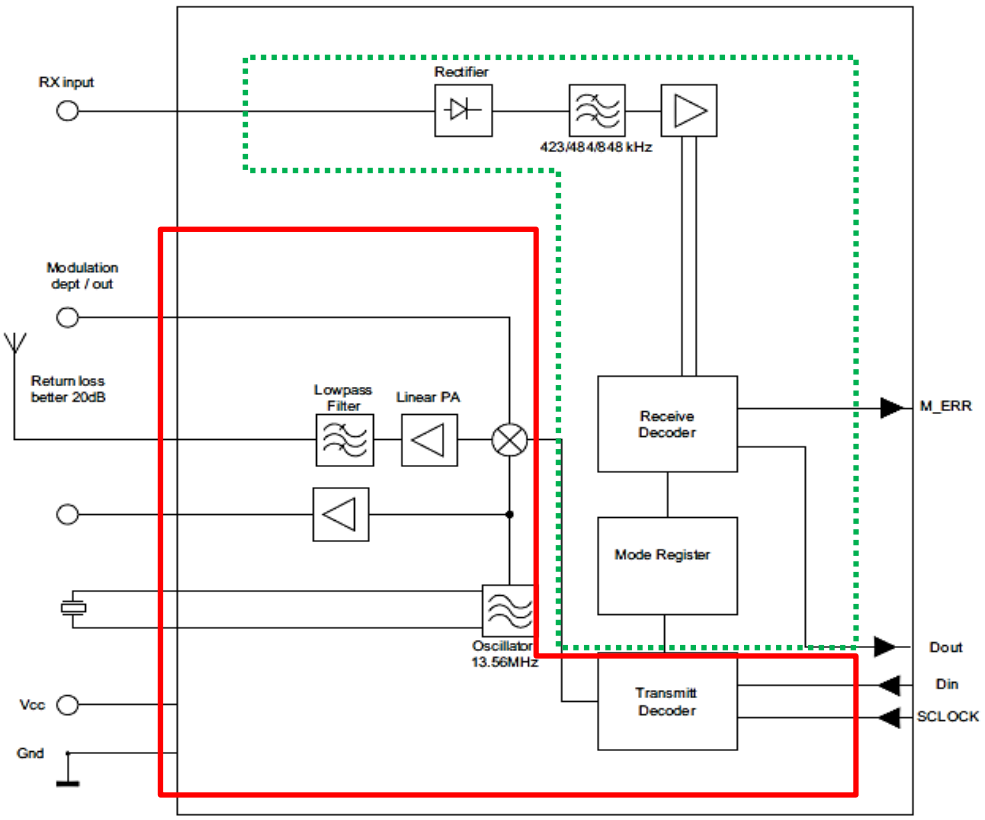

Figure 44: RI-R6C-003A block diagram (adapted from Texas Instruments, 2005)

The complete operation of the device is presented in the block diagram in Figure 45 and the full circuit schematic of the device is presented in Figure 46. A clearer picture of the schematic can be found on Appendix I.

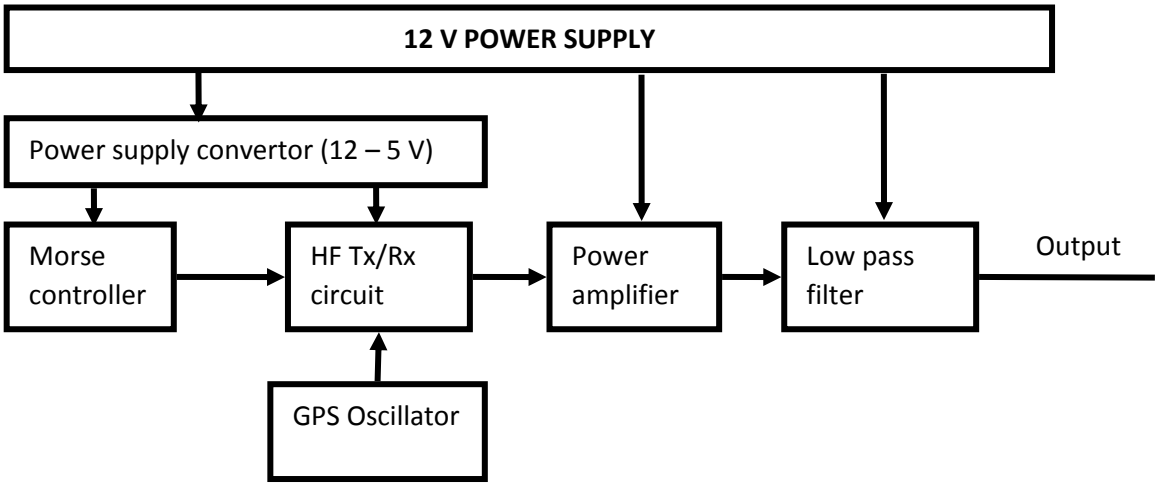

Figure 45: Block diagram of the complete HF beacon

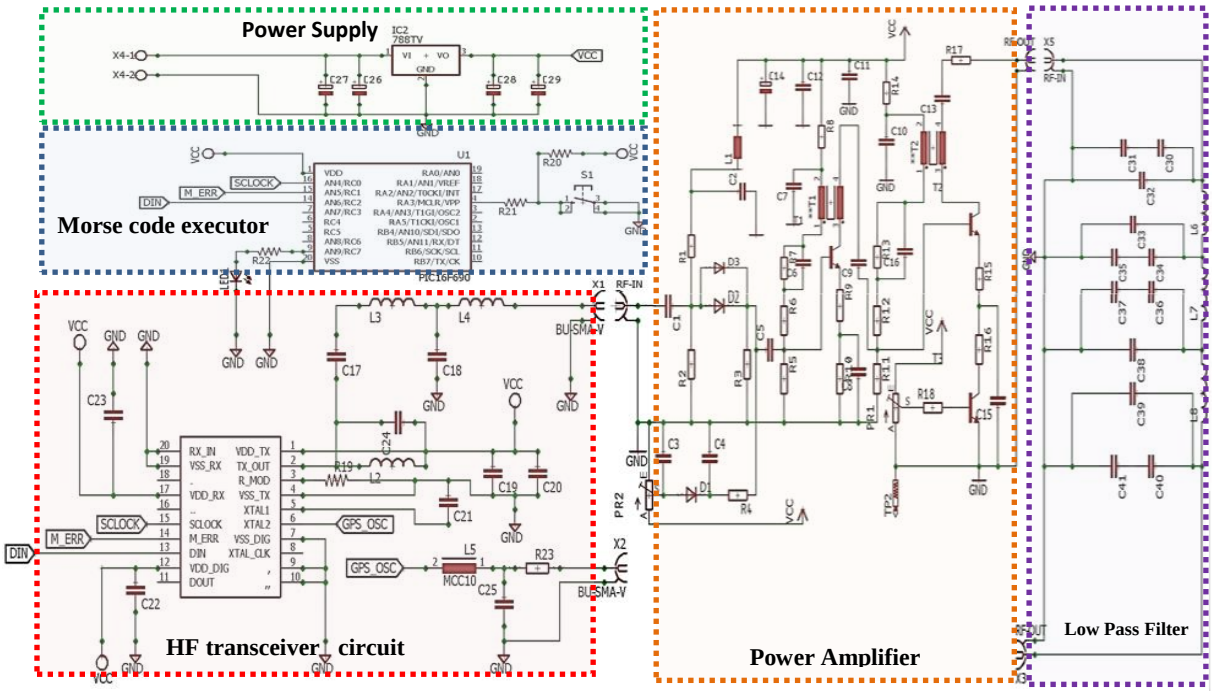

Figure 46: Complete circuit schematic of the HF beacon (adapted from Texas Instruments, 2005)

3.2. POWER SUPPLY

Even though the transceiver chip requires 5V biasing, it is specified to operate between 3V and 5.5V. The current drain is dependent on the antenna impedance and the output matching network but the transceiver chip is specified to consume a maximum power of about 500mW.

Power supply ripple and noise are some of the factors that degrade system performance. The 5V regulator circuit in Figure 47 was designed to bias the transmitter circuit. The component values is given in Table 3. The power supply that will be used in Antarctica is a 12V battery. Batteries are mostly stable but it is important to design a power supply regulator that can handle a noisy supply.

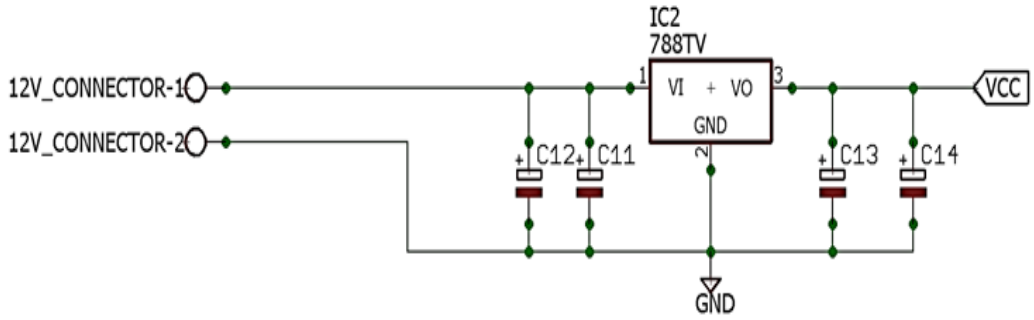

Figure 47: +5V supply circuit used as Vcc

Table 3: Power supply component values

Component	Value	Function
C12	0.1uF	This is called a bypass capacitor. It is used in this circuit to bypass extremely short duration spikes down to ground.
C11	1000uF	This is a filter capacitor and it is utilised in this circuit to stabilise the slow changes in the voltage applied at the input of the circuit.
C13	1000uF	This capacitor assists C11 in stabilising the slow changes of the input signal; it is also a filter capacitor.
C14	0.1uF	This is a bypass capacitor, like C12. It is considered the "last line of defense" against very small period spikes.
IC2	7805	This is a positive 5V DC regulator and its purpose is to keep the output steady at a constant value of 5V even though the input may be varying.

3.3. TRANSMITTER CIRCUIT

Figure 48 presents a circuit that comes highly recommended by Texas Instruments for the use of the RI-R6C-003A IC.

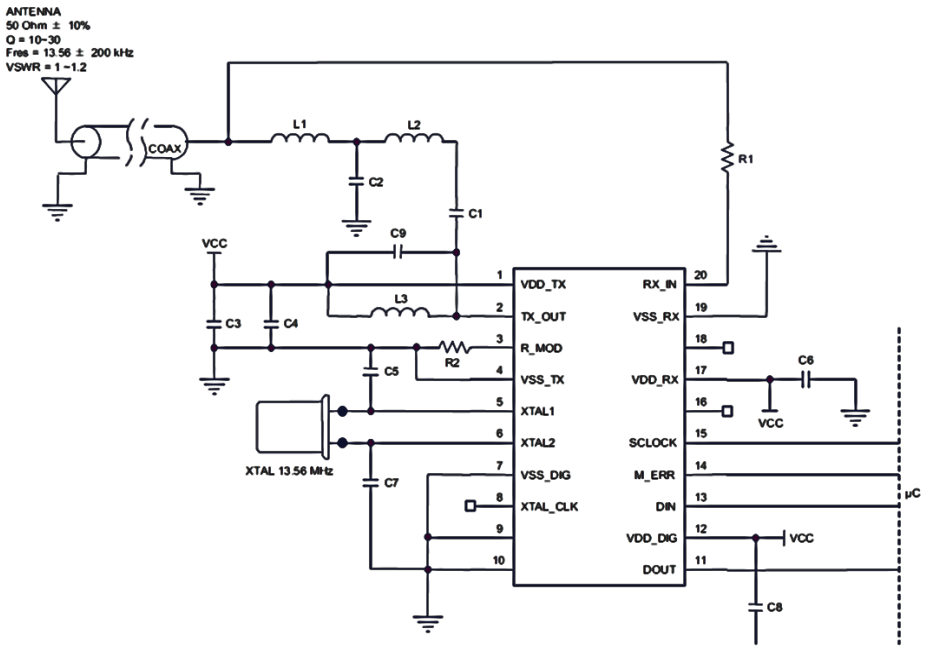

Figure 48: Wireless Identification application circuit using RI-R6C-003A transceiver (adapted from Texas Instruments, 2005)

To accommodate the HF transmitter application, the following changes have been made to the circuit:

- The 13.56 MHz crystal oscillator has been replaced by an external clock.
- The receiver is not utilised and is therefore connected to ground.

In Figure 49, these two changes are circled in red.

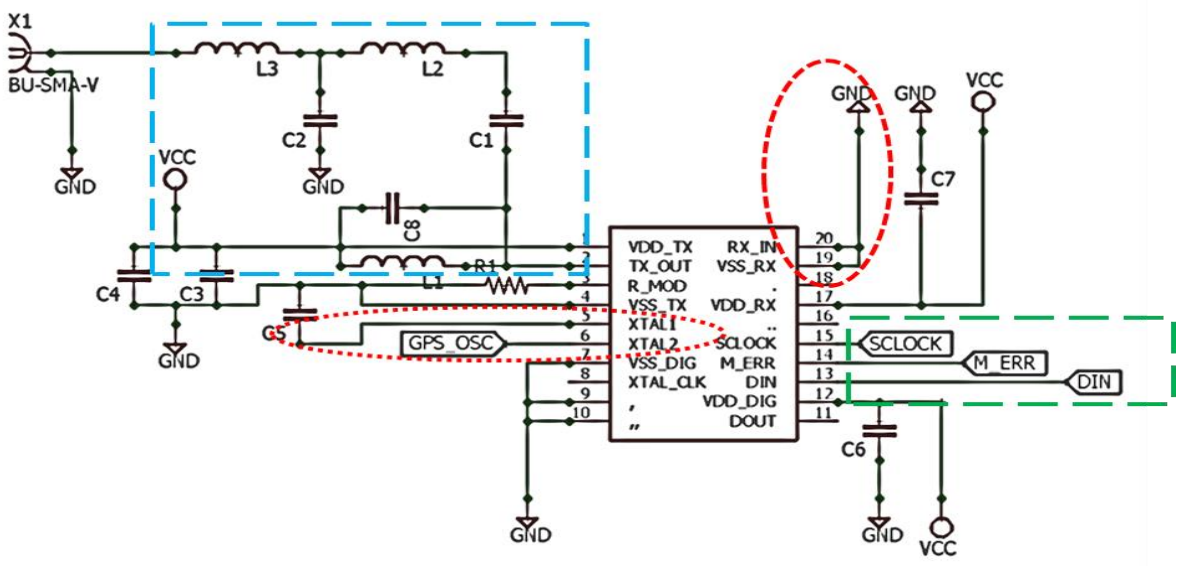

Figure 49: Modified RI-R6C-001A circuit

In the above circuit, the input RF signal that would normally be produced by a crystal oscillator will be fed from an external source, which will be discussed next. Since the receiver is not utilised, it is grounded to avoid noise. The green highlighted area is made up of connections to the reader or microcontroller. The blue highlighted area is the filter circuit of the transmitter. The circuit is given with recommended values for the filter circuit at 13.56 MHz. New values were calculated for the filter circuit in order to optimise the circuit for operation at 12.57 MHz, a load impedance of 50 Ω, a Q factor of 30 and a source or chip impedance of 5 Ω.

Filter calculations

The filter circuit is designed as a double L-matching circuit, which results in a T-matching network configuration. An equivalent impedance matching filter network is presented in Figure 50.

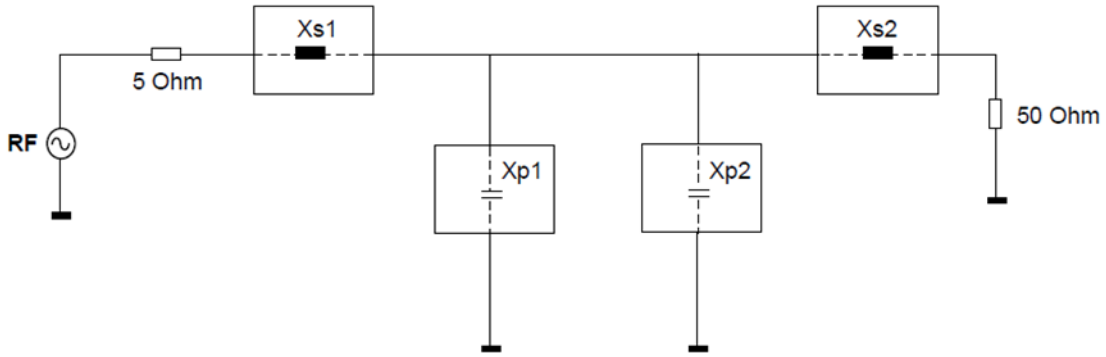

Figure 50: Double L matching circuit for the HF beacon circuit

For this circuit:

$R_L = 50\ \Omega$ - load resistance

$F_{res} = 12.57\ MHz$ - resonating frequency

$R_S = 5\ \Omega$ - source resistance

$Q = 30$ - Q factor

The virtual resistance of the parallel section (X_{P1} // X_{P2}) is given by:

$R = Rs \cdot (Q^2 + 1)$

$= 5 \times (901)$

$= 4505\ \Omega$

The inductive resistance of the first series inductor is given by:

$X_{S1} = Q \cdot R_S$

$= 30 \times 5$

$= 150\ \Omega$

The inductance of the first inductor is calculated as:

$$L_1 = \frac{Xs1}{2.\pi.f} = \frac{150}{2\pi \text{ x } 12.57\text{x}10^6} = 1.9\ uH$$

The quality or Q factor of the second series inductor is given by:

$$Q_2 = \sqrt{\frac{R}{R_L} - 1} = \sqrt{\frac{4505}{50} - 1} = 8.5$$

The inductive resistance of the second series inductor is given by:

$X_{S2} = Q_2 \cdot R_L$

$= 8.5 \times 50$

$= 425$

The inductance of the second series inductor is calculated as:

$$L_2 = \frac{Xs2}{2.\pi.f} = \frac{425}{2\pi \text{ x } 12.57\text{x}10^6} = 5.4\ uH$$

The capacitive resistances of the capacitors are given by:

$$X_{P1} = \frac{R}{Q} = \frac{4505}{30} = 150.2$$

$$X_{P2} = \frac{R}{Q2} = \frac{4505}{8.5} = 530$$

The equivalent capacitive resistance of the parallel capacitor is given by:

$$X_P = \frac{Xp2 \,.Xp1}{Xp2+Xp1} = \frac{150.2 \text{ x } 530}{680.2} = 117$$

The capacitance of the parallel capacitor is now calculated as:

$$C = \frac{1}{2\pi f Xp} = \frac{1}{2\pi \text{ x } 12.57\text{x}10^6 \text{ x } 117} = 108\ pF$$

Formulas and calculations adapted from (Texas Instruments, 2003)

3.4. EXTERNAL CLOCK

In order to accurately observe the motion of the ionosphere, it was required by the SANSA technical team that the frequency of the transmitter must be stable enough to measure a wave velocity of not more than 1 m/s when there is no motion between the transmitter and receiver. The maximum frequency deviation for this condition is given by:

$$\Delta f = \frac{v}{\lambda} = \frac{1}{23.9} = 41.8mHz \qquad (47)$$

$$\Delta f = \frac{41.8x10^{-3}}{12.57x10^6} = 3.3x10^{-9} = 3.3ppb$$

where:

Δf - frequency deviation in Hz

v – wave velocity in m/s

λ - wavelength

To achieve the minimum frequency drift of 41.8 mHz that is specific to this project, several clocks were considered.

- In-house developed oscillator circuit:
  Developing oscillator circuits in-house poses several technical challenges in terms of frequency stability and controlling the operating frequency digitally. After much deliberation, it was decided not to pursue this avenue, but rather investigate off-the-shelf alternatives for a stable, controllable oscillator.
- Crystal oscillator:
  Quartz crystal oscillators are timing devices with quartz crystal resonators and active oscillation circuits to generate the desired frequency output waveforms. There are several varieties of crystal oscillators, namely:
  - Crystal oscillator (XO):
    This is a first choice because of their low cost and availability. One of the major challenges with crystal oscillators is, however, the fact that they do not allow change of frequency; one would need to actually have an oscillator made for every frequency that is needed for operation. This type of package, also named a Simple Package Crystal Oscillator (SPXO), usually operates inefficiently at temperatures below 0°C in terms of frequency stability.
  - Temperature controlled crystal oscillator (TCXO):
    This is an improvement on the SPXO as the TCXO is designed to adjust its frequency deviation as the ambient temperature changes. It is more expensive than an SPXO and harder to source too.
  - Oven-controlled crystal oscillator (OCXO):
    This oscillator offers even better frequency stability. It actually has an oven (heating) block that monitors and regulates the temperature of the crystal oscillator and other temperature sensitive components to ensure frequency stability.
- GPS Disciplined Oscillator (GPSDO):
  The GPSDO was the preferred choice because of its superior stability and its ability to be programmed over a wide range of frequencies. This will be discussed further in Section 3.5.

Table 4 summarises the typical frequency stability performance of the abovementioned devices over different temperature ranges.

Table 4: Frequency stability of various oscillators

	XO	TCXO	OCXO	GPSDO
0°C to 70°C	±10 ppm	±0.5 ppm	±0.003 ppm	± 1 ppt
-20°C to 70°C	±25 ppm	±0.5 ppm	±0.003 ppm	± 1 ppt
-40°C to 85°C	±30 ppm	±1 ppm	±0.02 ppm	± 1 ppt
-55°C to 125°C	±50 ppm	N/A	N/A	N/A

3.5. GPS DISCIPLINED OSCILLATOR

A GPS disciplined oscillator (GPSDO) is a device that combines the sophisticated technology of GPS receivers with the reliability of stable high quality oscillators. The outputs of these oscillators (usually rubidium and quartz oscillators) are synchronized with signals that are broadcast by GPS and GNSS satellites. These oscillators are used as a reference in a variety of timing applications because of their accuracy.

Figure 51: Low jitter precision GPSDO reference oscillator (2 Ports) (adapted from Riley, 2016)

The low jitter GPS-locked precision frequency reference oscillator manufactured by Leo Bodnar Ltd in Figure 51 was chosen for this project because of the following reasons:

- Variable Frequency:
  The flexibility of frequency variability is always a desirable quality for most applications, including this project. The precision GPSDO reference oscillator can be programmed to output any frequency from 450 Hz – 800 MHz in 1Hz steps.
- Frequency stability:
  One of the primary requirements of this project is frequency stability and the precision GPSDO reference oscillator is expected to have a 1 ppb frequency deviation in less than a minute after it has locked its receiver to the GPS signal.
- User interface:
  The precision GPSDO requires no expert knowledge of any programming language as it comes with a software interface that is user-friendly. Figure 52 shows the user interface.

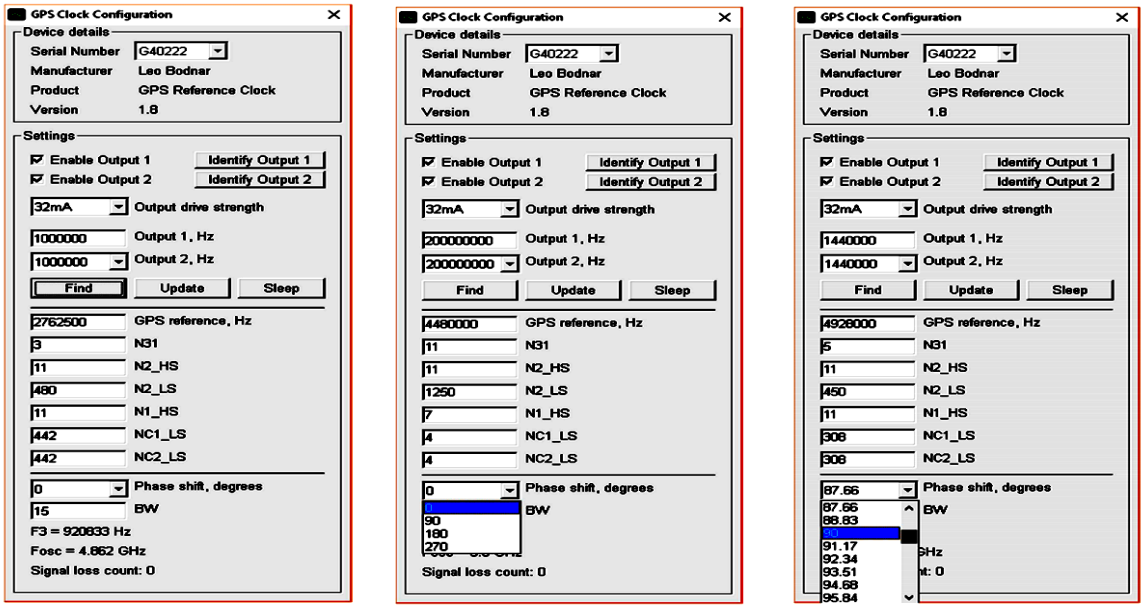

Figure 52: GPSDO software user interface illustrated for different frequencies settings (adapted from Riley, 2016)

The two outputs of the GPSDO in Figure 51 can be individually enabled and set to different frequencies. If both outputs have the same frequency, their relative phase shift can be adjusted. This can be useful in applications that require two signals with 90° phase shift, such as an I/Q mixer. Directly setting the frequency synthesizer parameters makes it possible to get more frequency combinations.

As the frequency of the GPSDO is decreased, the shape of the signal becomes more distorted until it is more like a square wave. It is more preferable to work with a sine wave than a square wave for this project because:

- the RI-R6C-001A transceiver datasheet specifically states that the external oscillator input must be a sine wave; and
- a square wave produces numerous harmonics.

Therefore, it is necessary to shape the signal using a low pass filter as shown in Figure 53.

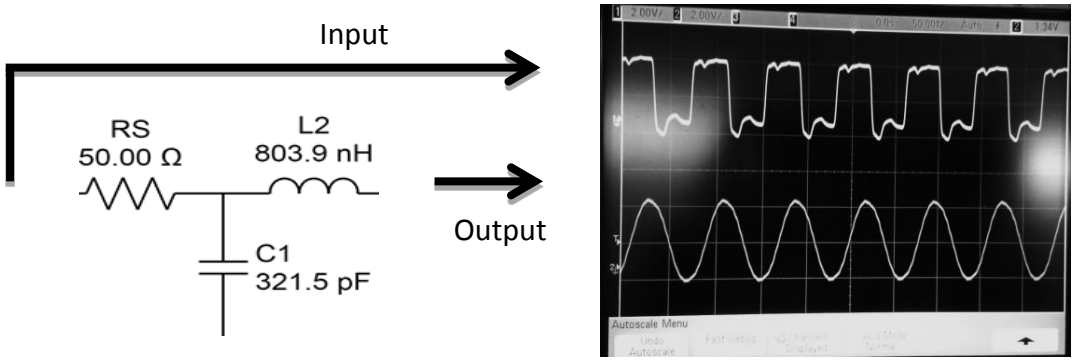

Figure 53: Low pass filter input and output

The cut-off frequency of the low pass filter in Figure 53 is given by:

$$f_c = \frac{1}{\pi\sqrt{LC}} \tag{48}$$

$$f_c = \frac{1}{\pi \cdot \sqrt{803.9\text{x}10^{-9} \cdot 321.5\text{x}10^{-12}}}$$

$$f_c = 19.8\,MHz$$

The rated short term stability of the GPS disciplined oscillator, i.e. immediately after it has been switched on and operated overnight, is shown in Figure 54. It is evident that the stability of the oscillator improves over time. The average frequency offset is specified to be approximately $+7.3\text{x}10^{-13}$ Hz over the period of a night.

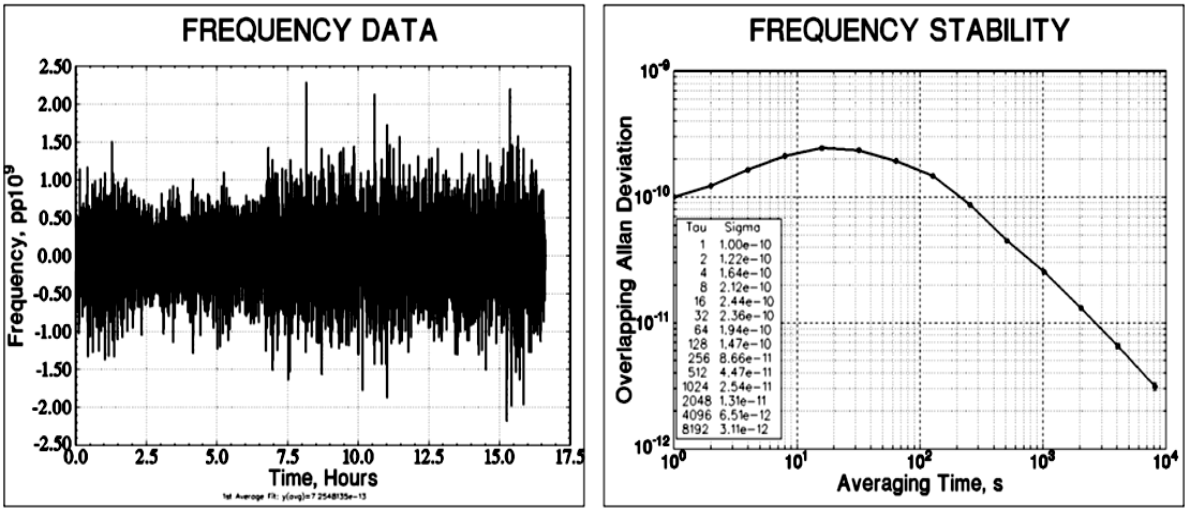

Figure 54: Frequency stability of GPSDO over time (adapted from Riley, 2016)

3.6. TRANSMITTER FREQUENCY

SuperDARN radars operate at frequencies between 8 MHz and 20 MHz. As mentioned earlier, the GPSDO can operate over this frequency range (and well beyond). However, the HF transceiver chip is only specified to operate between 4 MHz and 16 MHz. This may present a challenge for transmitters that have to operate above the specified maximum operation of the chip. This project will not be facing such a challenge as the nominal operating frequency is specified as 12.57 MHz.

3.7. PERIPHERAL INTERFACE CONTROLLER

The Peripheral Interface Controller (PIC) is a microcontroller that is developed by Microchip Technology and is found in many different applications, and mostly in automation. A PIC is a Reduced Instruction Set Computer (RISC) that makes it perform better than the Complex Instruction Set Computer (CISC) in terms of cycles per instruction. There are various packages and sizes of these PICs.

A PIC16F690 is utilised in this project as a controller that switches the transmitter between CW and Morse code as well as store the predefined ‘word’ that will be encoded into a Morse code when the transmitter is not set to CW.

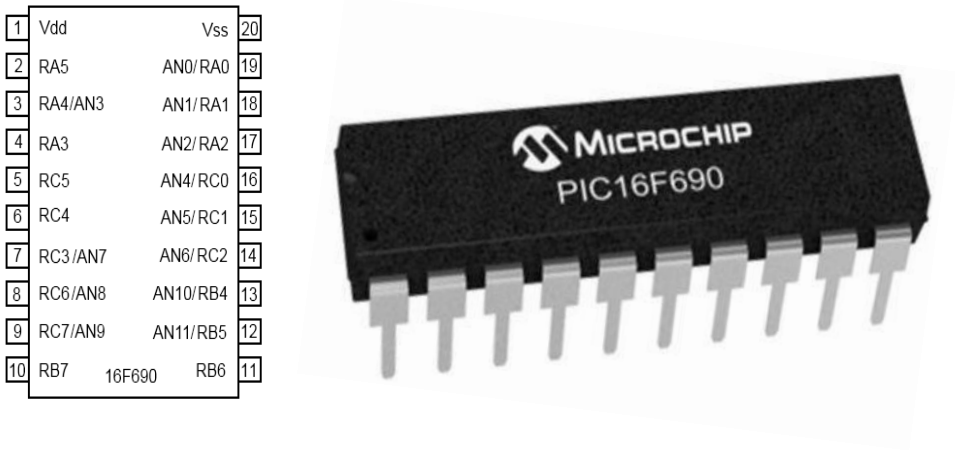

Figure 55: A PIC 16F690 pin label (left) and a its dual in-line package IC

The cost as well as the flexibility and availability of PIC microcontrollers make them popular for most projects. The abovementioned PIC in Figure 55 is a 20-pin IC and has an internal 4 MHz oscillator; thus, eliminating the need for an external crystal oscillator that is mostly used in other microcontrollers that are not equipped with internal oscillators. The pin description of the PIC16F690 may be found in Appendix F.

CHAPTER 4 DESIGN VERIFICATION AND EXPERIMENTAL RESULTS

4.1. INTRODUCTION

Tests need to be carried out in order to verify that the design meets the specifications of the project. The HF transmitter testing follows the blocks as shown in Figure 56.

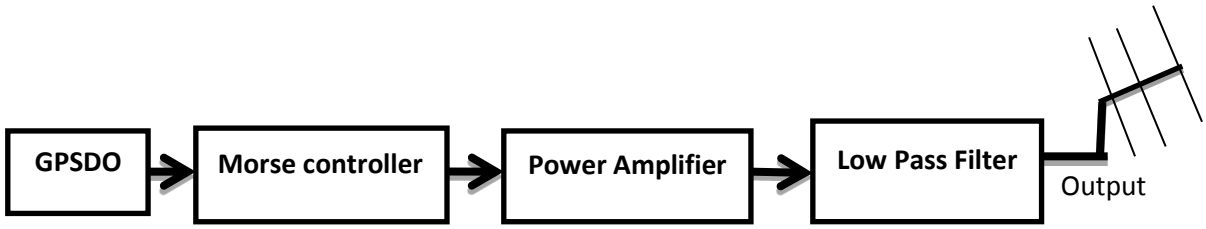

Figure 56: Block diagram of the HF transmitter stages

The tests are divided into 3 sections:

- Device laboratory tests:

The device under test (DUT) is powered to observe functionality. Key parameters, such as frequency stability and power output, of each stage are measured, verified and recorded.

- Propagation tests:
  The device is tested with a real antenna as a load and an attempt is made to receive the signal over a distance of approximately 1300 km, between Hermanus and Pretoria.
- Temperature test:
  The DUT is exposed to a wide range of temperatures that are expected in Antarctica. Any changes in power and frequency stability are monitored and recorded.

4.2. DEVICE LABORATORY TESTS

4.2.1. GPS Oscillator

The equipment in Figure 57 is necessary in order to carry out this test.

It is important to note that the equipment used for these measurements itself is not equipped with a GPS synchronised reference clock and can, therefore, measure only up to a level specified in Table 5 before it introduces frequency drift into the measurement.

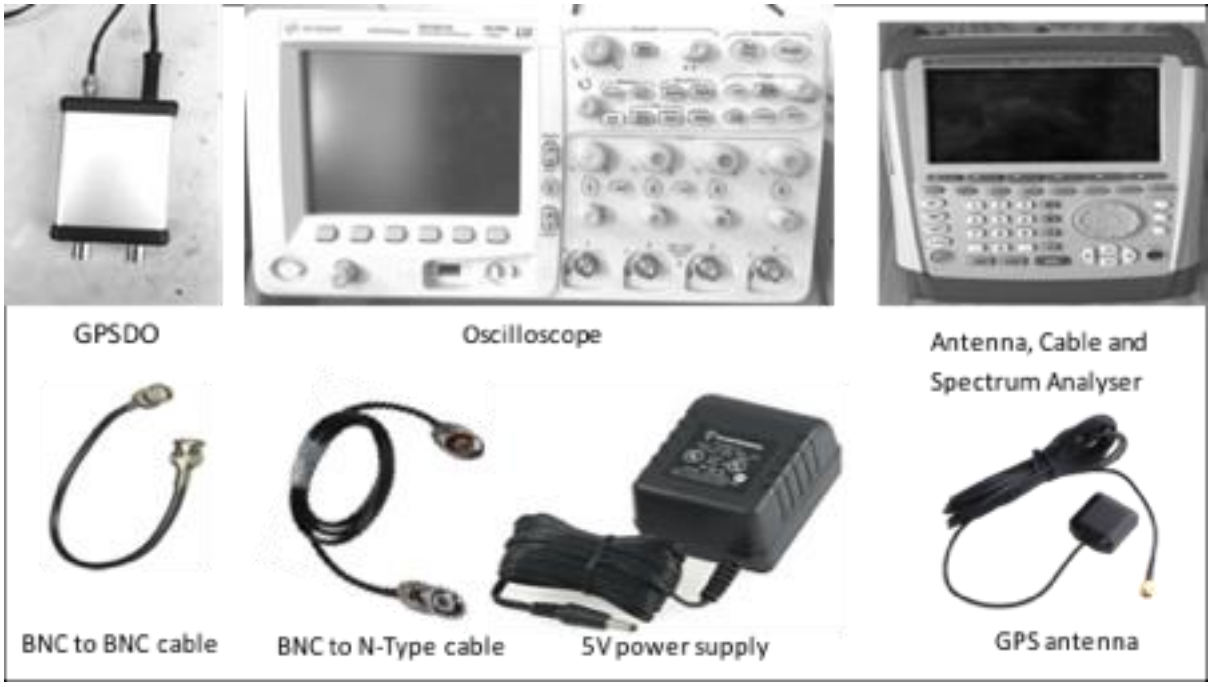

Figure 57: Equipment used for the GPSDO test

Table 5 below shows all the necessary information about the frequency accuracy and stability of the spectrum analyser used.

Table 5: Rhode & Schwarz ZVH4 cable and antenna analyser frequency performance

Frequency range	R&S®ZVH4	100 kHz to 3.6 GHz
	R&S®ZVH8	100 kHz to 8 GHz
Frequency resolution		1 Hz

Reference frequency, internal		
Total reference accuracy		±(time since last adjustment × aging rate) + temperature drift + calibration accuracy
Aging per year		$\pm 1 \times 10^{-6}$
Temperature drift	0 °C to +50 °C [1]	$\pm 1 \times 10^{-6}$
Achievable initial calibration accuracy		$\pm 5 \times 10^{-7}$
Reference frequency, with R&S®HA-Z240 GPS receiver option		
Frequency accuracy	GPS on, ≥ 1 min after satellite lock	$\pm 2.5 \times 10^{-8}$
	up to 30 min after losing satellite lock	$\pm 5 \times 10^{-8}$
Reference frequency, with R&S®FSH-Z114 precision frequency reference option		
Aging per year		3.6×10^{-9}
Temperature drift	0 °C to +50 °C	4×10^{-10}
Achievable initial calibration accuracy		1×10^{-9}
Total reference uncertainty	R&S®FSH-Z114 connected	
	≥ 30 s after oscillator lock	(time since last adjustment × aging rate) + temperature drift + 3 × calibration accuracy (nominal)
	≥ 2 min after oscillator lock	(time since last adjustment × aging rate) + temperature drift + calibration accuracy

Frequency readout		
Marker resolution		0.1 Hz
Accuracy		±(marker frequency × reference accuracy + 10 % × measurement bandwidth + ½ ($(f_{stop} - f_{start})$ / (data points – 1) + 1 Hz)

It may be observed from Table 5 that the instrument will have limitations measuring frequency accuracy to the level needed, but for the lack of better equipment, this was the best option. The equipment would be sufficient to measure the desired frequency level if it was synchronised with an external GPS timing device. However, this is a swept type of spectrum analyser, which means it can only detect a CW signal without any phase information. Also it is unsuitable for testing the Morse code part of this project.

Figure 58 depicts the configuration used during the test. Since the oscillator has 2 ports, both ports can be set to the same frequency and each port may be connected to a testing device i.e. an oscilloscope or spectrum analyser. However, only one port is utilised in this project, i.e. Port 1. This means that only one testing device may be connected at a time.

Figure 59 is a picture of the results displayed by the oscilloscope that is connected to Output_1 of the GPS oscillator. As mentioned before, the oscillator produces a distorted and almost square wave shape as the frequency of operation is reduced.

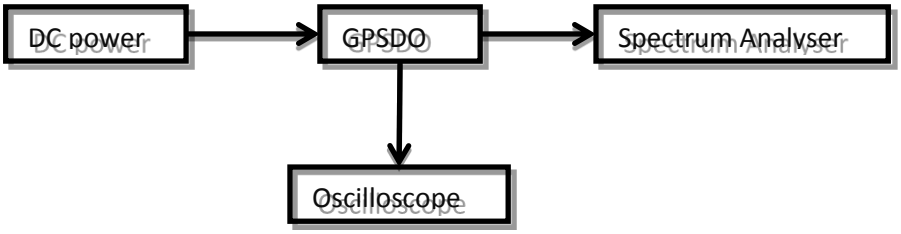

Figure 58: Layout of the test setup for the GPSDO

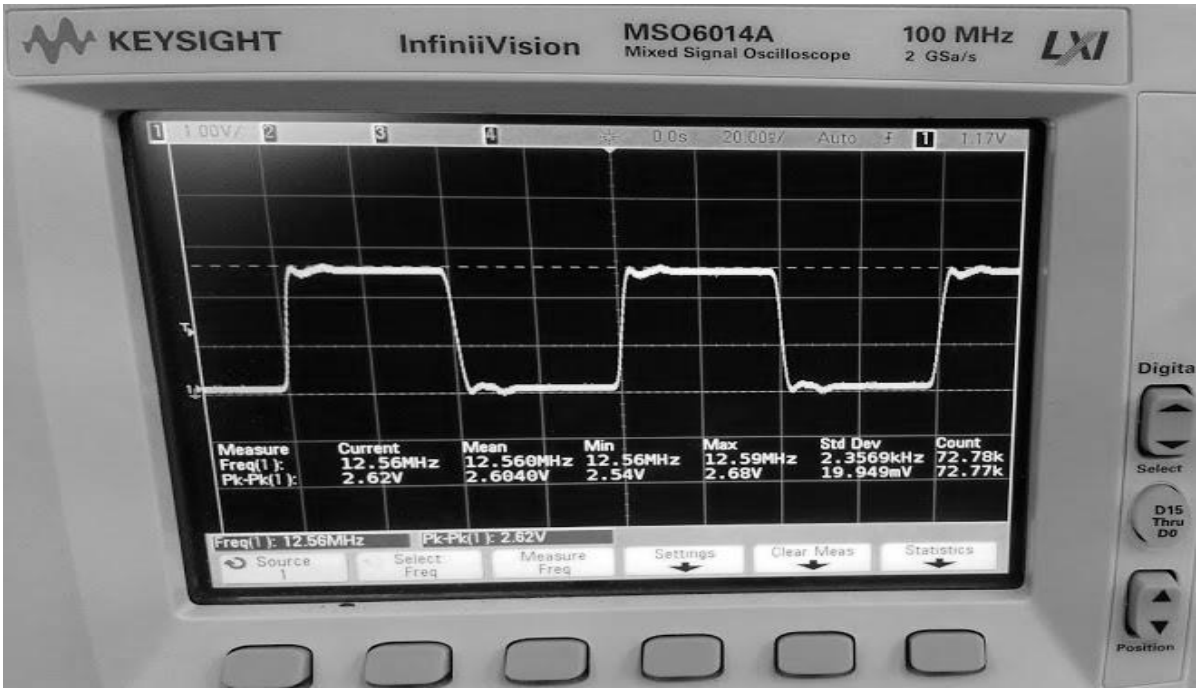

Figure 59: Oscilloscope displaying GPSDO output

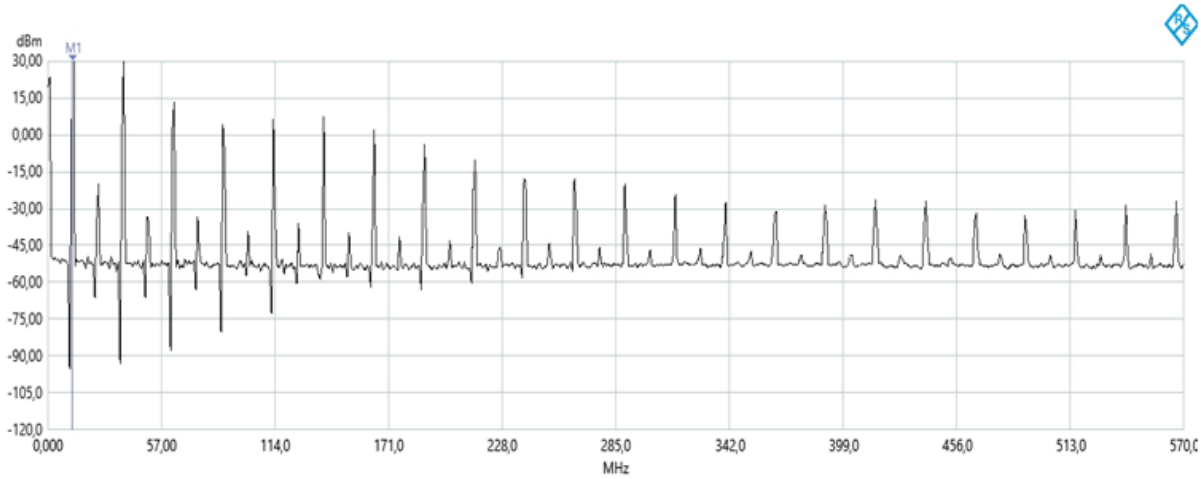

Figure 60: GPSDO power output spectrum displayed on the spectrum analyser

The measured output of the GPS disciplined oscillator, shown in Figure 60, is approximately 14 dBm at a frequency of 12.57 MHz and harmonics are observed as is expected from a square wave shaped signal. The filter is designed to minimise such harmonics.

4.2.2. Program execution

The PIC16F690 is utilised in this project to operate the transmitter in either continuous wave or Morse coded transmission. Figure 61 presents a flowchart of the code that is running on the PIC controller whenever is it switched on. The operation of the transmitter is looped to ensure the transmitter is always operational as it will be unattended.

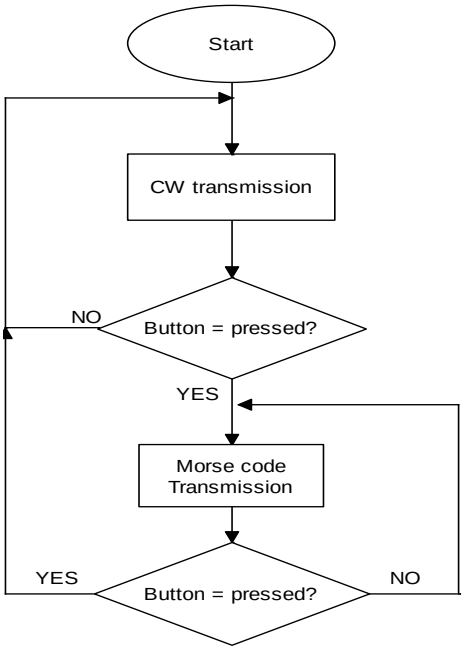

Figure 61: HF transmitter operation flow diagram

Some programming knowledge of embedded system software is necessary for this part as the programming language used for this project is C/C++. This is a general purpose programming language that was designed in favour of system programming and embedded systems.

For ease of programming and efficient use of time, it is best to write code in an integrated development environment (IDE) that supports a graphical user interface (GUI). An IDE is a software application that usually combines a debugger, build automation tools as well as a source code editing platform that provides facilities for software development to programmers. MPLAB X IDE is used in this project because it provides a single integrated "environment" to develop code for embedded microcontrollers. MPLAB X IDE runs on a PC to develop applications for Microchip microcontrollers and digital signal controllers. It supports various C/C++ compilers and some open source compilers, such as:

- MPLAB XC8, which supports 8-bit microcontrollers and is used for this project;
- MPLAB XC16, which supports 16-bit;
- HI-TECH C, which supports 8-bit microcontrollers; and
- Small Device C Compiler (SDCC), which is an open source programming software.

The programmer used for this project is a PICkit 3. PICkit is a range of programmers for PIC microcontrollers that Microchip developed to debug as well as program microcontrollers and EEPROMs.

Figure 62 shows a picture of a PICkit programmer and pin labels. The PICkit 3 programmer can also be used as a power supply for the microcontroller during programming, but this feature must be disabled when the chip is programmed in a circuit that has its own power source. The ability to program a chip in a live circuit is called in-system programming (ISP).

Figure 62: PICkit 3 and pin-out

4.2.2.1. Morse code execution

This stage of the circuit has mainly 2 purposes in this project, namely:

- to integrate the HF signal from the GPS oscillator with the control signal from the microcontroller to produce a Morse code encoded signal; and
- to pre-amplify the signal from the GPS oscillator.

Morse code is an information transmission method that is characterised by a series of on and off signals, such as tones, lights, clicks, etc. This form of encoding represents each ISO basic Latin alphabet with a standardized sequence of short and long signals that are called dots and dashes, respectively. Figure 63 shows the standard for encoding and decoding Morse code as defined by the International Telecommunications Union (ITU).

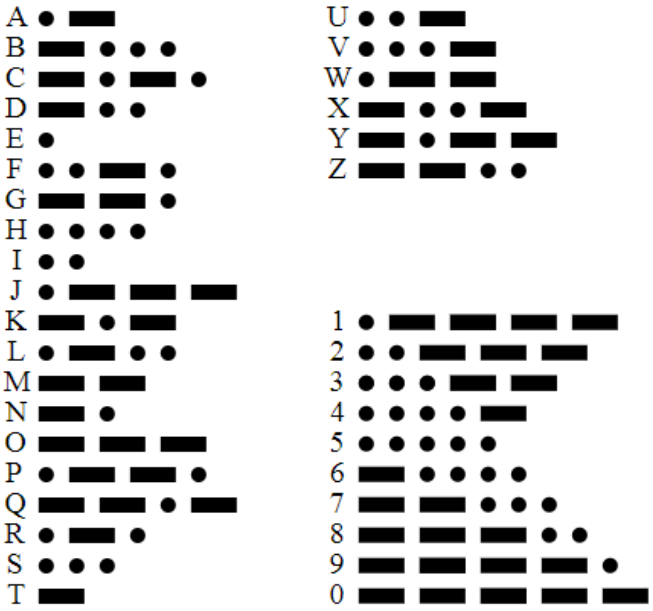

Figure 63: International Morse code character and number chart (ITU-R, 2009)

The guidelines for Morse code applications are as follows:

- the length of a dot is one unit;
- a dash is three units;
- the space between parts of the same letter is one unit;
- the space between letters is three units; and
- the space between words is seven units.

The output of the transceiver circuit is shown in Figure 64 as seen on an oscilloscope. This stage has two purposes in this project: to code the signal and to pre-amplify the signal from the GPS disciplined oscillator. This can be verified in Figure 65. The output power of this stage is recorded to be about 19 dBm, which is 5 dB above the input from the GPSDO. The purpose of pre-amplification has been achieved. The encoding of the RF signal has been achieved as can be seen in Figure 64.

Figure 66 shows a picture of the circuit implementation of this stage of the design.

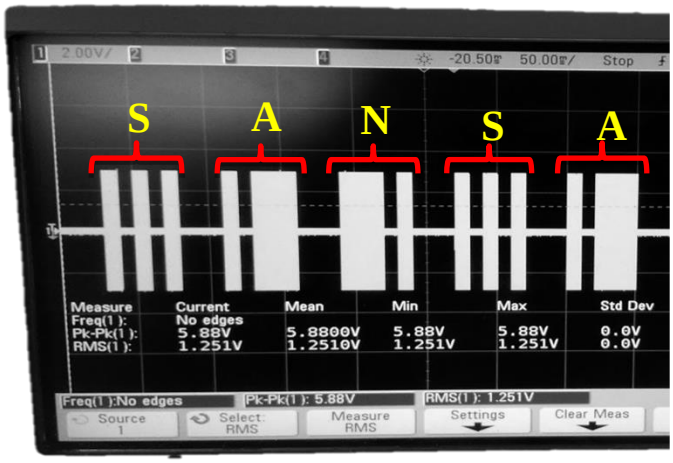

Figure 64: Morse coded RF signal from RI-R6C-001A

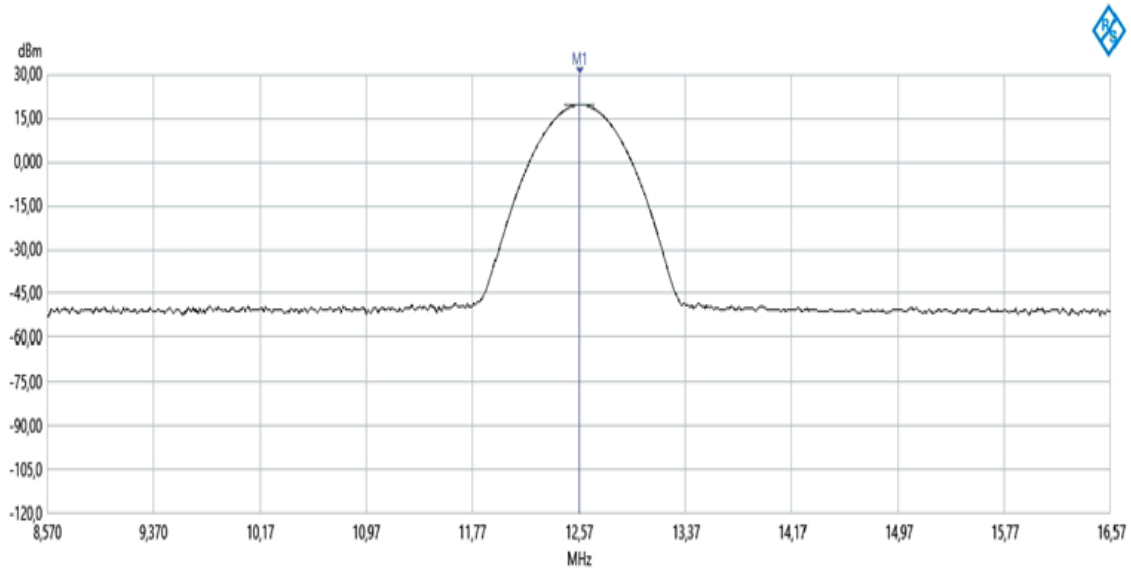

Figure 65: Output of the HF transceiver chip on the spectrum analyser

Figure 66: Morse controller section on a printed circuit board

4.2.3. Power amplifier

The power amplifier used in this project was adapted from an old SuperDARN radar transmitter circuit. It had been utilised as a pre-amplification circuit and it was decided that it would be suitable for the application. It was quickly noted that the power amplifier in use had limited efficiency but it was specified to meet the specifications of this project.

The measured output signal of the power amplifier is presented in Figure 67. The output was observed to be a pure sine wave up to an output level of 24 dBm, but distorted considerably towards 26 dBm. The distortion of the signal resulted in harmonics. This indicates that the amplifier is no longer operating in its linear region and that leads to a lot more power consumption without much notable difference in the output power at the fundamental frequency. It is therefore advisable to operate the transmitter in its linear region to avoid harmonic noise whenever possible. When a power level of 26 dBm is required, a low pass filter (LPF) can be used to minimise harmonics and their influence. The maximum gain of the power amplifier was recorded to be 7 dB at 12.57 MHz, and it achieved an efficiency of less than 20% at the nominal frequency.

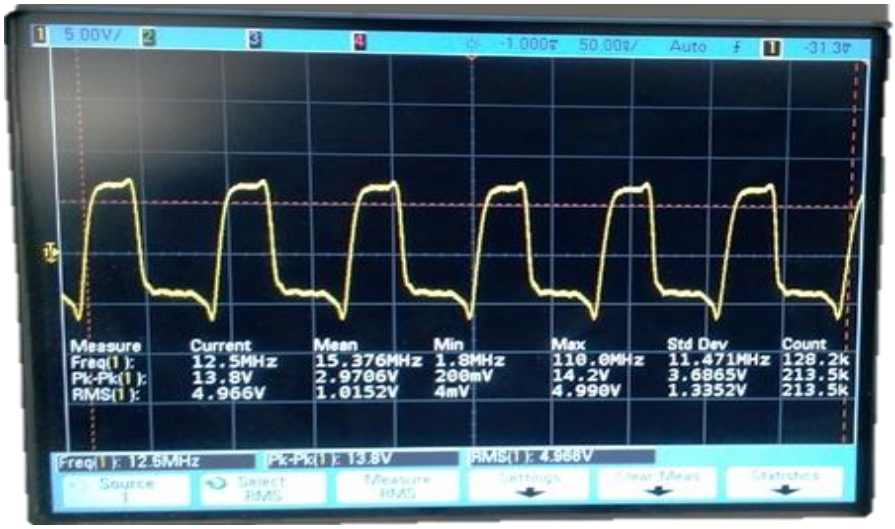

Figure 67: Output signal of the power amplifier

4.2.4. HF low pass filter

The low pass filter (LPF) used in this project was also taken from a decommissioned radar circuit. The filter circuit is rated to operate up to 20 MHz, which is the maximum frequency of SuperDARN radars.

Figure 68 shows the circuit configuration of the LPF that was utilised for this project, and its physical implementation on a PCB. The insertion loss of the filter was observed to be so low that it was considered negligible as it introduced no attenuation. The measured results obtained from the LPF are presented in Figure 69, and were obtained with a spectrum analyser.

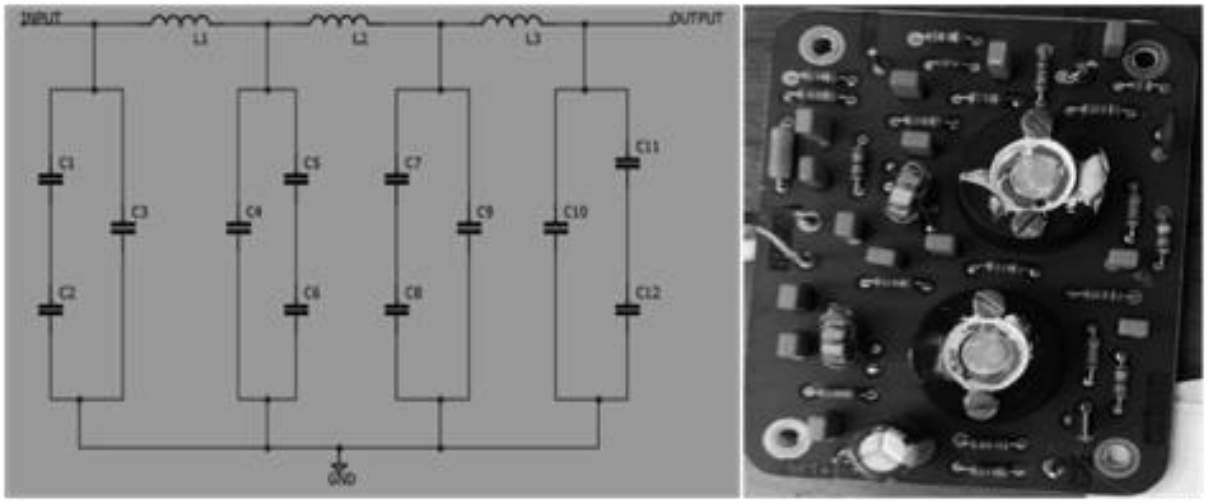

Figure 68: HF low pass filter

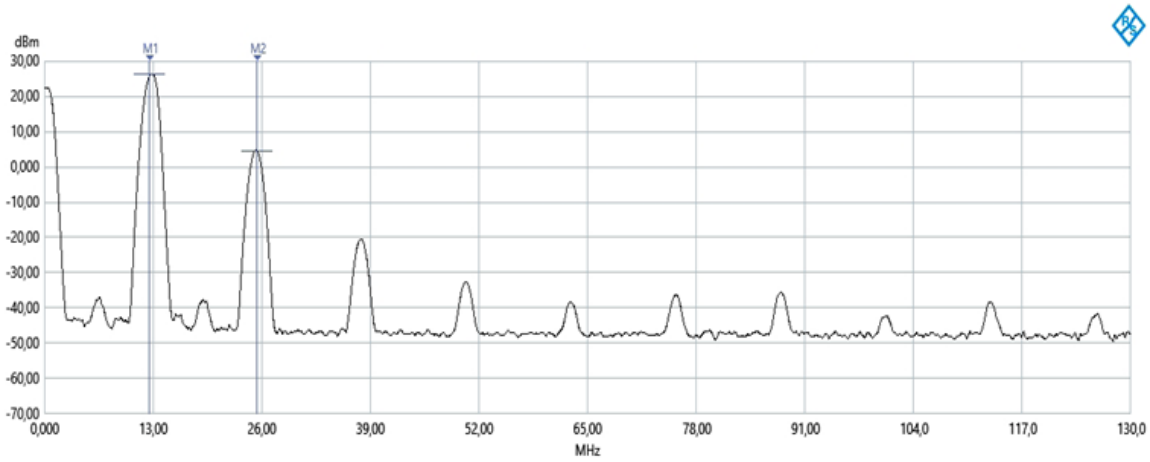

Figure 69: Output signal of the low pass filter

The output of the power amplifier was now observed to be sinusoidal up to 26 dBm with small harmonics, as expected. It may be observed that the power of the first harmonic of the operational frequency is more than 20 dB lower than the power of fundamental frequency signal.

4.3. PROPAGATION TESTS

Propagation tests were conducted in 2 different scenarios, which are discussed in the following sections.

4.3.1. Line-of-sight test

Line-of-sight tests are necessary for this project to demonstrate that the transmitter can operate with an actual HF antenna as a load. These tests were carried out at the Cape Peninsula University of Technology (CPUT) over a distance of 100m (about 4 wavelengths at the fundamental frequency).

Figure 70 shows how the two testing antennas were placed during the tests. The antennas used at CPUT have limited bandwidth and are tuned to 14.0999 MHz for a previous satellite

missions. The test was, therefore, carried out at 14.0999 MHz, which for the purpose of this test is close enough to 12.57 MHz that will be used during normal operations of the HF transmitter. The output power of the transmitter was set to 25 dBm. The output power of the transmitter was measured to be 25.36 dBm (see Figure 71). The VSWR of the transmit antennas used, is shown in Figure 72. It is measured to be 1.36 at the operating frequency.

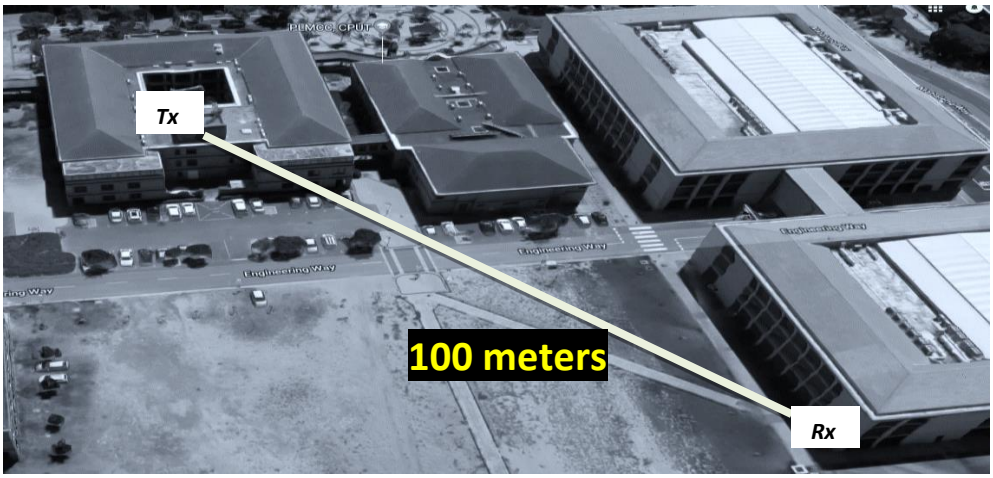

Figure 70: Antenna setup for line-of-sight tests

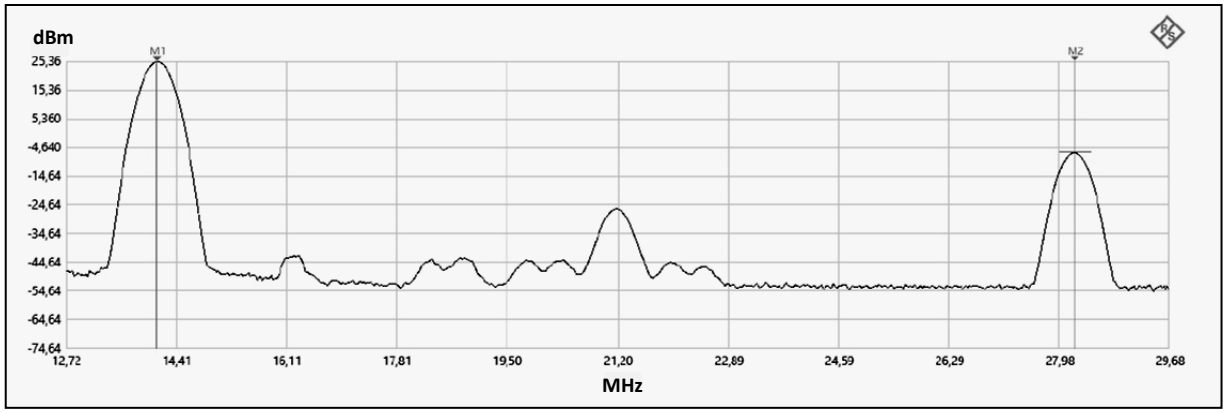

Figure 71: Power spectrum of the HF transmitter output

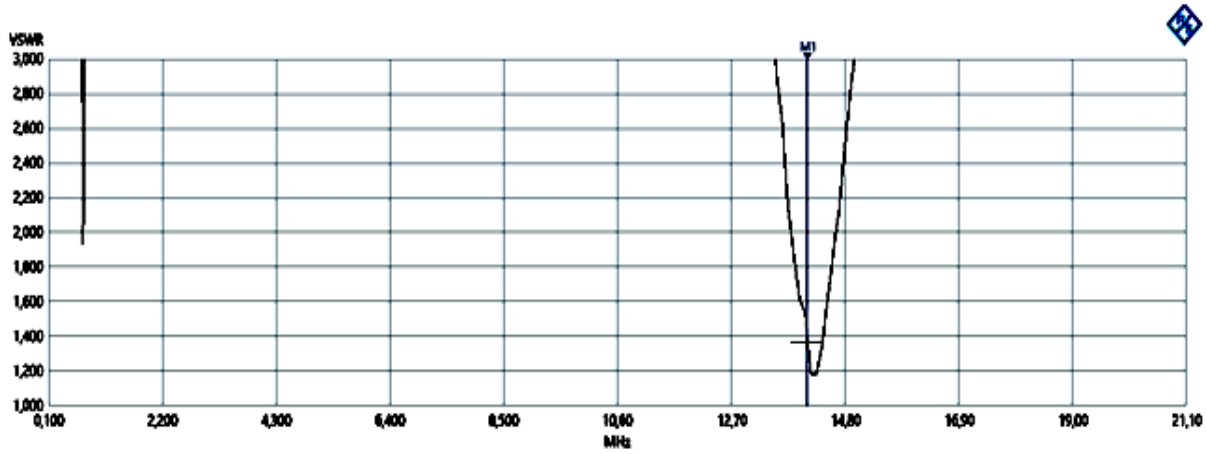

Figure 72: Transmitting dipole antenna measured VSWR

The measured VSWR presented in Figure 72 is as expected from the dipole. A similar dipole antenna with almost the same operational characteristics was used for reception during this experiment.

The received signal, measured with a spectrum analyser, is shown in Figure 73. The received power is -16 dBm at the fundamental frequency.

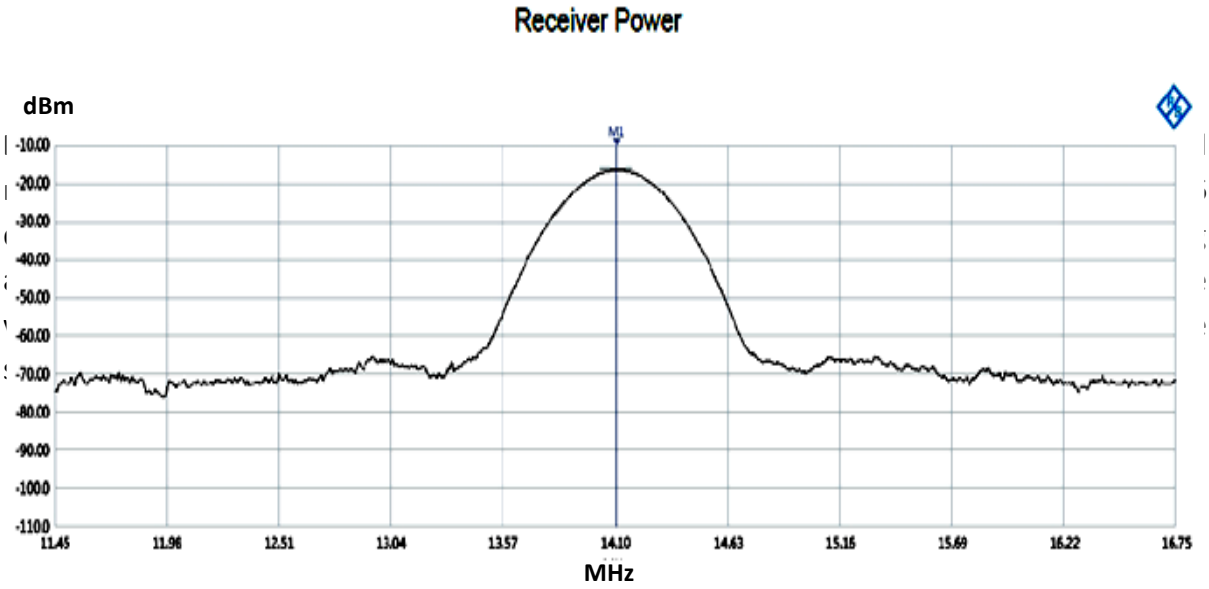

Figure 73: Received signal level at 100 meters

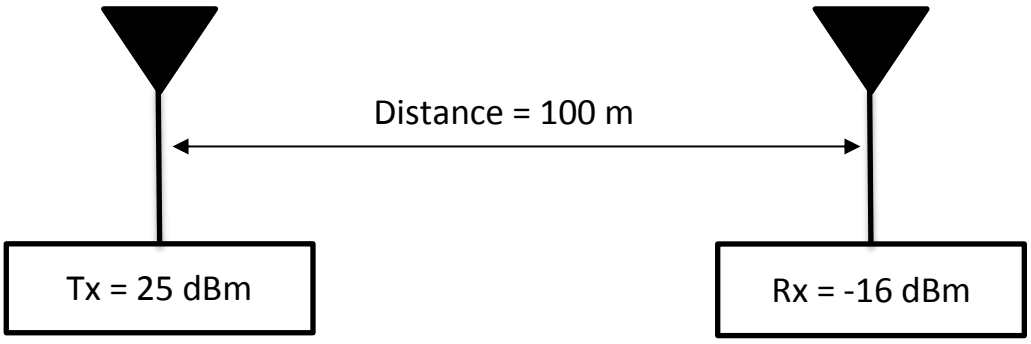

Figure 74: Block diagram representation of the line-of-sight test

The free space propagation loss for the test scenario in Figure 74 are given as:

$$FSPL = 32.45 + 20\ \log d_{km} + 20\ \log f_{MHz} = 34.4\ \text{dB}$$

And the theoretical total loss is given by:

$$L_T = FSPL + L_M = 34.4 + 7.3 = 41.7 \text{ dB}$$

Therefore, the received signal is given by equation (27) as:

$$P_{RX} = P_{TX} + G_{TX} - L_{Total} + G_{RX} = 25.36 + 1.8 - 41.7 + 1.8 = -12.74 \text{ dBm}$$

NB: The calculations above assume minimal cable, antenna and connector losses, and perfect radiation efficiency of both antennas, as well as perfect alignment.

The received signal is approximately 3 dB lower than the calculated value. This can be ascribed to imperfections of the link components. Also, the link budget equation applies to free space propagation and where the transmitter and receiver are removed by several wavelengths. In this case, the separation is only 4 wavelengths, and reflections from the ground and buildings can be expected.

4.3.2. Hermanus to Pretoria long-distance test

This propagation test is especially important for this project as it seeks to demonstrate the practical implementation of sky-wave communication, as well as to establish reasonable evidence of the success of the project. This test was conducted between a SANSA site at Hermanus, South Africa, and GEW Technologies, a company situated in Pretoria, South Africa. Before the tests were conducted, it was important to check the estimated optimal transmission frequencies of the day between the two sites to determine whether transmitting at 12.57 MHz would be supported during the course of the day.

As may be observed from Figure 75, the estimated lowest usable frequency (LUF) is well below 10 MHz the entire day. The maximum usable frequency (MUF) is above 15 MHz for most of the day. This means transmitting at 12.57 MHz on this day over this distance should be supported by the ionosphere. An omni-directional antenna that was already in place in Hermanus was utilised for this test; it is mounted approximately 20 m above ground. The sites are more than 1300 km apart with no line-of-sight path.

The performance of the antenna in the HF range is observed to be satisfactory; the VSWR of the antenna is displayed in Figure 76. A similar antenna was used for reception. The radiation pattern of the antennas in use is assumed to be similar to the radiation pattern in Figure 77.

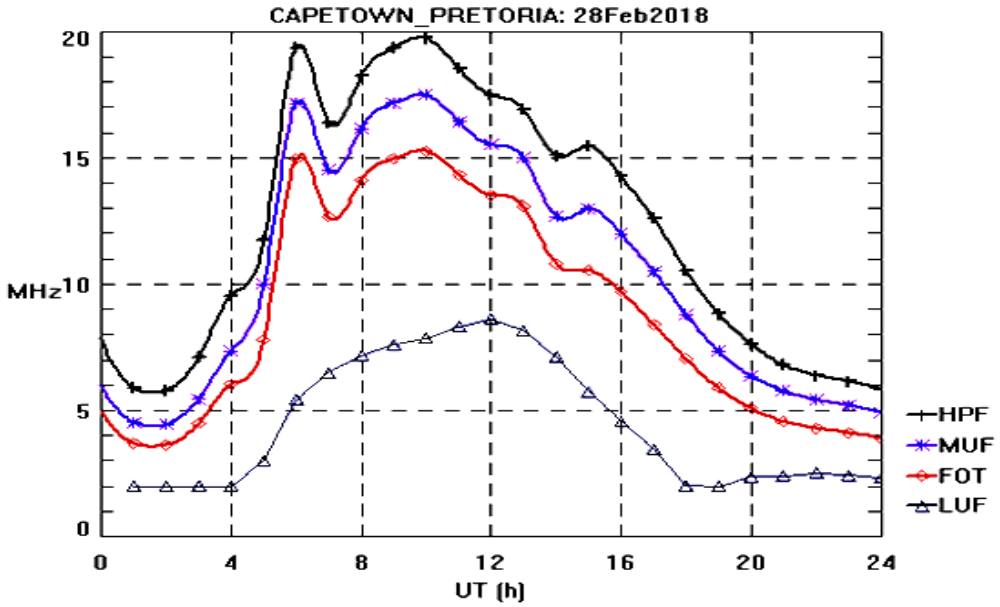

Figure 75: Estimated sky-wave frequencies between Pretoria and Cape Town/Hermanus adapted from SANSA online resources

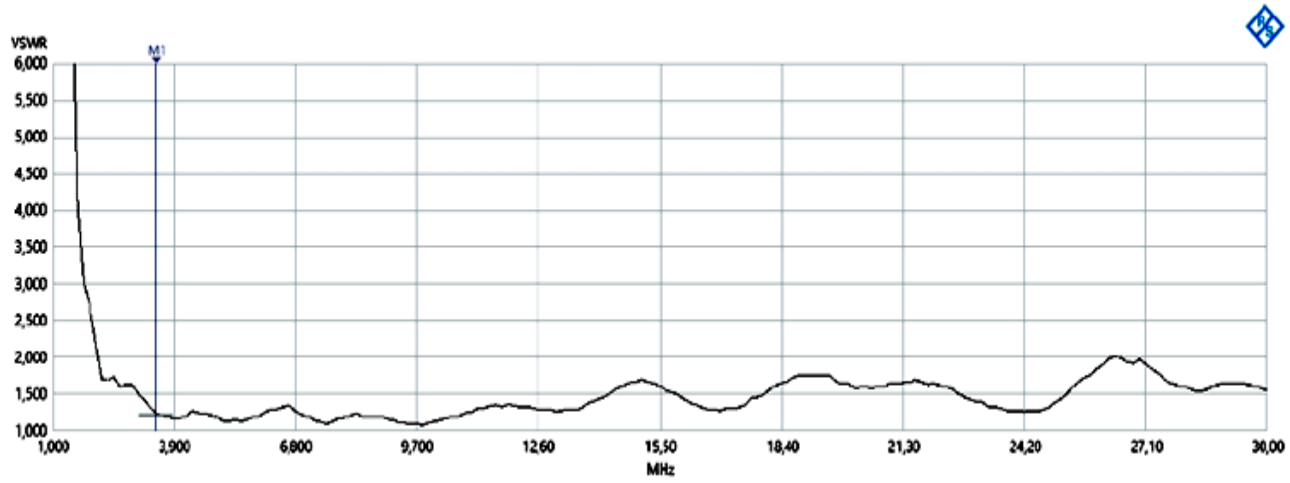

Figure 76: SWR of the transmitting antenna

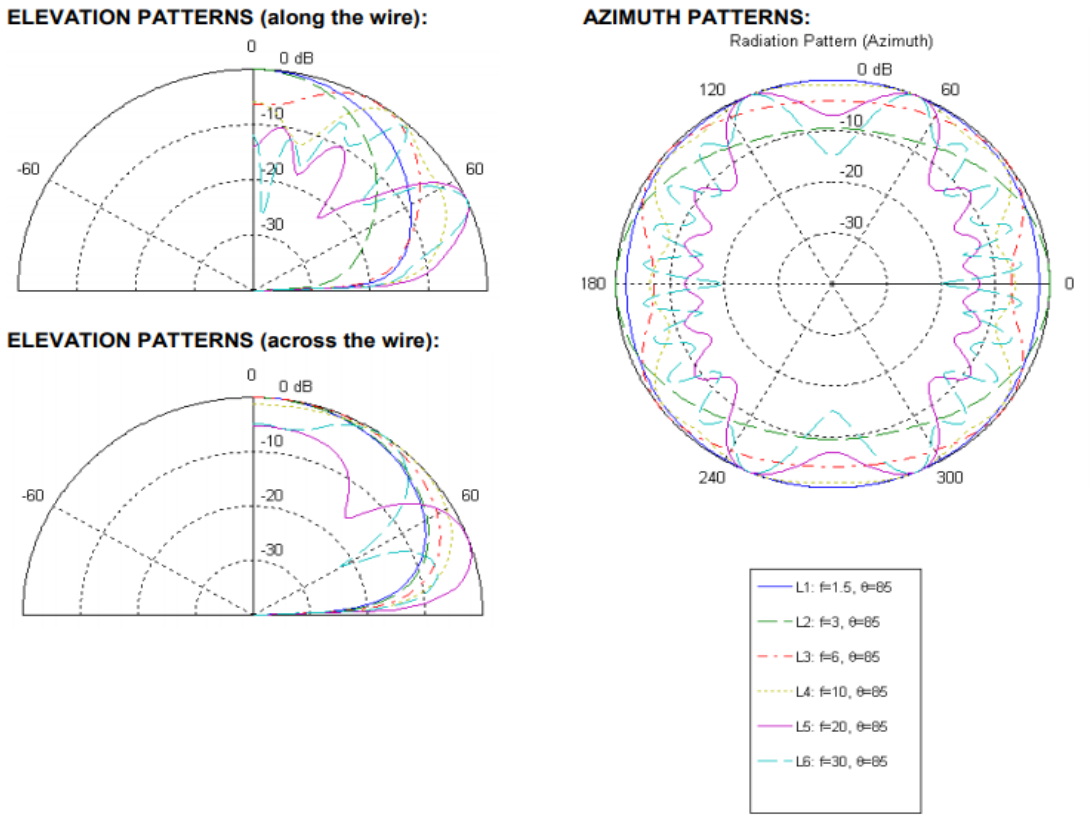

Figure 77: Radiation pattern of the transmitting and receiving antennas in the HF range (Adapted from Alaris antennas, 2017)

The receiver at Pretoria has the following specifications and settings:

- Receiver sensitivity: -124 dBm
- Signal to Noise Ratio: 10 dB
- Bandwidth: 2.7 kHz
- Noise Floor: -110 dBm

The signal received was rather faint; so much so that it was inaudible. It could only be observed on the spectral waterfall displayed on the radio at the receiving end. In order to prove that it was indeed the wanted signal being received, the transmitter was switched on and off several times; the received signal appeared and disappeared, respectively.

The approximate received signal level can be calculated from the link budget equation (27), and assuming omni-directional antennas with 0 dB gain and a propagation path of 1300 km:

$$P_{RX} = P_{TX} + G_{TX} - L_{Total} + G_{RX} = 25.36 + 0 - 117 - 7.3 + 0 = -98.94 \text{ dBm}$$

This is about 25 dBm above the sensitivity of the receiver and 11 dBm above the noise floor. The signal should, therefore, have been audible. However, a smaller signal would have been received in practice due to the following factors:

- The antennas is not perfectly omni-directional, and the gain may have been less than 0 dB in the transmit and receive elevations of the propagation path of the sky-wave.
- The fixed antennas could not be pointed at the desired elevation and azimuth angles to ensure maximum gain in the required direction for optimal transmission and reception. (It may also be observed from Appendix D that shorter distances require lower launching angles.)
- The sky-wave path would have been longer than the direct distance of 1300 km used in the above calculation. Also, the path close to Hermanus might have been obscured by mountains and the escarpment (see Figure 78).

These factors will explain the lower received signal than theoretically expected and for the signal to be inaudible but still observable in the spectrum waterfall of the received signal.

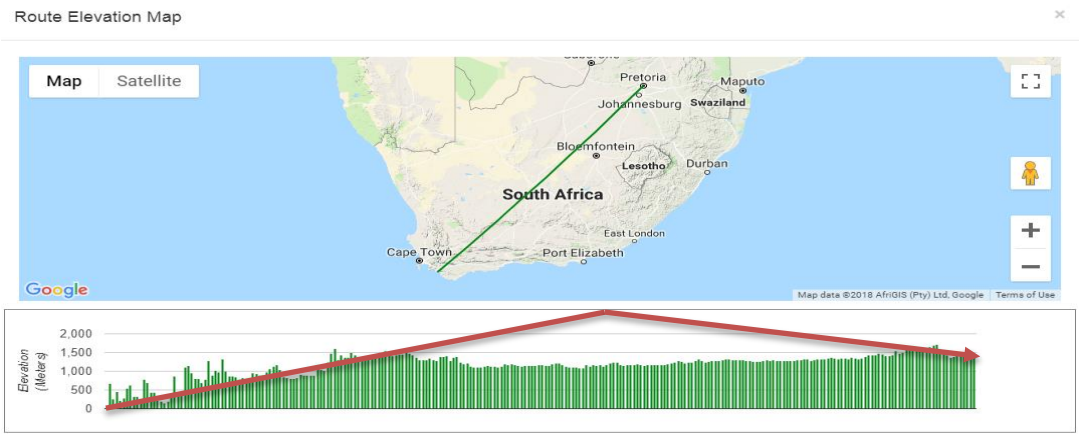

Figure 78: Distance and elevation between the transmitting and the receiving site

4.4. THERMAL TEST

Antarctica is located in a region that is colder than most areas since it is a high latitude region. Temperatures are expected to reach -40°C. It is, therefore, important to ensure that the device is able to operate in such conditions. The thermal test was carried out and the device is observed for any changes in terms of power and frequency of operation.

Figure 79: Setup for thermal test

Figure 79 shows the setup during the temperature test of the device. An environmental chamber is a device that can simulate environmental conditions, such as temperature,

humidity and pressure. In this project, temperature was the only parameter controlled to expose the DUT to different temperatures for several hours.

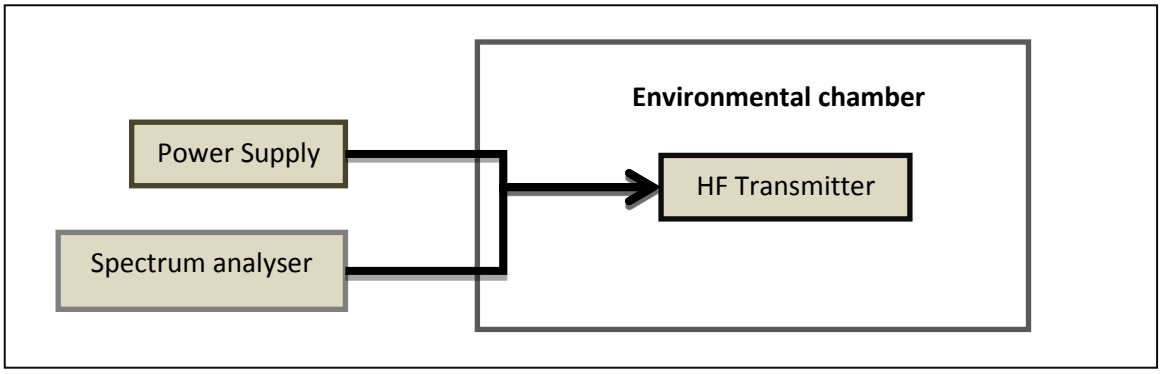

Figure 79: Setup for thermal test

During the experiment, the power supply and the measuring equipment were placed outside the environmental/thermal chamber. Only the device-under-test (DUT) and temperature sensor probes were placed inside the chamber as shown in the diagram in Figure 79.

The DUT was exposed to a range of temperatures between 40°C and -45°C (NB: -40°C is the specified value) as such negative temperatures are to be expected in Antarctica. It is a good engineering practice to test a device marginally past the specified values because conditions in the field are not always as expected. While the temperatures inside the chamber varied, the output performance of the devices was monitored for any changes in operational frequency and output power. The recorded temperature profile over 18 hours is presented in Figure 80. The data was recorded with Agilent data logging software.

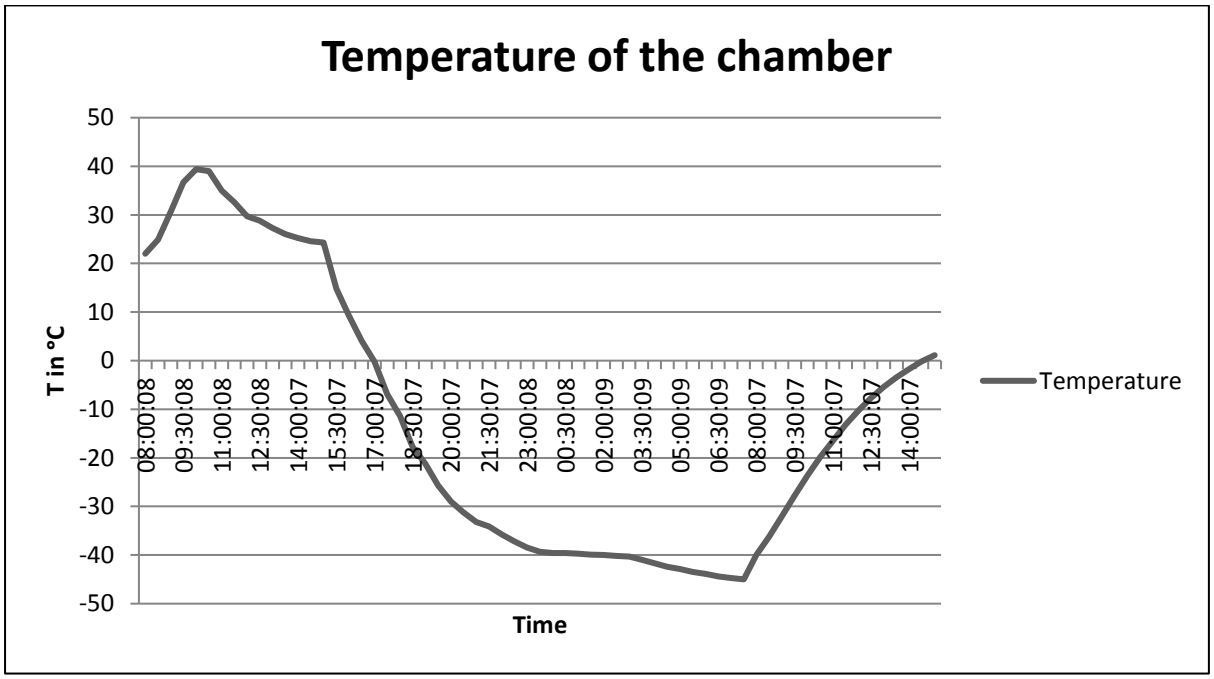

Figure 80: Recorded temperature profile of the chamber during tests

The output of the device was observed to be stable in terms of power as well as operating frequency over the full thermal cycle. Figure 81 presents the results displayed on the spectrum analyser during the entire period of the experiment. The output of the device was set to 24 dBm for the period of the test and no changes were observed. The frequency was as stable as the measuring equipment would allow as specified and mentioned earlier.

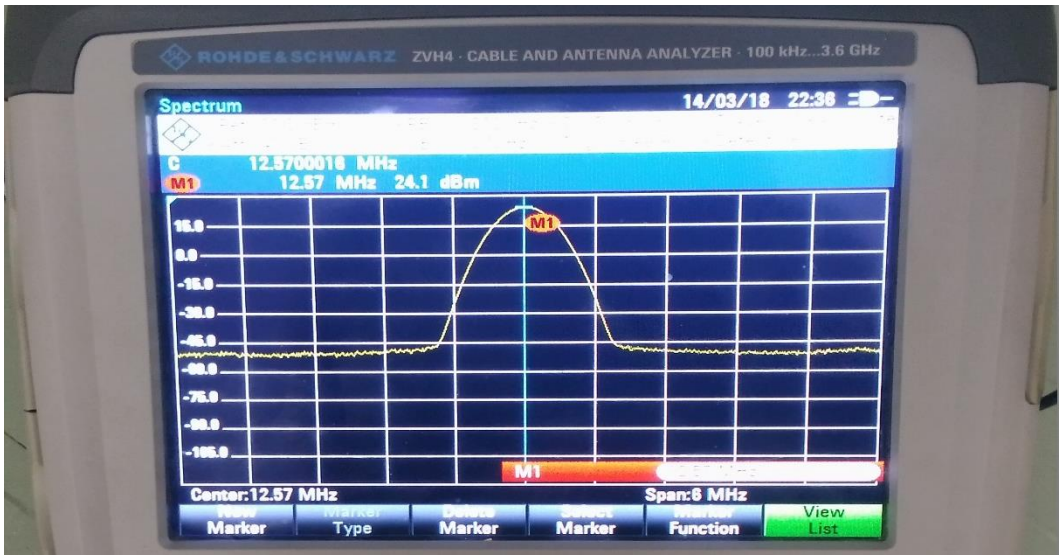

Figure 81: Output of the HF during temperature test displayed on the spectrum analyser

5.1. CONCLUSION

The primary objectives of the project, namely the design and verification of an HF transmitter, have been achieved. From Section 1.6, the transmitter had to meet the following specifications (repeated here):

- The device should be powered by a 12V DC supply.
- The output power of the device should be 100 mW at a maximum of 10 W input power.
- The device must operate over a range of 8 – 20 MHz with a nominal frequency of 12.57 MHz because the SuperDARN radar operates at this specific frequency.
- The device must operate in temperatures that range from -40 °C to 0 °C.
- The frequency of the device must be stable enough to achieve a Doppler shift observation better than 1 m/s for TID studies. This implies a maximum frequency offset of 41.8 mHz, or 3 parts-per-billion (ppb) at a nominal frequency of 12.57 MHz.
- The device must be able to transmit CW and Morse code signals.

A low cost HF beacon that has an output power of almost quadruple the specified power requirement and operates without any measurable power or frequency deviation between the temperature levels of 40^{o}C to -45^{o}C was designed, simulated and tested successfully in the laboratory and in the field.

Table 6 presents the specified and calculated values against the experimental values obtained with this project.

Table 6: HF transmitter experimental results

	Specified value	**Achieved device value**
Frequency stability	< 42 mHz @ 12.57 MHz or < 3 ppb	The average frequency offset of the GPSDO is specified to be of the order 1 ppb (see Figure 54) over time. This could, however, not be verified experimentally due to the available test equipment.
Output power	100 mW	≈ 400 mW
Operating Temperature	0^{o}C to -40^{o}C	40^{o}C to -45^{o}C

Several frequency clocks were studied and compared in order to achieve the minimum Doppler shift observation of 1 m/s as per the specification of the project, which was achieved and tested with the available equipment. The rest of the circuitry introduced no frequency

drift to the signal from the GPS disciplined oscillator used as a source clock. The frequency was observed to be stable when tested over a wide range of negative temperatures.

The propagation studies and link budgets were conducted with the data available to determine if sky-wave propagation will be possible in Antarctica. Experimental propagation test were conducted over a reasonable distance in South Africa. The elevation of the transmitting site and an obstacle in the direction of the receiving site presented a challenge during the propagation tests that resulted in the received signal being much weaker than expected.

The ionospheric research models available are rather limited when high latitude regions are considered. However, they were utilised in order to get some ionospheric data, such as gas concentrations required to determine the collision frequencies of the D layer. The electron density was also obtained from the estimations of the IRI model and are also assumed to be less accurate than desired. The use of the VITMO models was of some significance in determining the absorption levels expected in Antarctica. It should, however, be noted that these predicted values are expected to be different from the real values of the Antarctic ionosphere.

5.2. RECOMMENDATIONS

During the process of the project, several ways came up on how this project could be improved for different scenarios. These recommendations are mentioned below.

- When an external clock is used with an RI-R6C-001A chip where the maximum power output from the IC is required, a pre-amplifier must be placed between the output of the clock and the input of the RI-R6C-001A chip. The external oscillator used in this project provided a signal with a level of approximately 2.6 V peak-to-peak (see Figure 59) instead of the 5V peak-to-peak as for the input of the transceiver chip as specified by the chip manufacturer. This resulted in the transceiver chip being unable to produce the required maximum output of 200mW. This is, however, advantageous for this project as it has a power amplifier driven by the chip. Driving the power amplifier with more power would have simply resulted in more harmonics.
- A more efficient HF amplifier needs to be researched and designed for transmitters in the 1W – 10 W range for applications that require more power and simple operation. The amplifier in use for this project was adapted from an old radar system, which utilised it as a pre-amplifier for a 600 W transmitter. It is only suitable for this project because of the operational frequency range and the fact that its output power meets the power needs and specifications of this project.
- For experimental propagation tests, a transmitting station/site should be chosen to make sure that there are no obstacles that may impair propagation. The transmission site should be more elevated to avoid obstacles that may present a challenge for sky-

wave propagation, especially when it is not possible to adjust antenna radiation angles and direction.

- The calculations done for the link budget for the proposed deployment in Antarctica assumed a 10 dB transmitting antenna. A more directional HF antenna, such as a Yagi antenna, could be installed at the beacon at the South Pole. The South Pole is not a high wind location but accumulates snow at the rate of approximately 20 cm per year. This would not be a problem for a Yagi either as it can be mounted on a structure with good ground or ice clearance.

BIBLIOGRAPHY

Alaris antennas. (2017, 04 04). *Alaris antennas.* Retrieved 01 25, 2018, from http://www.alarisantennas.com/wp-content/uploads/2017/06/brochures/DIPL-A0056%20Version%203.4.pdf

Albulet, M. (1962). *RF Power Amplifiers.* Atlanta: Noble Publishing Corporation.

Alpers, W., & Huang, W. (2011, March). On the Discrimination of Radar Signatures of Atmospheric Gravity Waves and Oceanic Internal Waves on Synthetic Aperture Radar Images of the Sea Surface. *IEEE Transactions on Geoscience and Remote Sensing, 49*(3), 1114-1126.

Antenna Handbook MCRP 8-10B.11 . (2016).

Bahl, I. J. (2008). *Fundamentals of RF and Microwave Transistor Amplifiers.* Hoboken: John Wiley & Sons, Inc.

Baker, J. B. (2011). The Super Dual Auroral Radar Network (SuperDARN). Virginia: VT SuperDARN Group .

Baker, J. B., Ruohoniemi, J. M., Sheperd, S. G., McWilliams, K. A., Greenwald, R. A., & Bristow, W. A. (2008, August 7-16). Those DARN Radars: New Directions for the Super Dual Auroral Radar Network. *International Union of Radio Science*.

Bakshi, U. A., Bakshi, A. V., & Bakshi, K. A. (2008). *Antenna & Wave Propagation.* Pune: Technical Publications Pune.

Balthazor, R. L., & Moffett, R. J. (1997). A study of atmospheric gravity waves and travelling ionospheric disturbances at equatorial latitudes. *Annales Geophysicae*, 1048 - 1056.

Berngardt, O. I., Kutelev, K. A., Kurkin, V. I., Grkovich, K. V., Yampolsky, Y. M., Kashcheyev, A. S., . . . Kusonsky, O. A. (2015). BISTATIC SOUNDING OF HIGH-LATITUDE IONOSPHERIC IRREGULARITIES USING A DECAMETER EKB RADAR AND AN UTR-2 RADIO TELESCOPE: FIRST RESULTS. *Radiophysics and Quantum Electronics, 58*(6).

Bertrand, R. (2002, April). *Online Radio & Electronics Course.* Retrieved 06 25, 2017, from Propagation: http://www.radioelectronicschool.com/

Bevelacqua, P. J. (2015). *Friis Transmission Equation*. Retrieved 10 03, 2017, from http://www.antenna-theory.com/basics/friis.php

Breit, G., & Tuve, M. A. (1926). A Test of the Existence of the Conducting Layer. *American Physical Society*.

Bristow, W., & Greenwald, R. (1997, June 1). On the spectrum of thermosperic gravity waves observed by Super Dual Auroral Radar Network. *Journal of Geophysical Research, 102*, 11585 - 11595.

Cander, L. R., & Zolesi, B. (2013). *Ionospheric Prediction and Forecasting.* Springer Science & Business Media.

Carr, J. (2001). *The Technician's Radio Receiver Handbook: Wireless and Telecommunication Technology.* Newnes.

Chisham, G., Yeoman, T. K., & Sofko, G. J. (2008). Mapping ionospheric backscatter measured by the SuperDARN HF radars – Part 1: A new empirical virtual height model. *Annales Geophysicae, 26*, 823 - 841.

Coleman, D. D., & Westcott, D. A. (2006). *CWNA Certified Wireless Network Administrator Study Guide: (Exam PW0-100).* Indianopolis: Wiley Publishing Inc.
Cripps, S. C. (2006). *RF Power Amplifiers for Wireless Communications* (2nd ed.). Norwood: ARTECH HOUSE, INC.

Davies, K. (1965). *Ionospheric Radio Propagation.* Washington DC: National Bureau of Standards.

Dellinger , J. H. (1937, October). Sudden Disturbances of the Ionosphere. *Proceedings of the Institute of Radio Engineers, 25*(10), pp. 1253 - 1290.

Ding, F., Wan, W., Liu, L., Afraimovich, E. L., Voeykov, S. V., & Perevalova, N. P. (2008). A statistical study of large-scale traveling ionospheric disturbances observed by GPS TEC during major magnetic storms over the years 2003 - 2005. *JOURNAL OF GEOPHYSICAL RESEARCH*, 1-8.

Ellingson, S. W. (2016). *Radio Systems Engineering.* Cambridge: Cambridge University Press.

Faruque, S. (2017). *Popular Electronics*. Retrieved November 11, 2017, from https://popularelectronics.technicacuriosa.com/2017/03/08/radio-frequency-modulation-made-easy/

Floyd, T. L. (2000). *Electronic Devices* (5th ed.). (L. Ludewig, Ed.) London: Prentice-Hall International (UK) Limited.

Freeman, R. L. (1999). *Fundamentals of Telecommunications.* New York: John Wiley & Sons, Inc.

Goodman, J. M. (2006). *space weather & telecommunications* (Vol. 782). Alexandria: Springer Science & Business Media.

Graham, A. (2011). *Communications, Radar and Electronic Warfare.* West Sussex: John Wiley and Sons Ltd.

Grebennikov, A. (2007). *RF and Microwave Transistor Oscillator Design.* Chichester: John Wiley & Sons.

Green, D. (1978). *Radio System TEC level 2.* Pitman Publishing.

Harden, P. (2005). Solar Activity & HF Propagation. *FDIM Symposium*, (pp. 81-88). Dayton Hamvention.

Harris, T., Cervera, M., & Meehan, D. H. (2012). Investigations into Small-Scale Disturbances in the Ionosphere Using SpICE. *Journal of Physical Research, 117*, 1 - 12.

Hickey, M. P. (2011). Atmospheric Gravity Waves and Effects in the Upper Atmosphere Associated with Tsunamis. *Cdn.Intechweb.Org*, 667 - 690.

Hocking, W. K. (2001, January 10). *Western University*. Retrieved 10 30, 2017, from Buoyancy (gravity) waves in the atmosphere: http://www.physics.uwo.ca/~whocking/p103/grav_wav.html

Hum, S. V. (2007). *University of toronto.* Retrieved 09 2017, from ECE422 Radio and Microwave Wireless Systems: http://www.waves.utoronto.ca

Hunsucker, R. D., & Hargreaves, J. K. (2003). *The High-Latitude Ionosphere and it's Effects on Radio propagation.* Cambridge: The Press Syndicate of the University of Cambridge.
INGV Roma2 | ionosphere. (1999). Retrieved January 29, 2018, from http://roma2.rm.ingv.it/en/research_areas

Issakov, V. (2010). *Microwave Circuits for 24 GHz Automotive Radar in Silicon-based Technologies.* London: Springer Science & Business Media.
ITU-R. (2009, October). *International Morse code.* Retrieved February 15, 2018, from https://www.itu.int/dms_pubrec/itu-r/rec/m/R-REC-M.1677-1-200910-I%21%21PDF-E.pdf

Jackman, S. M., Swartz, M., Burton, M., & Head, T. W. (2011). *CWDP Certified Wireless Design Professional Official Study Guide: Exam PW0-250.* John Wiley & Sons.

Jenkins, B., Jarvis, M. J., & Forbes, D. M. (1998). Mesospheric wind observations derived from Super Dual Auroral Radar Network (SuperDARN) HF radar meteor echoes at Halley, Antarctica: Preliminary results . *Radio Science, 33*(4), 957 - 965.

Johnsen, T., & Olsen, K. E. (2006). *Bi- and Multistatic Radar Terje.* Kjeller: Norwegian Defence Research Establishment.

Khoder, K. (2014). Monitoring of ionosphere propagation conditions using opportunistic HF signals. The Hague: IEEE.

Kulpa, K. (2005). CONTINUOUS WAVE RADARS–MONOSTATIC, MULTISTATIC AND NETWORK. *Advances in Sensing with Security Applications.* Tuscany: NATO Advanced Study Insitute.

Lanzerotti, L. J. (2013). *Space Weather Effects on Technologies.* (H. J. P. Song, Ed.) Washington, D. C: American Geophysical Union.

Lee, J. G. (1991). *An introduction to Radio Wave Propagation.* London: Bernard Babani Ltd.

Malindi, P. (2013, November). *Doc Malindi.* Retrieved September 13, 2017, from Publications: https://doc.malindi.co.za

Masinde Muliro University of Science and Technology. (1999). Retrieved December 12, 2017, from http://mmust.elimu.net/BSC(ELEC_COMM)/Year_4/ECE%20451%20L_Radar_Eng_and_Facsimile/Introduction_to_Radar/Introduction_to_Radar.htm

Maslin, N. M. (2003). *HF Communications: A Systems Approach.* CRC Press.

Mitchell, C. N., Rankov, N. R., Bust, G. S., Miller, E., Gaussiran, T., Calfas, R., . . . Dekine, I. (2017). Ionospheric data assimilation applied to HF geolocation in the presence of traveling ionospheric disturbances. *Radio Science*, 829 - 840.

Ogawa, T., Nishitani, N., Otsuka, Y., Shiokawa, K., Tsugawa, T., & Hosokawa, K. (2009). Medium-scale traveling ionospheric disturbances observed with the SuperDARN Hokkaido radar, all-sky imager, and GPS network and their relation to concurrent sporadic E irregularities. *JOURNAL OF GEOPHYSICAL RESEARCH, 114*(A3). doi:10.1024/2008JA013893

Oshiorenoya, A. E. (2004, July). Plasma in the Ionosphere Ionization and. Umea, Sweden.

Owens, J. E. (2004). *Ionospheric sounding using a modified frequency chirp.* New York.

Patrick, D. R., & Fardo, S. W. (2008). *Electricity and Electronics* (2nd ed.). Lilburn: The Fairmont Press Inc.

Podlesnyi, A. V., Kurkin, V. I., Laryunin, O. A., Pezhemskaya, M. D., & Chistyakova, L. V. (2014). *Studying travelling ionospheric disturbances from near-vertical ionosphere sounding with high temporal resolution.* Beijing: IEEE.

Poole, I. (1999). *Radio Waves and the Ionosphere.* Burlington: Newnes.

Poole, I. (2016). *Electronics notes*. Retrieved July 01, 2017, from Ionospheric Absorption of Radio Signals: www.electronics-notes.com

Riley, W. J. (2016, May 23). *Leo Bodnar Electronics Ltd.* Retrieved November 30, 2017, from http://www.leobodnar.com

Rishbeth, H. (1989). Surface Wave Propagation. In M. P. Hall, & L. W. Barclay, *Radiowave Propagation* (pp. 75-94). London: Peter Peregrinus Ltd.
Scientific, C. (2016). Retrieved March 16, 2017, from Campbell Scientific: https://s.campbellsci.com/documents/us/technical-papers/link-budget.pdf

Senior, A., Kosch, M. J., Yeoman, T. K., Rietveld, M. T., & McCrea, I. W. (2006). Effects of high-latitude atmospheric gravity wave disturbances on artificial HF radar backscatter. *Annales Geophysicae*, 2347 - 2361.

Senior, J. M. (2009). *Optical Fiber Communications Principles and Practice* (3rd ed.). Essex: Pearson Education Limited.

Seybold, J. S. (2005). *Introduction to RF Propagation.* New Jersey: John Wiley & Sons, Inc.

Sharma, D. K., Mishra, A., & Saxena, R. (2010). Analog & Digital Modulation Techniques: An Overview. *International Journal of Computing Science and Communication Technologies, III*, 551 - 561.

Shepherd, S. G. (2017, August 14). Elevation angle determination for SuperDARN HF radar layouts. *Radio Science, 52*(8), 938-950.

Silver , H. W. (2008). *The ARRL Extra Class License Manual for Ham Radio.* (M. Wilson, Ed.) American Radio Relay League.

Silver, H. W., Ford, S. R., & Wilson, M. J. (Eds.). (2013). *The ARRL Handbook for Radio Communications* (90 ed.). Newington: American Radio Relay League.

Singh, A., Shah, V., & Sarnaik, A. (2013). Moving Target Indication Radar. *International Journal of Student Research in Technology & Management, 1*(1), 27-38.

Sisodia, M. L., Gupta, V. L., & Agrawal, J. P. (2011). *Microwave and Radar Engineering* (1st ed.). Jaipur: Anshan.

Sklar, B. (1997). Rayleigh fading channels in mobile digital communication systems. I. Characterization. IEEE.
Space weather impacts. (2016). Retrieved June 27, 2016, from https://www.metoffice.gov.uk/services/public-sector/emergencies

Straw, R. D. (Ed.). (1997). *THE ARRL ANTENNA BOOK* (18th ed.). Newington, Connecticut: The American Radio Relay League, Inc.

Tang, J. (2015). Unlocking Potentials of Microwaves for Food Safety and Quality. *Journal of Food Science, 80*(8), 1776 - 1793.

Terman, F. E. (1943). *Radio Engineering Handbook* (1st ed.). New York: McGraw-Hill Book Company inc.

Texas Instruments. (2005). *HF Reader System Series 6000*. Retrieved July 23, 2017, from http://e2e.ti.com/support/wireless_connectivity

Tolstikov, M., Medvedev, A., & Ratovsky, K. (2012). METHOD OF RECONSTRUCTION OF WAVE FRONT OF TRAVELING. *Mathematical Methods in Electromagnetic Theory* (pp. 573-574). Kyiv: IEEE.

Walker, J. L. (Ed.). (2011). *Handbook of RF and Microwave Power Amplifiers.* New York: Cambridge University Press.

Weston, D. A. (2001). *Electromagnetic Compatibility: Principles and Applications, Second Edition .* New York: Marcel Decker Inc.

Whitaker, J. C. (Ed.). (1996). *The Electronics Handbook.* CRC Press.

Willis, N. J., & Griffiths, H. D. (Eds.). (2007). *Advances in Bistatic Radar.* SciTech Publishing Inc.

Wilson, M. J., & Ford, S. R. (Eds.). (2009). *The ARRL Handbook for Radio Communications.* Newington: ARRL- The National Association for Amateur Radio.

Wirth, A., & Hofer, L. (2017). *Gravity Waves*. Retrieved October 8, 2017, from http://www.eumetrain.org/resources

Zolesi, B., & Cander, L. R. (2014). *Ionospheric Prediction and Forecasting.* New York: Springer Science and Business Media.

APPENDICES

Appendix A: Season variation of South Pole

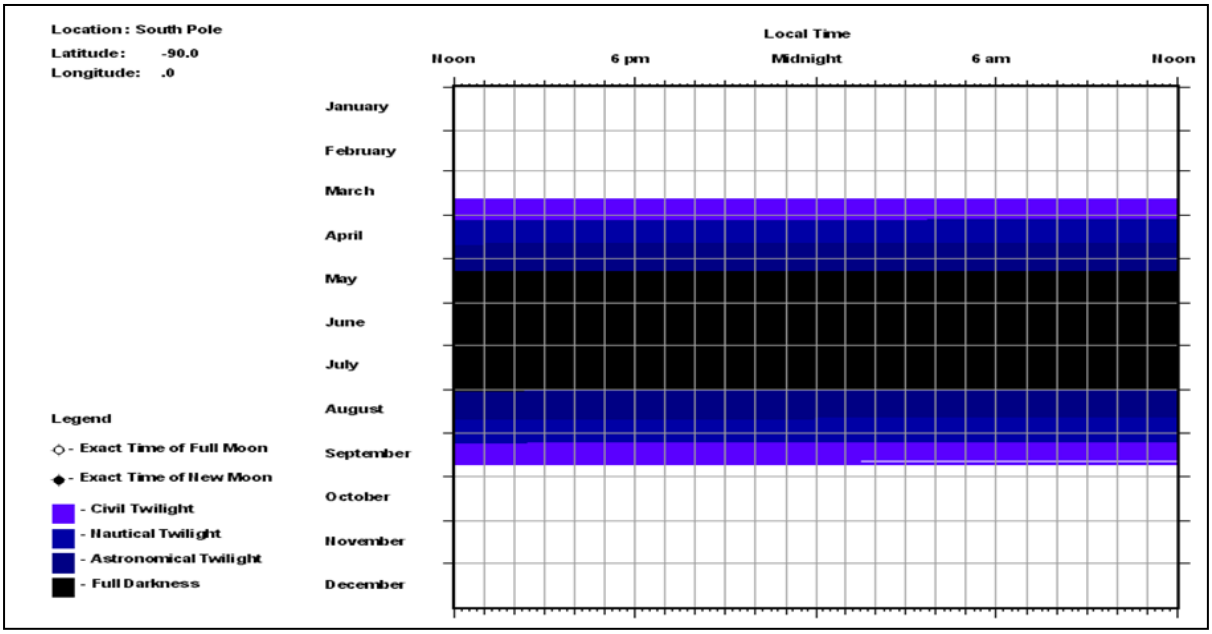

Appendix B: Direction of radiation for the HF beacon.

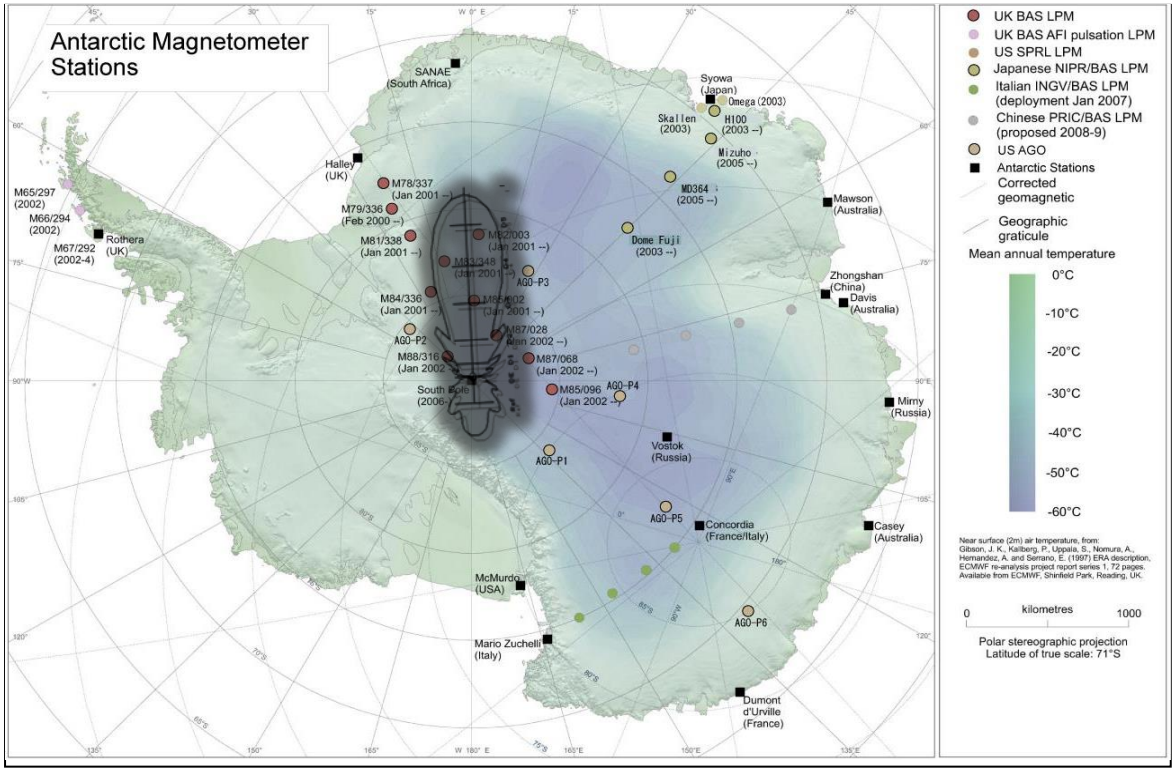

Appendix C:

1. SuperDARN network that currently exists in both hemispheres

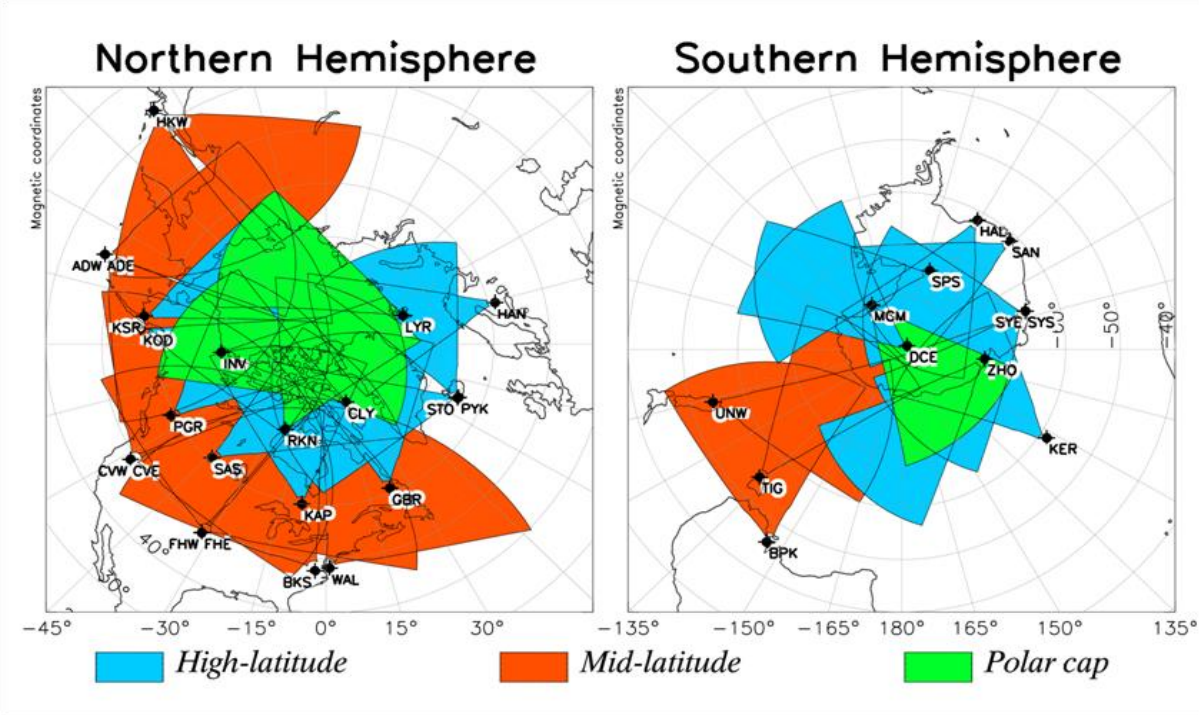

2. Beam 6 of the SuperDARN radar at SANAE pointing towards South Pole

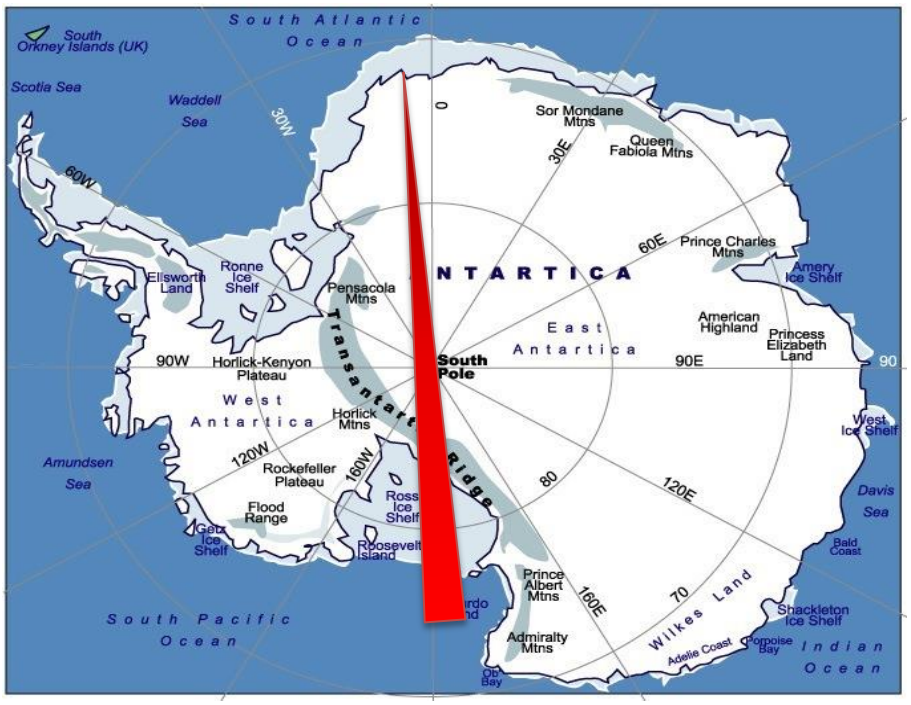

Appendix D:

1. Online ray tracer illustrating ray propagation between SANAE and South Pole during summer

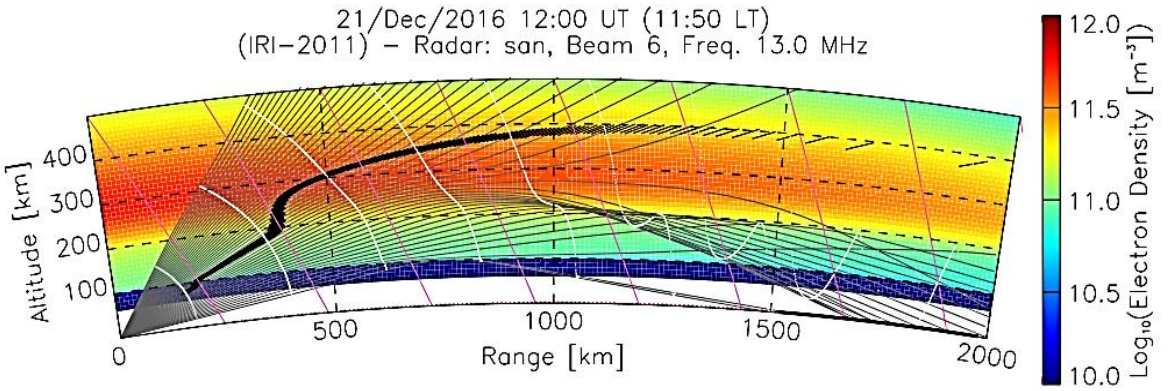

2. Online ray tracer illustrating ray propagation between SANAE and South Pole in winter

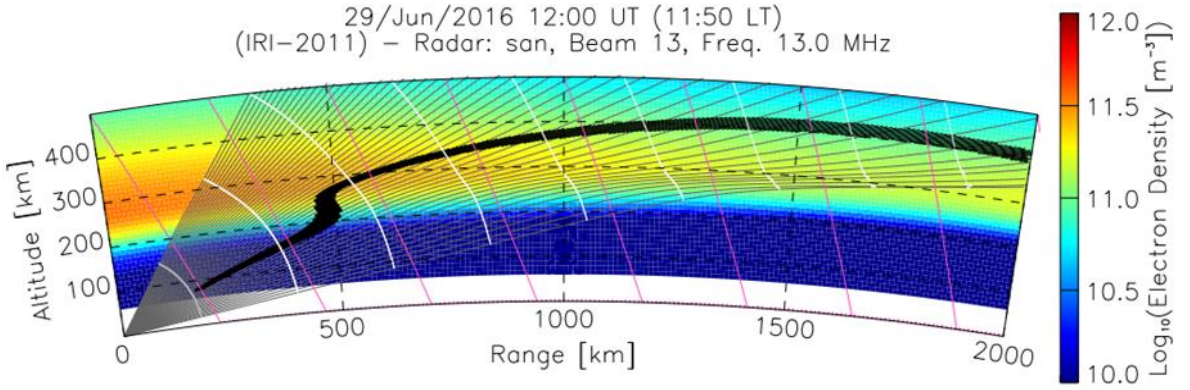

3. Online ray tracer illustrating ray propagation between SANAE and South Pole during Equinox

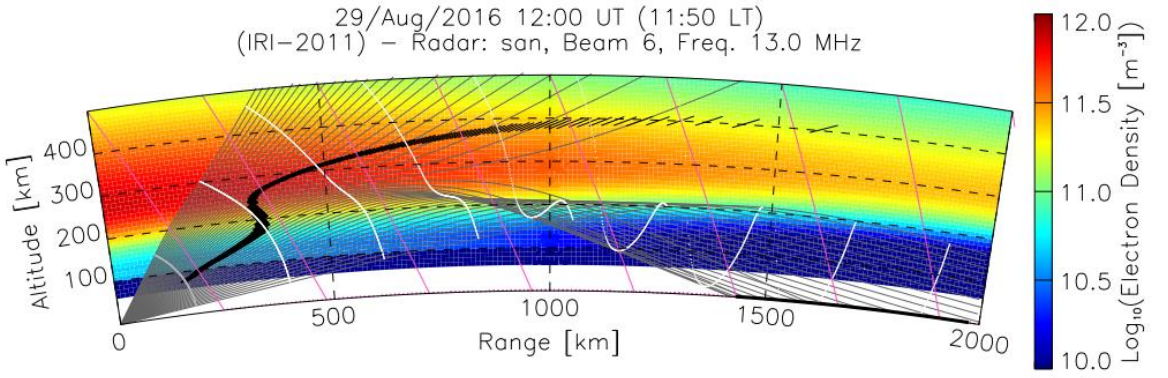

Appendix E:

1. Pin Description of the RI-R6C-001A transceiver IC

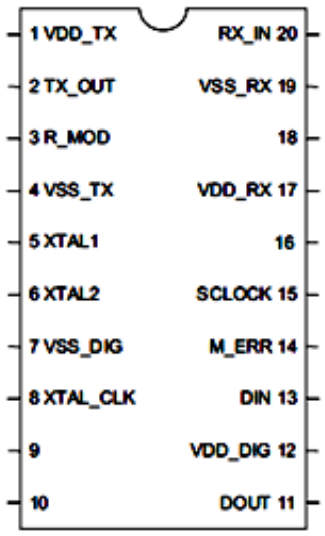

PIN NUMBER	SIGNAL NAME	DESCRIPTION
1	VDD_TX	Transmitter power supply
2	TX_OUT	Output transistor drain connection
3	R_MOD	External resistor to set 10% modulation depth mode
4	VSS_TX	Transmitter section ground
5	XTAL1	Pin 1 of Xtal resonator
6	XTAL2	Pin 2 of Xtal resonator and external system clock input
7	VSS_DIG	Digital section ground
8	XTAL_CLK	Buffered output of Xtal oscillator
9	not used	Grounded for normal operation
10	not used	Grounded for normal operation
11	DOUT	Data output for serial link
12	VDD_DIG	Digital section power supply
13	DIN	Data input for serial link
14	M_ERR	Manchester Protocol error flag
15	SCLOCK	Serial link clock
16	not used	Leave open for normal operation
17	VDD_RX	Receiver section power supply
18	not used	Leave open for normal operation
19	VSS_RX	Receiver section ground
20	RX_IN	Receiver input

2. Timing description of the transceiver

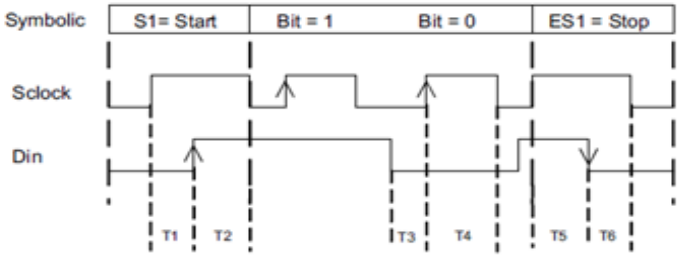

Minimum timings

T1: 300ns T4: 600ns
T2: 300ns T5: 300ns
T3: 66ns T6: 300ns

Definition of Start (S1), Stop (ES1) and Data Bit

Start, stop, and data are indicated by the sequences:

- Start (S1) is defined as the start of the communication sequence between the Transceiver IC and the micro-controller. It is a low-to-high transition on the DIN line while SCLOCK is held high.
- Stop (ES1) is defined as the end of the communication sequence and is a high-to-low transition on the DIN line while SCLOCK is held high.
- Each data bit is latched by the rising edge of SCLOCK. The value of the data bit must be settled and has to remain the same while SCLOCK is high.
- The data on DIN can be changed while SCLOCK is low.

Appendix F: Pin description of a PIC16F690

Name	Function	Input Type	Output Type	Description
RA0/AN0/C1IN+/ICSPDAT/ ULPWU	RA0	TTL	CMOS	General purpose I/O. Individually controlled interrupt-on-change. Individually enabled pull-up.
	AN0	AN	—	A/D Channel 0 input.
	C1IN+	AN	—	Comparator C1 positive input.
	ICSPDAT	TTL	CMOS	ICSP™ Data I/O.
	ULPWU	AN	—	Ultra Low-Power Wake-up input.
RA1/AN1/C12IN0-/VREF/ICSPCLK	RA1	TTL	CMOS	General purpose I/O. Individually controlled interrupt-on-change. Individually enabled pull-up.
	AN1	AN	—	A/D Channel 1 input.
	C12IN0-	AN	—	Comparator C1 or C2 negative input.
	VREF	AN	—	External Voltage Reference for A/D.
	ICSPCLK	ST	—	ICSP™ clock.
RA2/AN2/T0CKI/INT/C1OUT	RA2	ST	CMOS	General purpose I/O. Individually controlled interrupt-on-change. Individually enabled pull-up.
	AN2	AN	—	A/D Channel 2 input.
	T0CKI	ST	—	Timer0 clock input.
	INT	ST	—	External interrupt.
	C1OUT	—	CMOS	Comparator C1 output.
RA3/$\overline{\text{MCLR}}$/VPP	RA3	TTL	—	General purpose input. Individually controlled interrupt-on-change.
	$\overline{\text{MCLR}}$	ST	—	Master Clear with internal pull-up.
	VPP	HV	—	Programming voltage.
RA4/AN3/$\overline{\text{T1G}}$/OSC2/CLKOUT	RA4	TTL	CMOS	General purpose I/O. Individually controlled interrupt-on-change. Individually enabled pull-up.
	AN3	AN	—	A/D Channel 3 input.
	$\overline{\text{T1G}}$	ST	—	Timer1 gate input.
	OSC2	—	XTAL	Crystal/Resonator.
	CLKOUT	—	CMOS	FOSC/4 output.
RA5/T1CKI/OSC1/CLKIN	RA5	TTL	CMOS	General purpose I/O. Individually controlled interrupt-on-change. Individually enabled pull-up.
	T1CKI	ST	—	Timer1 clock input.
	OSC1	XTAL	—	Crystal/Resonator.
	CLKIN	ST	—	External clock input/RC oscillator connection.
RB4/AN10/SDI/SDA	RB4	TTL	CMOS	General purpose I/O. Individually controlled interrupt-on-change. Individually enabled pull-up.
	AN10	AN	—	A/D Channel 10 input.
	SDI	ST	—	SPI data input.
	SDA	ST	OD	I^2C™ data input/output.
RB5/AN11/RX/DT	RB5	TTL	CMOS	General purpose I/O. Individually controlled interrupt-on-change. Individually enabled pull-up.
	AN11	AN	—	A/D Channel 11 input.
	RX	ST	—	EUSART asynchronous input.
	DT	ST	CMOS	EUSART synchronous data.

Legend: AN = Analog input or output; CMOS = CMOS compatible input or output; OD = Open Drain
TTL = TTL compatible input; ST = Schmitt Trigger input with CMOS levels
HV = High Voltage; XTAL = Crystal

Name	Function	Input Type	Output Type	Description
RB6/SCK/SCL	RB6	TTL	CMOS	General purpose I/O. Individually controlled interrupt-on-change. Individually enabled pull-up.
	SCK	ST	CMOS	SPI clock.
	SCL	ST	OD	I^2C™ clock.
RB7/TX/CK	RB7	TTL	CMOS	General purpose I/O. Individually controlled interrupt-on-change. Individually enabled pull-up.
	TX	—	CMOS	EUSART asynchronous output.
	CK	ST	CMOS	EUSART synchronous clock.
RC0/AN4/C2IN+	RC0	ST	CMOS	General purpose I/O.
	AN4	AN	—	A/D Channel 4 input.
	C2IN+	AN	—	Comparator C2 positive input.
RC1/AN5/C12IN1-	RC1	ST	CMOS	General purpose I/O.
	AN5	AN	—	A/D Channel 5 input.
	C12IN1-	AN	—	Comparator C1 or C2 negative input.
RC2/AN6/C12IN2-/P1D	RC2	ST	CMOS	General purpose I/O.
	AN6	AN	—	A/D Channel 6 input.
	C12IN2-	AN	—	Comparator C1 or C2 negative input.
	P1D	—	CMOS	PWM output.
RC3/AN7/C12IN3-/P1C	RC3	ST	CMOS	General purpose I/O.
	AN7	AN	—	A/D Channel 7 input.
	C12IN3-	AN	—	Comparator C1 or C2 negative input.
	P1C	—	CMOS	PWM output.
RC4/C2OUT/P1B	RC4	ST	CMOS	General purpose I/O.
	C2OUT	—	CMOS	Comparator C2 output.
	P1B	—	CMOS	PWM output.
RC5/CCP1/P1A	RC5	ST	CMOS	General purpose I/O.
	CCP1	ST	CMOS	Capture/Compare input.
	P1A	ST	CMOS	PWM output.
RC6/AN8/$\overline{SS}$	RC6	ST	CMOS	General purpose I/O.
	AN8	AN	—	A/D Channel 8 input.
	$\overline{SS}$	ST	—	Slave Select input.
RC7/AN9/SDO	RC7	ST	CMOS	General purpose I/O.
	AN9	AN	—	A/D Channel 9 input.
	SDO	—	CMOS	SPI data output.
VSS	VSS	Power	—	Ground reference.
VDD	VDD	Power	—	Positive supply.

Legend: AN = Analog input or output; CMOS = CMOS compatible input or output; OD = Open Drain
TTL = TTL compatible input; ST = Schmitt Trigger input with CMOS levels
HV = High Voltage; XTAL = Crystal

Appendix G:

1. Morse code character encoding as defined by the ITU (International Telecommunications Unit, 2009)

a	.−	i	..	r	.−.
b	−...	j	.−−−	s	...
c	−.−.	k	−.−	t	−
d	−..	l	.−..	u	..−
e	.	m	−−	v	...−
e	..−..	n	−.	w	.−−
f	..−.	o	−−−	x	−..−
g	−−.	p	.−−.	y	−.−−
h	....	q	−−.−	z	−−..

1	.−−−−	6	−....
2	..−−−	7	−−...
3	...−−	8	−−− ..
4	....−	9	−−−−.
5	.....	0	−−−−−

2. Morse code punctuation marks and miscellaneous signs encoding as defined by the ITU (International Telecommunications Unit, 2009)

Full stop (period)	[.]	.-.-.-
Comma	[,]	--..--
Colon or division sign	[:]	---...
Question mark (note of interrogation or request for repetition of a transmission not understood)	[?]	..--..
Apostrophe	[']	.----.
Hyphen or dash or subtraction sign	[-]	-....-
Fraction bar or division sign	[/]	-..-.
Left-hand bracket (parenthesis)	[(]	-.--.
Right-hand bracket (parenthesis)	[)]	-.--.-
Inverted commas (quotation marks) (before and after the words)	[" "]	.-..-.
Double hyphen	[=]	-...-
Understood		...-.
Error (eight dots)		.....
Cross or addition sign	[+]	.-.-.
Invitation to transmit		-.-
Wait		.-...
End of work		...-.-
Starting signal (to precede every transmission)		-.-.-
Multiplication sign	[×]	-..-
Commercial at[1]	[@]	.--.-.

Appendix H: C code of the program running on the PIC

```
int main(int argc, char** argv)
{

    Init_Ports();                   //Setup ports as inputs or outputs

    mode = cw;                      // CW transmission as default mode
    while(1)
    {
        while(mode==cw)
        {
            LED = 0;
            switch_on();            //Transmission begins
            if(!RC5)                // Checking Puss-button state
            {
                __delay_ms(100);    //de-bouncing delay
                if(!RC5)            // Confirm Puss-button state
                {
                    while(!RC5);    // Wait for button to be released
                    switch_off();   // Stop transmission
                    mode=morse;     // Switch mode to Morse code
                }
            }

        }

        while(mode==morse)
        {
            LED=!LED;               //Toggle LED after every message

            //Message begins
            _S_();                  //South
            _A_();                  //African
            _N_();                  //National
            _S_();                  //Space
            _A_();                  //Agency
            //Message ends


            if(!RC5)                //Check push button status
            {
                __delay_ms(100);    //De-bouncing delay
                if(!RC5)            //Verify push button status
                {
                    while(!RC5);    // Wait for button release
                    mode = cw;      // Switch to CW transmission
                }
            }
        }
    }

    return (EXIT_SUCCESS);
}
```

Appendix I: Complete HF transmitter circuit

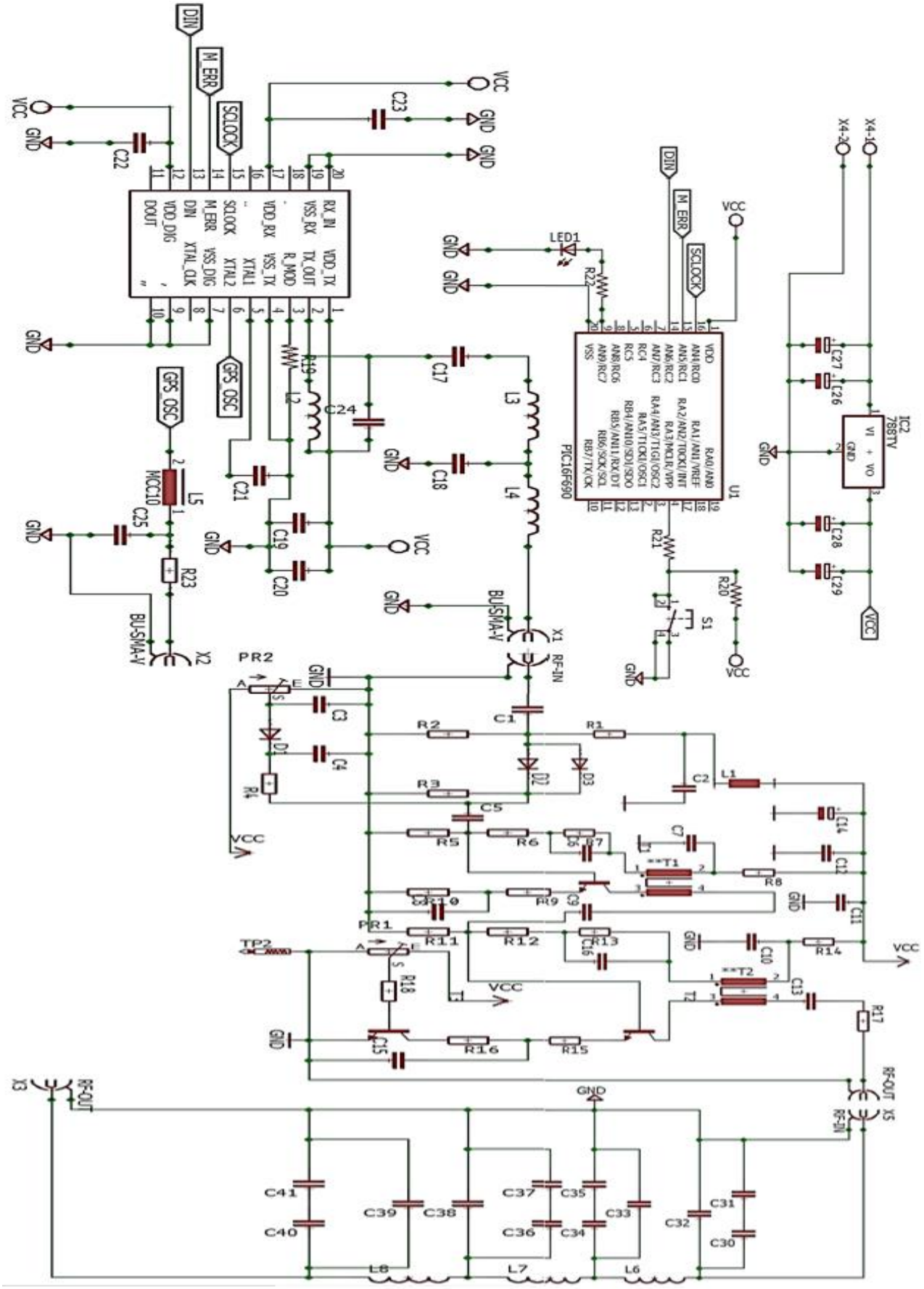

Appendix J: HF beacon circuit

1. Circuit layout as designed on Eagle software

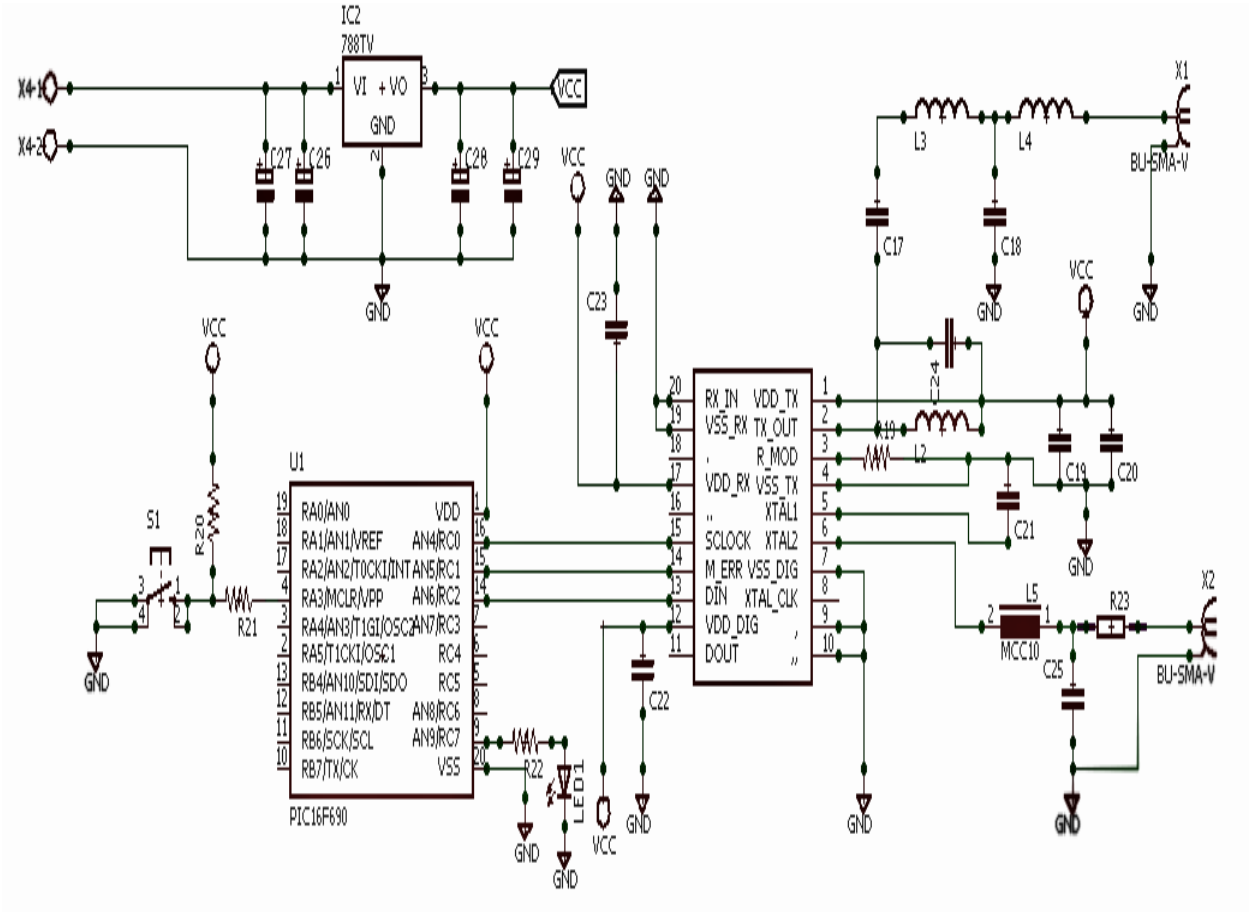

2. PCB layout as designed on Eagle software

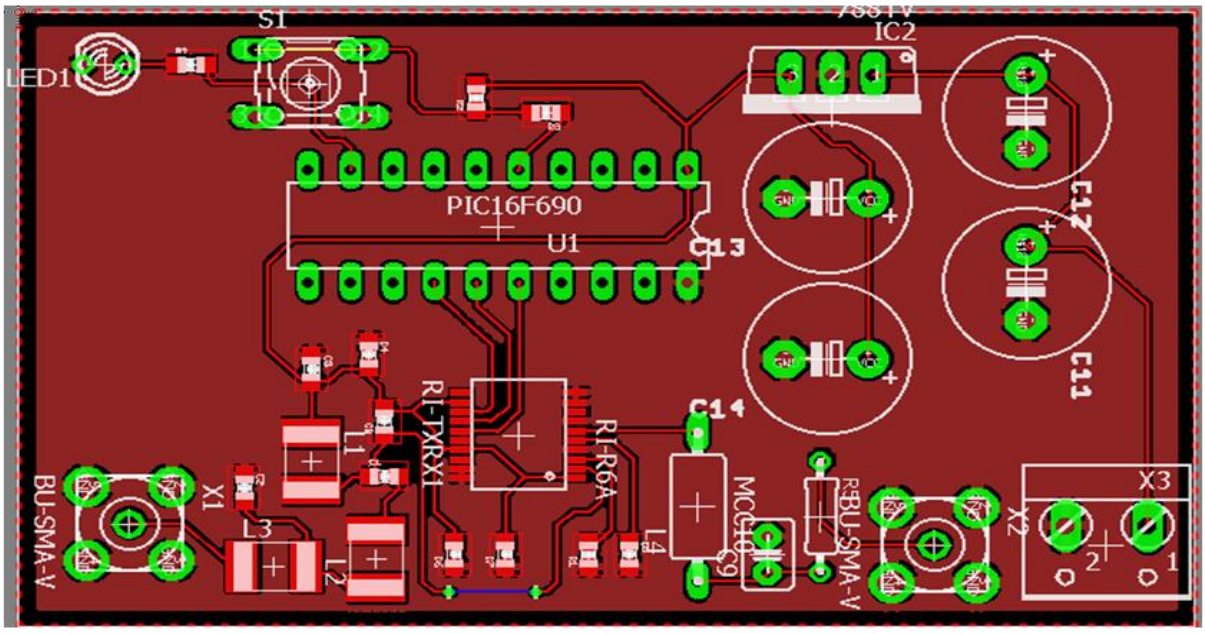

3. Physical implementation of the HF beacon circuit

Appendix K: HF Beacon circuitry ready for temperature tests

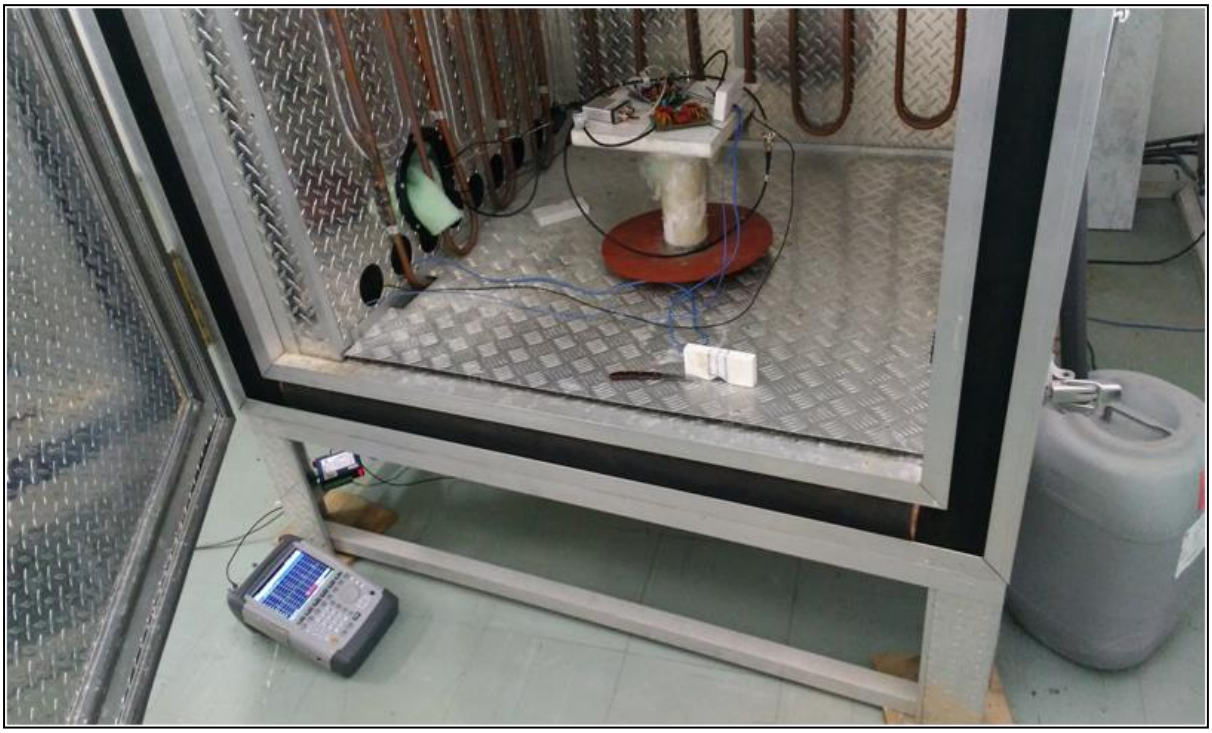

Appendix L: Long-distance experimental verification of HF transmitter

a. Ground distance between the transmitter at Hermanus and a receiver in Pretoria

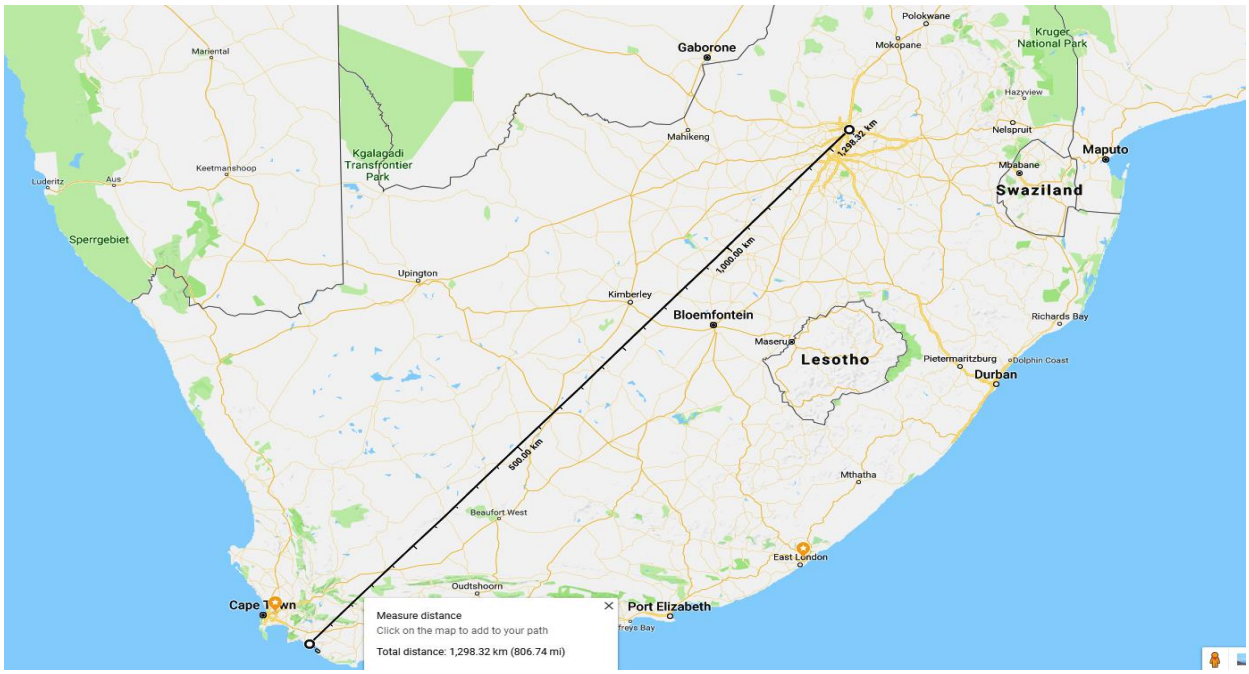

b. Ground distance between the beacon at South Pole and the radar at SANAE IV